CHEMICAL REVIEWS

pubs.acs.org/CR

Review

# Dilute Alloys Based on Au, Ag, or Cu for Efficient Catalysis: From Synthesis to Active Sites

Jennifer D. Lee, Jeffrey B. Miller, Anna V. Shneidman, Lixin Sun, Jason F. Weaver, Joanna Aizenberg, Juergen Biener, J. Anibal Boscoboinik, Alexandre C. Foucher, Anatoly I. Frenkel, Jessi E. S. van der Hoeven, Boris Kozinsky, Nicholas Marcella, Matthew M. Montemore, Hio Tong Ngan, Christopher R. O'Connor, Cameron J. Owen, Dario J. Stacchiola, Eric A. Stach, Robert J. Madix, Philippe Sautet,* and Cynthia M. Friend*

Cite This: *Chem. Rev.* 2022, 122, 8758−8808

Read Online

ACCESS | Metrics & More | Article Recommendations

**ABSTRACT:** The development of new catalyst materials for energy-efficient chemical synthesis is critical as over 80% of industrial processes rely on catalysts, with many of the most energy-intensive processes specifically using heterogeneous catalysis. Catalytic performance is a complex interplay of phenomena involving temperature, pressure, gas composition, surface composition, and structure over multiple length and time scales. In response to this complexity, the integrated approach to heterogeneous dilute alloy catalysis reviewed here brings together materials synthesis, mechanistic surface chemistry, reaction kinetics, in situ and operando characterization, and theoretical calculations in a coordinated effort to develop design principles to predict and improve catalytic selectivity. Dilute alloy catalysts—in which isolated atoms or small ensembles of the minority metal on the host metal lead to enhanced reactivity while retaining selectivity—are particularly promising as selective catalysts. Several dilute alloy materials using Au, Ag, and Cu as the majority host element, including more recently introduced support-free nanoporous metals and oxide-supported nanoparticle "raspberry colloid templated (RCT)" materials, are reviewed for selective oxidation and hydrogenation reactions. Progress in understanding how such dilute alloy catalysts can be used to enhance selectivity of key synthetic reactions is reviewed, including quantitative scaling from model studies to catalytic conditions. The dynamic evolution of catalyst structure and composition studied in surface science and catalytic conditions and their relationship to catalytic function are also discussed, followed by advanced characterization and theoretical modeling that have been developed to determine the distribution of minority metal atoms at or near the surface. The integrated approach demonstrates the success of bridging the divide between fundamental knowledge and design of catalytic processes in complex catalytic systems, which can accelerate the development of new and efficient catalytic processes.

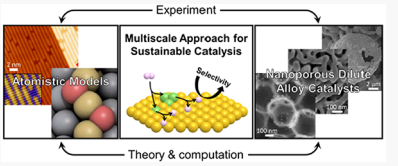




## CONTENTS



**Received:** November 17, 2021
**Published:** March 7, 2022

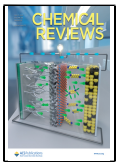





https://doi.org/10.1021/acs.chemrev.1c00967
*Chem. Rev.* 2022, 122, 8758−8808

## 1. INTRODUCTION

### 1.1. Background

Chemical production, which relies heavily on heterogeneous catalysis, now accounts for nearly 30% of industrial energy use.[1] Forecasts for global energy demand project this number will rise to 45% by 2040. Current trends in energy supply and use are unsustainable—economically, environmentally, and socially. Due to the potential for substantial energy savings, building a foundation of fundamental principles that can guide the development of new materials and new catalytic processes is a high priority around the world.[2]

Heterogeneous catalytic processes are extremely complex. Not only do they require optimization of factors across multiple length, time, pressure, and temperature scales, but development of efficient catalytic processes also mandates team science and an interdisciplinary approach, inclusive of materials synthesis, mechanistic surface chemistry, reaction kinetics, and in situ and operando characterization. Numerous studies show that complex metal/oxide interfaces, generally present in catalysts, appear to play an important synergistic role in determining reactivity. Further, since materials are often affected by the reaction environment, pre- and on-stream activation and optimization of performance is necessary.

Historically, heterogeneous catalytic processes have been designed empirically, with broad guidelines informed by prior experience in organic and organometallic chemistry. Recent advances in theory and experiments provide tools with the potential to move beyond the traditional "trial-and-error" approach to design principles that predict and develop highly efficient heterogeneous catalysis materials systems.

This review provides a multidisciplinary view of heterogeneous catalysis (Figure 1), wherein a combination of theory

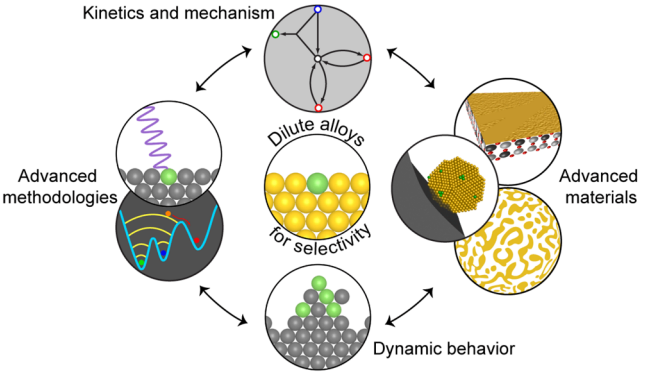


**Figure 1.** Graphical overview of the integrated theoretical−computational−experimental approach needed to bridge the divide between fundamental knowledge and design of catalytic processes in complex dilute alloy systems.

and fundamental studies together with advanced materials synthesis and characterization informs general principles toward the design of more efficient and stable, heterogeneous catalysts, with a vision to advance the fundamental science necessary to reduce the carbon footprint of the chemical industries sector. This is, naturally, a broad topic, spanning numerous materials classes and reactions. From this large range


https://doi.org/10.1021/acs.chemrev.1c00967
Chem. Rev. 2022, 122, 8758−8808

of materials, this review specifically focuses on dilute metal alloy catalysts where the majority element host is Au, Ag, or Cu, a class of heterogeneous catalysts which are particularly promising as industrial catalysts as they present a multitude of advantageous properties, including a significantly reduced use of ultrarare metals as Pt, Pd, or Rh, the possibility of a reduced carbon footprint, increased atom efficiency,[3] and resistance to poisoning.[4−6] This is due to the unique dual functionality they provide, in which a more reactive minority metal is key for bond activation in elementary steps and initiates the catalytic cycle, whereas the less reactive majority metal imparts selectivity by providing a different environment, coordination, and electronic properties to the active element.[7−14]

Importantly, dilute alloy catalysts are a particularly valuable system for a fully integrated theoretical−computational−experimental approach to bridge the divide between fundamental knowledge and design of catalytic processes, specifically by quantitatively scaling from model studies to catalytic conditions due to the relatively simple arrangement of atoms on the surface and the obtained low coverage of intermediates. Experimentally, isolated clusters or atoms (in the case of single atom alloys) of minority species facilitate imaging and interpretation of data in model surface science studies compared to other bimetallic heterogeneous catalysts. Meanwhile, the orbitals of isolated small cluster ensembles or individual atoms of minority species are tractable for theoretical calculations.[15,16]

**1.1.1. Dilute Alloy Catalysts Facilitate Scaling between Model and Catalytic Studies.** It is often challenging to scale between model and catalytic studies due to the typical orders of magnitude difference in temperature and pressure, e.g., $\sim 10^{-8}-10^{1}$ Pa in surface science studies, where the state of the surface is well-defined due to the low number of adsorbates, versus ∼0.1−100 atm in catalytic conditions. Surface science studies typically employ low temperatures to increase the surface lifetime of reactants and products as the relatively nonreactive metal host of dilute alloy catalysts is less likely to accumulate strongly bound species, while higher temperatures and high pressure are typically used in catalytic processes to increase the reaction rates. Ideally, the reactions investigated would not be sensitive to the surface structure; however, if the rates of reaction depend on surface structure, single crystals with different crystallographic orientation can be investigated using both theory and experiment to model the more complex catalytic materials that expose surfaces with a variety of crystallographic faces.

The elementary steps determined from fundamental studies provides a means of predicting and modeling reactivity and selectivity under catalytic conditions.[17] To scale between model systems and catalytic studies, the state of the surface must be similar for the two cases; this challenge is well-met by dilute Au-, Ag-, and Cu-based catalysts because accumulation at high coverage of strongly bound species that can modify the surface is less likely on these relatively low-reactivity host metals. For example, pure Au has an extremely low reactivity; hence, the state of the surface is readily controlled over widely varying conditions encountered during catalytic processes. The consequence is the successful bridging of a wide pressure range[18] and prediction of catalytic selectivity for oxidation reactions based on fundamental studies. Because Au has low reactivity, a second metal is required to initiate the catalytic cycle in the catalyst; for example, small amounts of Ag are used to activate $O_2$, the first step in selective oxidation reactions.[19−22] Similar approaches have been used with materials in which Ag or Cu is the majority element. Both of these metals are somewhat more reactive than Au, so that scaling between model and catalytic studies tend to be more challenging, yet possible. For example, Pd doping of Cu is used to initiate hydrogenation catalysis via $H_2$ dissociation, which does not readily occur on Cu.[23]

**1.1.2. Distribution of Minority Species.** The underlying principle governing the design of dilute alloy catalysts is that the reactive minority metal, e.g., Pd, Ni, Pt, or Ag, initiates the catalytic cycle, whereas the abundant and more "noble" host, e.g., Au, Ag, or Cu, imparts selectivity, either by performing part of the catalytic cycle itself or by electronically modifying the dilute dopant, compared to its bulk state (Figure 2). This simple paradigm requires that intermediates formed from bond activation on the reactive site, migrate ("spillover") across the less reactive majority site.[16] While simple, in principle, design of the catalytic system is complex in practice due to (1) variations in the structure and distribution of the reactive minority component in and on the catalyst, (2) differences in the reaction conditions, which can themselves affect this distribution, and (3) influence of the support both in terms of macroscopic transport phenomena and participation in the catalytic reaction.

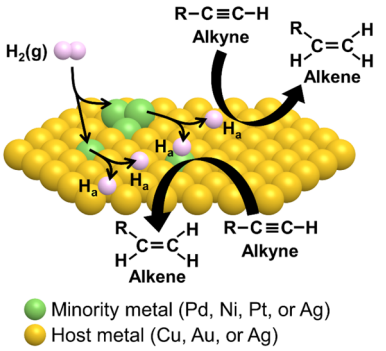


**Figure 2.** Schematic of the underlying design principle of dilute alloy catalysts using selective hydrogenation of alkynes to alkenes as an example. The catalytic cycle is initiated by the reaction minority metal (e.g., Pd, Ni, Pt, or Ag) where $H_2$ dissociates, followed by spillover across the abundant host metal (e.g., Au, Ag, or Cu) that imparts selectivity.

The distribution of the minority metal has three important effects. First, the minority metal must be on or near the surface of the catalyst to impart reactivity. Second, the ensemble size of the minority metal on the catalyst surface is important—for example, single atoms, small ensembles, and larger islands of the minority metal will all have different chemical properties. Third, the distribution and structure of the minority metal in the catalyst is dynamic and depends on the pretreatment and reaction conditions, including temperature and the composition of the reactant gas phase. The effect of adsorbates on surface composition and catalytic function is a key aspect of the research reviewed here. Indeed, reactive species such as CO, $O_2$, and others are known to alter the distribution of minority species as adsorbates may impart additional thermodynamic stabilization of the minority atom at the surface.[24] For example, adsorbed CO provides a thermodynamic driving force for Pd to reside at the surface of a model Pd/Ag(111) alloy at room temperature.[25]


https://doi.org/10.1021/acs.chemrev.1c00967
Chem. Rev. 2022, 122, 8758−8808

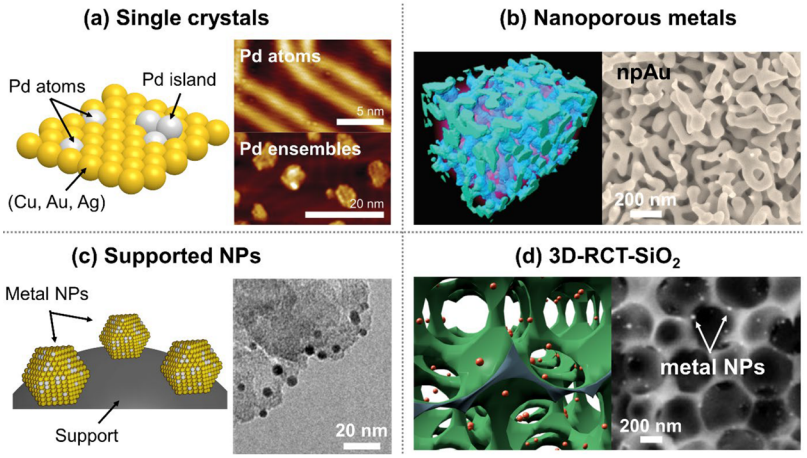


**Figure 3.** Examples of dilute alloy catalysts employed in fundamental studies and catalytic applications. Schematics (left) and example microscopy images (right) of (a) single crystals, (b) nanoporous metals, supported alloy NPs produced by (c) colloidal synthesis and (d) RCT approach. The corresponding microscopy images include (a) scanning tunneling microscopy (STM) image showing single Pd atoms and extended Pd ensembles on a Au(111) surface, (b) scanning electron microscopy (SEM) images of support-free, npAu, (c) transmission electron microscopy (TEM) image of $Pd_{0.15}Au_{0.85}$ NPs supported on carbon, and (d) SEM image of an RCT material consisting of Au NPs partially embedded in nanoporous $SiO_2$ support. The schematic of npAu in (b) is generated by fully atomistic molecular dynamics (MD) simulations. Adapted with permission from ref 28. Copyright 2009 Springer Nature. Images in (a), (c), and (d) are adapted with permission from refs 29, 30, and 31, respectively. Copyrights 2019 Royal Society of Chemistry, 2020 American Chemical Society, and 2018 John Wiley and Sons.

Temperature is another important variable that can alter the composition and distribution of the reactive metal on and near the surface.[4,7] In general, higher temperatures lead to higher activity and lower selectivity for any given chemical process because of the exponential dependence of reactivity on temperature. For dilute alloy catalysts, temperature affects the steady-state concentration of adsorbed species at a given pressure, which in turn may alter the thermodynamic stability of the minority atom at the surface. In addition, the rate of exchange of surface atoms and those in the bulk are affected by the temperature as diffusion rates increase with temperature. All in all, there is a complex interplay among temperature, pressure, gas composition, surface composition, and structure. We will show in this review how all of these aspects affect the dynamics, surface composition, and catalytic reactivity of dilute alloys.

**1.1.3. Materials to Test Concepts from Catalytic Studies.** A challenge in testing heterogeneous catalyst is often the nonuniformity and dynamic structure at the atomic or nanoscale level. There is thus an impetus to develop well-defined materials with controlled structure and composition. Heterogeneous catalysts come in the form of (1) model systems for ultrahigh vacuum studies (UHV) as well as (2) support-free and (3) supported materials for reactor studies (Figure 3). The synthesis of single or polycrystal dilute alloy catalysts for UHV studies as well as supported and unsupported nanoparticles (NPs) has been discussed in several review articles.[7,26,27] The current review provides illustrative examples from those works in section 2—but is by no means exhaustive—and highlights more recent materials developments in dilute alloy catalysts, namely, support-free nanoporous materials (section 2.3), which provide high surface-to-volume ratio, high surface curvature, and confinement with properties of extended 3D materials, including high thermal and electrical conductivity, and supported NPs, including the raspberry colloid templating (RCT) approach to prepare sinter-resistant supported dilute metal alloy NPs partially embedded in nanoporous oxide supports (section 2.4). The consistent nature of these materials in terms of composition and morphology throughout numerous catalysis and treatment conditions makes them amenable to a variety of characterization techniques and aids the connection to theoretical investigations, allowing for feedback between the fundamental surface science studies, calculations, and catalytic processes.

**1.1.4. Reactions, their Mechanisms and Kinetics, and Dynamic Behavior during Catalysis.** By correlating surface science studies with density functional theory (DFT) of well-defined systems, fundamental insights into mechanisms, energetics, and the role of structure toward understanding the selected oxidation and hydrogenation reactions can be obtained (section 3). The success of relating model studies to catalytic performance over dilute alloy catalysts has advanced the paradigm for control of a wide range of reactions, examples including CO and alcohol oxidation over Au-based dilute alloy materials (section 3.2) and non-oxidative dehydrogenation over Cu-based catalysts (section 3.3) are emphasized in this review due to the wealth of information acquired through fundamental and catalytic studies as well as their industrial relevance. The importance of introducing minority reactive metals in coinage metals is also reviewed for selective hydrogenation of carbon−carbon multiple bonds (section 3.4), where the difference in adsorption energy of reactant and product governs the high selectivity toward alkene. The dynamic changes in the surface structure and composition as well as adsorbate migration between reactive ensembles can have profound effects on the catalytic behavior of dilute alloys (section 4). This includes determining dynamic behavior in response to gas-phase composition and temperature and identifying reaction conditions that retain the optimal catalyst structure (section 4.2). The mechanisms for adsorbate migration between coexisting surface phases and their influence on reaction kinetics and surface restructuring can be demonstrated using model bimetallic surfaces (section 4.3).

**1.1.5. The Need for Development of Methodologies.** A major challenge in studying catalytic processes involving dilute alloys is tracking the minority component in the catalyst,


https://doi.org/10.1021/acs.chemrev.1c00967
Chem. Rev. 2022, 122, 8758−8808

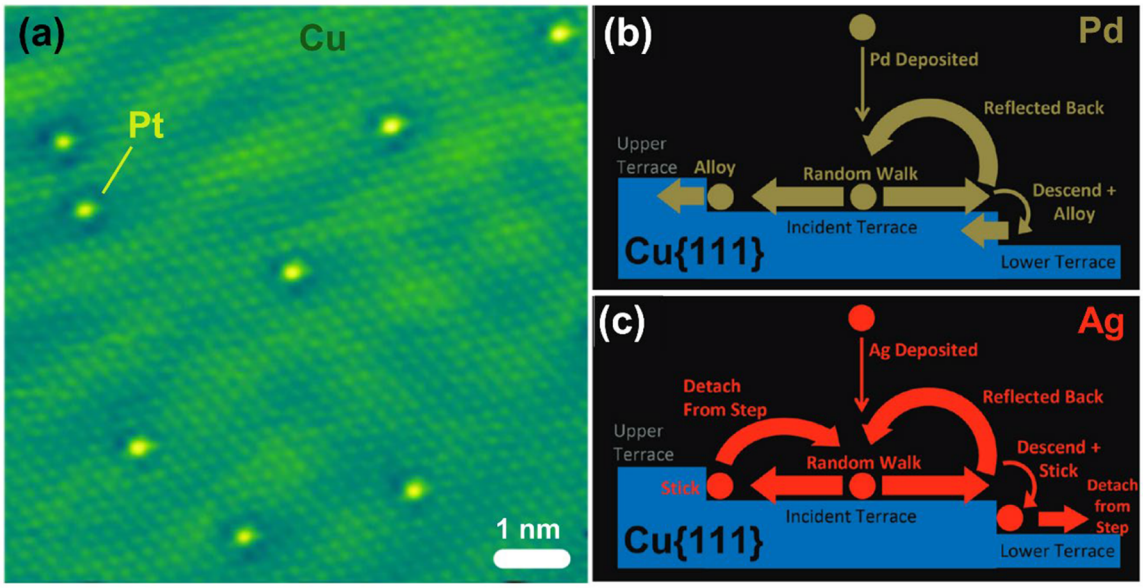


**Figure 4.** (a) STM image of a 0.02 ML Pt/Cu(111) surface. The bright spots correspond to Pt atoms substituted on the Cu(111) surface. Proposed mechanisms for alloying of (b) Pd and (c) Ag on Cu(111) surfaces, where the thickness of the arrows represents the relative prevalence of the events. The difference between the two minority species are attributed to their different binding strengths at ascending step edges, e.g., weakly binding for Ag and strongly (irreversible) for Pd. Adapted with permission from refs (a) 35 and (b,c) 34. Copyrights 2015 Macmillan Publishers and 2009 American Chemical Society.

including the amount and the sizes of reactive metal ensembles on the surface. Even more challenging is the fact that the surface composition and ensemble size will fluctuate because of temperature effects or the binding of reactants and products to the surface, creating the need for understanding kinetics and dynamics of material rearrangement and the relationship to reaction kinetics.

A concerted effort has been made to advance experimental tools to understand the state of the surface under different conditions (section 5). This requires a combination of spectroscopy, imaging, and simulation. One area of focus has been the advancement of analysis of extended X-ray absorption fine structure (EXAFS) data using machine learning (ML) methods to map out the atomic distribution of the metal atoms (section 5.2). Atomic-scale imaging complements the spectroscopic data, and together with in situ capabilities, materials under reaction conditions can be characterized (section 5.3). In both cases, the highly dilute nature of the alloys reviewed here push the boundaries of the methods. Theoretical tools that include ML methods and automation that accelerate molecular dynamics (MD) simulations are also under development to model the atomic-scale events that lead to rearrangement of the alloy surfaces and thus understand changes in materials properties, migration of reactants across boundaries in the material, and model reaction pathways (section 5.4).

The development of these and other methods is broadly useful in the field of heterogeneous catalysis and can also be applied to other materials and processes involving complex materials. Hence, considerable effort has been made by researchers in this area to both develop new methods and push the boundaries of existing tools.

### 1.2. Summary

The foundational concept underlying the research reviewed here is that fundamental surface chemistry studies combined with advanced materials synthesis and characterization provides a means of understanding and predicting catalyst function, opening the door to "catalysis by design", with a special focus on materials consisting of a Au, Ag, or Cu host and Pd, Pt, Ag, or Ni minority species due to their importance in a broad range of catalytic reactions. This review strives to provide an overview of how a highly interdisciplinary approach, inclusive of materials synthesis, mechanistic surface chemistry, reaction kinetics, and in situ and operando characterization, can be used to understand catalytic processes. Each of the subtopics discussed cannot be covered exhaustively; rather, the value of combining various methods is articulated, referring the reader to more complete reviews of those topics.

## 2. ADVANCED MATERIALS

### 2.1. Overview

The ability to reproducibly fabricate customizable and robust catalysts is critical to improve catalytic performance by quantitatively scaling from model studies to reaction conditions. A variety of dilute alloy materials have been developed to address these complexities (Figure 3). UHV surface science studies on single-crystal surfaces in the presence of low concentrations of reactants and other adsorbates are used to gain a fundamental understanding of the reaction pathways and surface restructuring, which can be directly correlated to DFT calculations. With an added level of complexity in materials design, support-free nanoporous metals have been introduced to bridge between surface science and catalytic reactor studies without the confounding effects introduced by a support. At the highest level of complexity are supported NPs, the structure of most heterogeneous catalysts currently employed in industry but the most challenging to characterize due to the complex interplay of phenomenon such as mass and thermal transport, accessibility of active sites, direct participation of the support in reactions, and metal−support interactions. As part of the multipronged approach to understanding dilute alloy catalysts, it is


https://doi.org/10.1021/acs.chemrev.1c00967
Chem. Rev. 2022, 122, 8758−8808

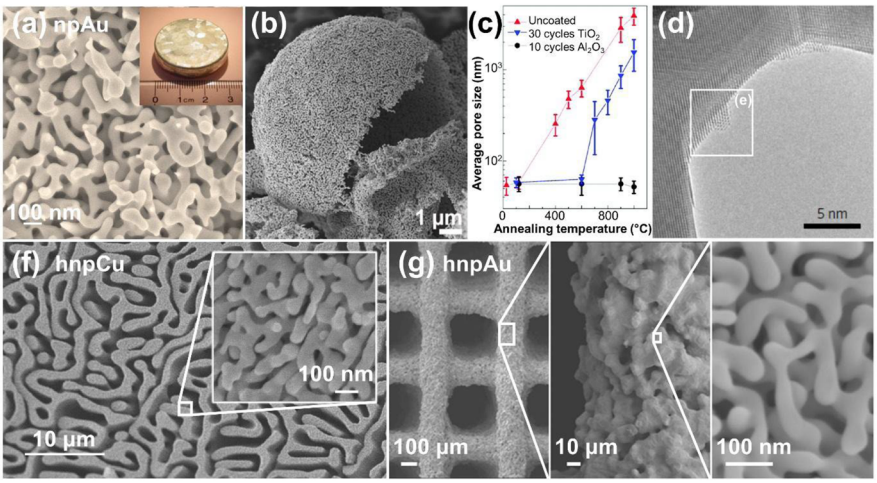


**Figure 5.** Varieties of nanoporous metal catalyst architectures have been synthesized to suit specific applications. SEM images of npAu in the form of (a) monolithic bulk sample and (b) hollow shells. Inset in (a) is a photograph of the starting alloy $Au_{0.3}Ag_{0.7}$. (c) Inhibition of coarsening of npAu when nanometer-scale $Al_2O_3$ and $TiO_2$ coatings are present. (d) TEM image of npAu demonstrating its single-crystalline character. Boxed area in (e) indicates the formation of highly crystalline metallic NPs after reduction by 0.1 Torr methanol at 423 K for 30 min. SEM images of (f) hierarchical npCu (hnpCu) made from a Cu-$CuAl_2$ starting alloy and (g) hierarchical npAu (hnpAu) with residual Ag fabricated by direct ink printing with increasing magnifications going from left to right. Images in (b), (c), and (d) are adapted with permission from refs (b) 55, (c) 58, and (d) 62. Copyrights 2015 and 2011 American Chemical Society and 2017 Springer Nature.

imperative to synthesize well-defined supported catalysts to be able to relate materials studies to catalytic activity in order to facilitate their further design. RCT has recently emerged as an approach to prepare supported NP catalysts with highly stable NPs that are uniform in size and distributed throughout the macroporous metal oxide support, allowing correlations between bulk material characterization techniques and local electron microscopy techniques.

This section discusses the most common synthetic routes for preparing the materials presented in Figure 3 and the corresponding characterization techniques, highlighting the systems that will be commented later on in the review. The ability to precisely synthesize and characterize these materials is critical to understand changes that occur in the dynamic environments experienced by catalysts and to guide material optimization.

### 2.2. Metal Foils for UHV Studies

Fundamental surface science studies of single atoms deposited on well-defined single-crystal metal surfaces led to the discovery of single and dilute atom alloy catalysts, a rare instance of fundamental studies initiating the development of a class of heterogeneous catalysts, as opposed to the more traditional approach of testing various catalysts and then turning to fundamental studies to gain mechanistic understanding and further optimize the catalyst.[7,26] Samples for UHV studies can be prepared by melting a quantitative amount of the two metals (e.g., Au slugs together with Pd granules) above their alloying temperature, followed by cold-rolling into a foil and annealing (e.g., ∼1100 K) for grain growth; the samples are then cycled between thermal treatments and Ar ion sputtering to remove impurities, with a final step of thermal treatment under UHV conditions for recrystallization.[32] A more ubiquitous strategy is to introduce the minority species by physical vapor or electron beam deposition onto the surface of a pristine metal substrate, which has a well-defined crystalline orientation and an exceptionally low defect and impurity density (often commercially obtained), e.g., Pd/Au(111), Pt/Ag(100), Pt/Cu(111), etc. During the deposition process, the substrate should be held at an appropriate temperature (typically ∼400 K), high enough to allow for diffusion of the minority species and its substitution onto surface sites but low enough to limit diffusion into the bulk.[7,33] Cycles of sputtering with nonreactive Ar ions followed by annealing (∼800−1000 K) under UHV conditions are standard methods of cleaning the surface prior to deposition of the minority species.

As these structures are planar, their surface is easily accessed by STM, allowing an atomic-scale view of the arrangement of minority species before, during, and after exposure to various reactants, adsorbates, and conditions. Figure 4a shows an example STM image of Pt deposited on a Cu(111) surface. STM has been employed, for example, to visual the distribution minority species deposited onto a host surface as a function of substrate temperature, identifying general principles regarding atom exchange at step edges versus terraces and the formation of isolated atoms versus clusters.[33] Such phenomena can then be modeled with DFT to aid the development of a mechanistic understanding of the alloying process.[33,34] The alloying processes involve minority species that either bind strongly (Figure 4b) or weakly (Figure 4c) to step edges of the host metal. STM images can be correlated with other experimental techniques; for example, temperature-programmed desorption (TPD) of CO and other probe molecules in a UHV system.[4]

### 2.3. Support-Free Nanoporous Alloys

Support-free nanoporous materials readily connect results from surface science studies to catalytic conditions due to their highly ordered character and low density of grain boundaries as well as their amenability to both UHV surface science tools and reactor studies.[36] Nanoporous alloys consist of metals with feature sizes on the order of tens of nanometers with morphology, uniformity, purity, and density controlled through the choice of synthetic route and parameters therein[37,38] (see examples produced by dealloying and selective leaching in Figure 5). The extended connected network provides beneficial properties such as high thermal and electrical


https://doi.org/10.1021/acs.chemrev.1c00967
Chem. Rev. 2022, 122, 8758−8808

conductivities. High thermal conductivity is of critical importance for process intensification in highly exothermic or endothermic reactions where the catalyst utilization becomes limited by thermal gradients;[39] high electrical conductivity is a prerequisite for electrochemical transformations such as electrochemical $CO_2$ reduction.[40−42] The electrical conductivity of monolithic nanoporous metals also facilitates fundamental surface science studies that rely heavily on electron spectroscopies (e.g., Auger electron spectroscopy and X-ray photoelectron spectroscopy (XPS)). At the same time, the highly curved surfaces of nanoporous metals mimic those of metal NPs, including a high density of undercoordinated surface sites, though they exhibit many saddle points where the principal radii of curvature are of opposite sign in contrast to NPs which are exclusively convex.[43]

Numerous approaches toward fabrication of monolithic nanoporous metals have been developed, and several review articles[44−46] provide an overview over the different synthesis techniques ranging from bottom-up approaches based on assembly of nanoscale objects such as metal NPs and nanowires to corrosion-based top-down approaches, templating, nanosmelting, and combustion. The various bottom-up approaches[44] offer different degrees of control over morphology, uniformity, purity, and density. Compositional tuning is generally performed in the preassembly stage, for example, by controlling the composition of the primary NPs to be assembled through electroless plating or galvanic exchange reactions.[47] The most common and universal top-down approach is dealloying via a corrosion-based process starting with binary ($M_1M_2$) or ternary ($M_{1a}M_{1b}M_2$) alloys, where $M_1$ represents the more noble alloy component(s) and $M_2$ is a less noble alloy component. The process generates a unique bicontinuous ligament pore morphology with unimodal nanoscale ligament/pore size distribution at a length scale of 10−100 nm depending on the details of the alloy composition and dealloying conditions (Figure 5).[48,49] Nanoporosity is generated by selective removal (leaching) of the less noble alloy component $M_2$ from the starting alloy, and the composition is controlled by the starting alloy and the specifics of the dealloying process; for example, nanoporous $Ag_{0.03}Au_{0.97}$ (npAgAu) is readily formed from a bulk AuAg alloy. A coherent nanoporous morphology, where the grain structure of the starting alloy is preserved, is produced from starting alloys in which components form a solid solution and both the starting alloy and the remaining more noble alloy component share the same crystal lattice and lattice constant.[36,50] The resulting crystallite size is orders of magnitude larger than the characteristic length scale of the ligaments and pores.

Combinations of bottom-up and top-down approaches typically include fabrication and assembly of larger particles made, for example, by templating[51] or ball milling[40] followed by dealloying. Dealloying is in fact a universal process: it can be performed with a variety of different starting alloys in the form of bulk materials (Figure 5a),[52] thin films,[53] or particles (Figure 5b)[54,55] as long as the alloy components have a sufficiently different corrosion behavior. Furthermore, various dealloying environments have been established with or without applied electrochemical potential in aqueous or ionic liquid electrolytes or even in molten metal[56] and the vapor phase.[57]

When the structure is further tuned, the feature size of both pores and ligaments can be adjusted from a few nanometers to a few microns by thermal annealing (Figure 5c).[58] The coarsening is self-similar; that is, the number of connections in a representative volume element remains constant, independent of the ligament size, thus providing an ideal platform to study size effects.[59] The coarsening kinetics depends strongly on alloy composition and surface chemistry, with both high melting point alloy components[60,61] and surface oxides[58] strongly suppressing coarsening (Figure 5c).

The classical example for a monolithic nanoporous metal made by dealloying is npAu prepared by selective corrosion dealloying of Ag from $Au_{1-x}Ag_x$ alloys ($x$ = 0.65−0.75). npAu is a Au-rich AuAg alloy where the residual Ag reflects the dealloying process is never 100% complete (Figure 5d).[63] The same dealloying process can be applied to many other alloy systems, including Ag-free npAu prepared by dealloying AuAl starting alloys,[64] npCu generated from CuMn,[50] CuAl[65], and CuZn[52] alloys, and npAg prepared from AgAl alloys.[66] While dealloying single-phase starting alloys generally generates a unimodal nanometer-scale pore size distribution, more complex, hierarchical pore size distributions can be obtained by dealloying multiphase starting alloys such as the two-phase Al-$CuAl_2$ eutectic alloy (Figure 5f). The presence of larger pores in these hierarchical nanoporous metals helps overcome mass transport limitations to improve the efficiency of nanoporous catalyst materials in the case where chemical reactions are fast compared to mass transport.[67] Besides the traditional metallurgical techniques, 3D metal printing can be used to create hierarchical nanoporous architectures where the macropore (∼0.1−1 mm in diameter) morphology is defined (and limited) by the resolution of the 3D printing process (Figure 5g).[68] This, for example, can be used to realize engineered pore architectures that are designed to improve mass transport properties.

In the case of bottom-up approaches, more reactive minority alloy components can be added after dealloying by a variety of methods including galvanic exchange, liquid impregnation, and atomic layer deposition.[47,60,69,70] For example, Ni has been added to npAu and npCu using a liquid impregnation technique.[47,67] Alternatively, more complex ternary starting alloys can be used to directly generate nanoporous dilute alloys if both the majority and minority components are more noble than the porosity forming alloy component. Examples include Pd-doped npAg and npAu fabricated from ternary AgPdAl and AuPdAl alloys, respectively. However, many of the ternary alloy systems are not thermodynamically stable at room temperature and thus require metallurgy techniques like melt spinning that realize extremely high cooling to keep the alloy system homogeneous. Catalytic studies employing such nanoporous materials are presented in Table 1 and discussed in more detail in sections 3.2.1, 3.2.2, and 3.3.1.

### 2.4. Supported Dilute Alloy Catalysts

Supported heterogeneous catalysts are used in a wide range of industrial applications. Thus the integration of dilute alloys with a support is an important step in advancing the field of dilute alloy catalysis toward industrial applications. Although the NPs often function as the catalytically active site, the support can play an important role in the performance of the catalyst, as well, affecting the overall activity, selectivity, and stability. Among others, the support determines the internal mass transport, accessibility of active sites, and stability of the incorporated metal NPs and can even directly participate in the catalytic cycle. Strategies for controlling metal−support interactions have been reviewed previously.[79]



https://doi.org/10.1021/acs.chemrev.1c00967
Chem. Rev. 2022, 122, 8758−8808

**Table 1. Support-Free Dilute Alloy Catalysts and the Corresponding Catalytic Reactions Summarized in This Review**

| target reactions | support-free materials |
|---|---|
| CO oxidation | $Ag_{0.007}Au_{0.093}$,[71] $Cu_{0.12}Au_{0.88}$[72] |
| oxidative self-coupling | $Ag_{0.03}Au_{0.97}$[55,68,73−75] |
| oxidative cross-coupling | $Ag_{0.03}Au_{0.97}$[76−78] |
| anhydrous aldehyde production | $Ni_xZn_{0.04}Cu_{0.96-x}$ ($x$ = 0.003, 0.01),[47,69,a] $Ni_{0.01}Cu_{0.99}$[60] |
| | $Ni_xAg_{0.03}Au_{1-x}$ ($x$ = 0.0001, 0.001, 0.002, 0.01)[60] |

[a]Residual Zn content depends on the dealloying conditions, with HCl resulting in lower Zn concentrations, and $H_3PO_4$ resulting in higher Zn concentrations.

Over the past decade, synthesis and material science efforts have enabled the preparation of dilute alloy NPs with well-defined size, shape, composition, and distribution of minority species, as well as their incorporation on and in a variety of supports for catalytic studies under reaction conditions. The variety of synthetic methods have been extensively discussed previously[7], and a brief summary is provided here.

A wide range of traditional catalyst preparation approaches have been applied to the synthesis of dilute alloy catalysts, including deposition precipitation[80,81] and impregnation[3,81−84] of the metal precursors on a support materials or wet-chemical approaches such as colloidal synthesis[9,30,35,85−89] and/or galvanic replacement. In deposition precipitation, metal salt precursors are deposited on a support by reducing their solubility in solution, followed by drying and calcination to decompose the salt and form NPs. Impregnation involves infiltrating the support with a metal precursor solution followed by drying and calcination. These two methods have been applied to produce dilute alloy NPs with sizes typically below 10 nm and consisting of a variety of metals combinations, including PdAu,[83,85] PdAg,[3] PdCu,[80] and PtCu.[90] The TEM image in Figure 6 shows an example of dilute $Pd_{0.025}Ag_{0.975}$ NP alloys synthesized via co-impregnation of $Pd(NO_3)_2$ and $AgNO_3$ on a $SiO_2$ support. A class of dilute alloy NPs containing singly dispersed active metal atoms embedded into a less active host metal are often referred to as single-atom alloys (SAAs).

The advantages of deposition precipitation and impregnation are the large quantity of catalysts that can be prepared in a single batch (typically several grams of material are obtained). However, ensuring homogeneity in particle size, metal composition, and distribution can be challenging. Recent advances in material science have enabled the synthesis of alloy NPs with well-controlled size, shape, and composition via colloid methods. Briefly, the alloy NPs are grown in solution prior to being deposited on a support (Figure 6c); the metal composition is tuned via the metal precursor concentrations in solution, and the size and shape are controlled via the reaction conditions (e.g., temperature, pH) and the type of organic ligands used to direct the particle growth. After depositing the NPs on the support, the ligands are removed via thermal treatment[91,92] or chemical washing[93] to ensure that the metal surface is accessible for catalysis. A wide range of dilute alloy catalysts have been prepared, including PdAu,[9] PdAg, PtCu,[35,94] PdCu,[87,88] and NiAu[95] NPs with sizes between 2 and 5 nm, supported on various metal oxide supports (e.g., $SiO_2$, $TiO_2$, $Al_2O_3$). Finally, it is possible to introduce a dilute

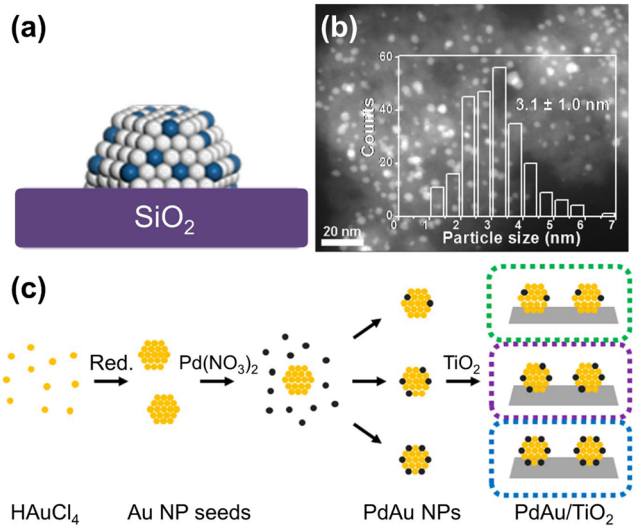


**Figure 6.** (a) Schematic and (b) TEM image of $Pd_{0.025}Ag_{0.975}$ NP catalyst supported on $SiO_2$ formed by wetness incipient co-impregnation of $Pd(NO_3)_2$ and $AgNO_3$ in a silica gel. The histogram in (b) shows the particle size distribution. (c) Schematic of a two-step colloidal synthesis of PdAu NPs followed by deposition onto a $TiO_2$ support. Here, Au NP seeds were synthesized in the first step with particle size determined by the reaction temperature. Pd is incorporated in the second step with the concentration depending on the Pd precursor concentration. The as-prepared PdAu NPs were then deposited onto a calcined $TiO_2$ support. Images are adapted from refs (a,b) 3 and (c) 9. Copyrights 2015 and 2018 American Chemical Society.

amount of the second metal onto an already existing metal NP via galvanic replacement.[7,95] This methodology can be applied if the metal host consists of a less noble metal (i.e., lower electrode potential) than the second/dopant metal and is therefore suitable for Ag and Cu host materials but not for Au.

A well-known deactivation mechanism of supported catalysts is NP migration and sintering, especially during reactions at elevated temperatures and pressures, although the support does substantially improve NP thermal stability compared to their unsupported counterparts.[96] In addition to reducing catalytic efficiency, variations in NP accessibility and size complicate the material characterization and understanding. Both the dopant distribution on the surfaces of dilute alloy NPs as well as the NPs themselves can suffer from metal redistribution and NP sintering, respectively, at the temperatures required to remove the stabilizing ligands from the NP surface (~573−673 K) or under the reaction conditions used.[7,97] Various strategies have been developed to stabilize the host NPs at high temperature and pressure, including confining NPs in pores or cavities of inorganic supports where encapsulation in porous materials allows for facile reactant and product transport but precludes NP migration. Encapsulating materials include zeolites[98] and metal oxides such as mesoporous $SiO_2$[97,99,100] or $ZrO_2$.[97]

Precise control over the material composition, support architecture, and NP distribution are desirable to perform fundamental studies and optimize catalyst design. A particularly promising route to substantially improve the thermal stability of dilute alloy NPs is to employ the recently developed RCT approach, wherein NPs are anchored in the 3D microporous metal oxide ($MO_x$) support at the pore interfaces, ensuring that every NP is accessible to the reactant stream.[101]


https://doi.org/10.1021/acs.chemrev.1c00967
Chem. Rev. 2022, 122, 8758−8808

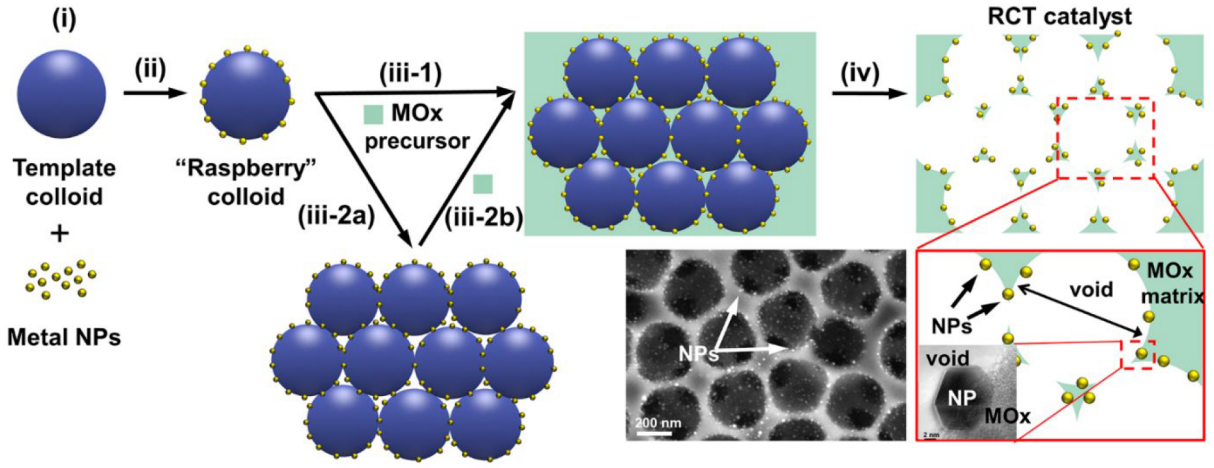


**Figure 7.** Schematic of the synthetic procedure to produce RCT materials. The procedure consists of (i) synthesis of ligand-capped polymeric template colloids and metal NPs of well-defined size and shape, (ii) attachment of NPs onto the colloid surface, and (iii) assembly of the resulting raspberry colloids either (iii-1) together with the $MO_x$ precursor in a process known as coassembly or without (iii-2a), followed by (iii-2b) infiltration by the $MO_x$ precursor. Once (iv) the template is removed, typically through calcination at 773 K in oxidative conditions, a porous RCT catalyst is formed, featuring interconnected voids with metal NPs at the air−$MO_x$ interface. The inset is a TEM image of a $Ag_xAu_{1-x}$ RCT-$SiO_2$ catalyst. The SEM image to the left is taken over the same catalyst. Adapted with permission from ref 31. Copyright 2018 John Wiley and Sons.

Importantly, anchoring of the NPs gives rise to the high sinter resistance of RCT materials, which has been demonstrated through extensive TEM studies and, more recently, 3D TEM imaging.[102] The NPs thus maintain a uniform spatial distribution and size throughout the microporous structure, as shown for a variety of treatment conditions and after multiple reaction cycles.[102−105] This exceptional uniformity allows for the application of bulk material characterization techniques in addition to more localized characterization techniques such as electron microscopy.

The synthetic route to RCT catalysts (Figure 7) entails self-assembly of sacrificial templating polymeric colloidal particles decorated with presynthesized NPs either together with (coassembly) or followed by infiltration with a $MO_x$ precursor. Once the template is removed—typically by calcination in oxidative conditions—a highly interconnected network of spherical voids results, where the void size is determined by the templating colloid (anywhere from 50−1000 nm, with ∼300−400 nm being the most common in the catalytic studies to date) and the windows (or necks) connecting them of ∼80−100 nm width are the result of $MO_x$ precursors not being able to fill the regions where the templating spheres had been in contact.

The RCT strategy is highly modular, enabling screening through various structural and compositional features independently or quasi-independently. Features that can be varied include the composition, phase, and microporosity of the $MO_x$ support, the composition, size, loading, and placement of the single- or multimetallic NPs, and the pore size and organization of the 3D $MO_x$ framework. RCT has been demonstrated for various combinations of mono- and multimetallic NPs (e.g., Au, Pt, Pd, $Ag_xAu_{1-x}$, $Pd_xAu_{1-x}$) and $MO_x$ (e.g., $SiO_2$, $TiO_2$, $CeO_2$).[101] Catalytic studies based on supported dilute alloy catalysts are summarized in Table 2 and discussed in more detail in sections 3.2.1, 3.2.2, 3.3.1 and 3.4.1.

**Table 2. Dilute Alloy NPs on Metal Oxide Supports and the Corresponding Catalytic Reactions Discussed in This Review**

| target reactions | supported dilute NPs |
|---|---|
| CO oxidation | $Pd_xAu_{1-x}$ RCT-$SiO_2$ ($x$ = 0.02, 0.04, 0.09)[105] |
| oxidative coupling | $Ag_xAu_{1-x}$ RCT-$SiO_2$ ($x$ = 0.1, 0.2, 0.5)[31] |
| | $Pd_xAu_{1-x}$ NPs/$TiO_2$ ($x$ = 0.014, 0.048, 0.071, 0.15)[9,30] |
| anhydrous aldehyde production | $Ni_xCu_{1-x}$ NP/$SiO_2$ ($x$ = 0.001,[47] 0.01,[106] 0.04,[89] 0.18[89]) |
| | $Pt_xCu_{1-x}$ NP/$SiO_2$ ($x$ = 0.003,[107] 0.01[106,107]) |
| | $Pd_{0.01}Cu_{0.99}$ NP/$SiO_2$[106,107] |
| | $Ni_xAu_{1-x}$ NP/$SiO_2$ ($x$ = 0.001, 0.002, 0.005, 0.01)[60] |
| selective hydrogenation of alkynes | $Pd_xAg_{1-x}$ NP/$SiO_2$ ($x$ = 0.005,[3] 0.01,[3,108] 0.15,[80] 0.025[3]) |
| | $Pd_xAu_{1-x}$ NP/$SiO_2$ ($x$ = 0.004,[109,110] 0.025,[3,108,111] 0.01,[111] 0.1[111]) |
| | $Pd_xAu_{1-x}$ RCT-$SiO_2$ ($x$ = 0.02, 0.04, 0.09)[104,112] |
| | $Pd_xCu_{1-x}$ NP/$SiO_2$ ($x$ = 0.006, 0.015, 0.025, 0.09)[80,108] |
| | $Pd_xCu_{1-x}$ NP/$TiO_2$ ($x$ = 0.02, 0.08)[80] |
| | $Pd_{0.18}Cu_{0.82}$ NP/$Al_2O_3$ ($x$ = 0.013,[113,114] 0.02, 0.04,[113,114] 0.1,[113,114] 0.18[87]) |

## 3. MECHANISMS AND KINETICS

### 3.1. Overview

A central goal in the rational design of dilute alloy catalysts is to predict reaction selectivity under catalytic conditions based on reaction mechanisms and kinetics determined from fundamental studies on metallic single crystals. The design principle for dilute alloy catalysts involves a small amount of reactive metal atom (minority species) activating one key reactant and the selective reactions followed on the less reactive host metal (majority species). Catalytic behavior is studied under flow and batch conditions, often using operando spectroscopy. Remarkable progress has been made on the research objective to advance the paradigm for control of selective oxidation and hydrogenation on dilute alloy catalysts and to quantitatively model their kinetics.

The mechanisms and kinetics are determined for model systems using experimental studies on well-defined single-


https://doi.org/10.1021/acs.chemrev.1c00967
Chem. Rev. 2022, 122, 8758−8808

crystal materials at low pressure and complemented by theoretical studies of bonding and activation barriers. This fundamental information on specific elementary steps is used to model and understand the behavior of catalysts. In selected cases, the reactions and kinetics are analyzed and refined using advanced transient pulse techniques at intermediate pressures and temperatures used in catalytic operation on the actual catalysts.

Thus far, dilute alloy catalysts based on Au, Ag, or Cu with Pd, Ni, Pt, or Ag as the minority species have been employed in several reactions, some of which have been described in previous review papers.[7,26] Here, the reactions have been intentionally selected to show how model studies and catalyst performance can be related in an integrative approach that employs the feedback between a combination of rationally designed materials, advanced characterization methodologies, and theoretical approaches. This section will focus on three main reactions (Scheme 1): (1) CO oxidation and oxygen-assisted coupling of alcohols, (2) non-oxidative dehydrogenation of alcohols for aldehyde and hydrogen production, and (3) selective hydrogenation of alkynes to alkenes.

**Scheme 1. Selected Reactions Reported on Au-, Ag-, and Cu-Based Dilute Alloys Reviewed in Section 3**

(a) CO oxidation (Section 3.2)

$$CO + \tfrac{1}{2}O_2 \longrightarrow CO_2$$

(b) Oxidative self-coupling (Section 3.2)

$$2\,R\text{-}CH_2\text{-}OH \longrightarrow R\text{-}\underset{H_2}{C}\text{-}O\text{-}\overset{O}{\overset{\|}{C}}\text{-}R$$

(c) Anhydrous aldehyde production (Section 3.3)

$$R\text{-}CH_2\text{-}OH \longrightarrow R\text{-}\overset{O}{\overset{\|}{C}}\text{-}H + H_2$$

(d) Selective hydrogenation of alkynes (Section 3.4)

$$R\text{-}C{\equiv}C\text{-}H + H_2 \longrightarrow R\text{-}\underset{H}{\overset{H}{C}}{=}\underset{H}{\overset{H}{C}}\text{-}H$$

## 3.2. Oxidation Reactions on Au-Based Materials

**3.2.1. CO Oxidation.** The catalytic converter is a critical technology in automotive emission control for reducing air pollution to meet air-quality regulations. The oxidation of CO is also often used as a prototype reaction to understand key steps in oxidation reactions. The general reaction mechanism of CO oxidation involves $O_2$ activation followed by the removal of adsorbed O by CO to produce $CO_2$. Hence, this process probes the efficacy of the critical $O_2$ activation step and provides insight into catalyst stability. Using CO oxidation as a probe reaction, it can provide insights into the catalytically optimal composition and structure of catalyst design that leads to enhanced activity, selectivity, and stability.

*3.2.1.1. CO Oxidation over Supported Au-Based Materials.* CO oxidation over supported Au-based materials has been studied extensively, starting with the discovery of high activity at or below room temperature over monometallic Au.[115] The CO oxidation activity correlates with the Au NP size,[115] the metal oxidation state,[116] and the choice of oxide support.[117,118] For instance, the earliest report has pointed to the interface between Au and the $TiO_2$ support as the active site for $O_2$ activation in CO oxidation based on comparing the catalytic behavior under different pretreatment conditions.[115,117] In this case, the turnover frequency increases as the Au particle size decreases, with 3.5 nm being the optimum size for CO oxidation.[115] The optimum Au cluster size was also confirmed by surface science studies of different thickness of Au on $TiO_2(110)$.[119] The structure sensitivity is the result of quantum size effect, where islands with two-atom-thick Au clusters are most effective for catalyzing CO oxidation.[119]

Microscopy study has revealed the unique Au bilayer (BL) nanoclusters that contain ~10 Au atoms to be the origin of CO oxidation activity in $FeO_x$-supported Au catalysts.[120] The presence of both metallic and cationic Au in MgO-supported catalysts reported based on spectroscopy evidence directs the catalytic activity, with CO acting as both a reactant and a reducing agent.[116] In contrast, CO oxidation has been reported to be more facile on metallic Au than oxidized Au clusters supported on $Fe_2O_3$ and $CeO_2$ supports.[118] The $CeO_2$-supported Au catalysts treated under $H_2$ at 673 K showed a 2-fold enhancement in CO oxidation reaction rate compared to that of the pristine catalysts. This enhancement is correlated with the change in Au oxidation states probed by UV−vis, X-ray absorption near-edge structure (XANES), and XPS. In the proposed reaction pathway, weakly bound CO on metallic Au reacts with $O_2$ adsorbed on undercoordinated Au sites or $O_2$ from the support.[121]

*3.2.1.2. CO Oxidation over Support-Free Au-Based Catalysts.* Introducing a minority component to Au-based catalysts has improved the catalyst design for CO oxidation. As introduced in section 2.3, the high surface-to-volume ratio and surface curvature of hierarchical nanoporous metals make them

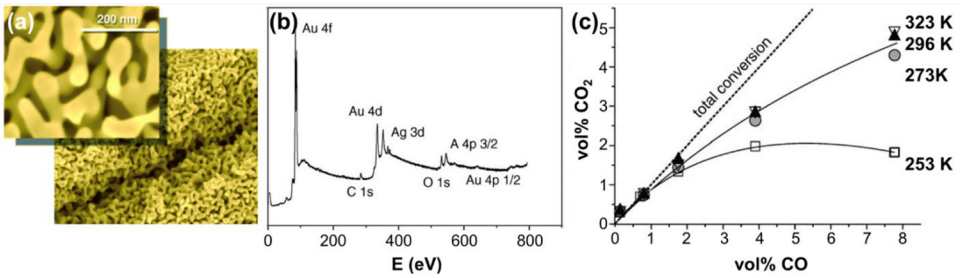


**Figure 8.** Characterization of the morphology and Ag content in npAu and its temperature-dependent CO oxidation activity. (a) SEM images of a npAu catalyst reveal a spongelike morphology consisting of ligaments with diameters on the order of several tens of nanometers and (b) corresponding XPS spectrum showing a Ag content of 4.4%. (c) Dependence of $CO_2$ concentration on CO concentration at temperature ranges between 253 and 323 K. Below 2 vol % CO, nearly total conversion to $CO_2$ is attained. Adapted with permission from ref 71. Copyright 2006 John Wiley and Sons.



https://doi.org/10.1021/acs.chemrev.1c00967
Chem. Rev. 2022, 122, 8758−8808

good candidates for catalytic studies. Minority alloy components can be present as residual from the selective corrosion dealloying process[63] or introduced after dealloying by various methods.[47,60,69,70] For example, npAu prepared by dealloying a AuAg alloy showed low-temperature CO oxidation activities similar to those of supported Au, without the contribution of Au-oxide interfaces.[21,71,122,123] The spongelike morphology of npAu consists of polycrystalline ligaments with diameters on the order of tens of nanometers (Figure 8a).[71] Based on the XPS spectrum (Figure 8b), 4.4% metallic Ag is present at the surface of the sample, where the total Ag content in the bulk is only 0.7% as determined by atomic absorption spectroscopy. High catalytic activity for CO oxidation was found in the temperature range of 273−323 K (Figure 8c). Even at 253 K, the turnover at CO concentrations up to 2 vol % is close to total conversion. Similarly, npAu containing 12% Cu prepared via leaching of ordered AuCu showed comparable activity to $Au/TiO_2$ catalysts.[72]

The low-coordination Au sites from the curved shape of ligaments in npAu adsorb CO while residual impurities (e.g., Ag or Cu) facilitate $O_2$ activation, which has been supported by both experimental observations and theoretical studies.[124] The surface structure of npAu with ∼2% of Ag predicted by theoretical calculations suggests the presence of Ag-rich step sites, and only these sites will facilitate $O_2$ dissociation (see section 3.2.3).[125] The contribution of impurities is evident by the poor activity toward CO oxidation over extremely pure npAu[122] and by varying the amount of residual Ag.[20] In situ TEM observations further reveal the stabilization of steps and kinks on the Au ligaments by residual Ag suppressing the surface reconstruction dynamics.[123,124,126] However, deactivation due to the coarsening of the porous structure often leads to reduced catalytic activity.[58,123,127] The faceting and coarsening of the nanopores after exposure to reaction gas mixture observed via environmental high-resolution transmission electron microscopy (HRTEM) is the result of increased mobility of the Au-containing species.[127] Introducing oxides onto npAu is an efficient way to improve the thermal stability of porous materials and improve CO oxidation activity.[20,58] For instance, depositing a thin $TiO_2$ layer via atomic layer deposition followed by annealing at high temperature demonstrates improved CO oxidation activity compared to uncoated npAu.[58]

Because of the nanostructured nature of npAu, reactants may be hindered from accessing regions deep inside the material. By combining npAu structures measured with STM, lattice−Boltzmann fluid dynamics simulations, and DFT-based thermodynamic predictions, it was shown that this hindrance can have significant consequences for the surface structure and reactivity of npAu.[128] Specifically, $O_2$ partial pressures can be quite low for internal regions of npAu, leading to a lack of Ag at the surface and a consequent lack of catalytic activity for oxidation reactions. Hence, npAu samples are often crushed into fine powders for reactor studies to avoid these transport limitations. As the temperature increases, Ag is predicted to increasingly prefer the subsurface or bulk, consistent with studies that show that high temperatures can lead to lower activity for AgAu alloys.[129,130]

The pretreatment condition of npAu can also affect its CO oxidation activity. For instance, npAu can be activated via reactant gases (CO and $O_2$) at ∼348 K for CO oxidation but remains inactive after $O_3$ treatment.[55] No $CO_2$ production was observed under standard operation conditions over $O_3$-activated npAu catalysts. On the other hand, $O_3$ activates npAu for oxygen-assisted alcohol coupling by removing carbonaceous residuals resulting from synthesis and thus increases accessible surface area. As a result, the activity and selectivity for alcohol coupling are different for $O_3$-activated materials. Therefore, it is important to understand adsorbate-triggered dynamic changes of morphology and surface composition, which will be discussed further in section 4.2.

*3.2.1.3. CO Oxidation over Supported Au-Based Catalysts.* Alloying Pd with Au to increase $O_2$ dissociation activity and improve catalyst stability has been shown as an efficient catalyst design for CO oxidation.[131,132] Higher turnover rates were observed for PdAu NPs at 473 K compared to those of the parent monometallic NPs, where high Pd content was present (25−75%).[133] The enhanced CO oxidation activity was attributed to the charge transfer between Pd and Au due to alloying based on CO diffuse reflectance infrared Fourier transform spectroscopy (DRIFTS) and XPS studies.[131] However, the same electronic effect was also reported to have little effect on CO oxidation in PdAu alloys with lower Pd content.[134] The CO oxidation activity is also affected by the Pd cluster size in PdAu NPs.[81] By exploring different Au/Pd molar ratios in PdAu alloys, it was shown that only contiguous Pd atoms are capable of catalyzing CO oxidation whereas isolated Pd atoms are not.

Other studies reveal the correlation between Pd surface segregation with CO oxidation activity. Pd preferentially segregates to the surface of PdAu NPs due to a stronger binding to CO under reaction conditions.[134−136] This was demonstrated by a combined X-ray absorption fine structure (XAFS)/DRIFTS approach to characterize the restructuring.[135] The pristine catalysts exhibit surface PdO islands, which are reduced to metallic Pd under reaction conditions and followed by the formation of a Pd-rich shell. A similar restructuring was observed in Pd-doped Au nanoclusters supported on $TiO_2$, where Pd migration from the core to the surface was supported by operando DRIFTS spectroscopy.[136] This is consistent with surface science studies of PdAu bimetallic model catalysts, where at elevated CO pressure, Pd segregates to the surface and forms contiguous Pd sites to catalyze CO oxidation.[137] The PdAu alloy shows superior reactivity compared with monometallic Pd as a result of reduced CO inhibition. The structural changes were supported by in situ polarization-modulation infrared reflection absorption spectroscopy (PM-IRAS) studies during CO oxidation conditions.[137]

Despite the success in introducing Pd to Au to increase $O_2$ dissociation activity for CO oxidation, there are limited reports on PdAu with low Pd concentration. As described in section 2.4, the recent development of RCT materials improves the thermal stability of NPs by embedding them in an interconnected 3D microporous $MO_x$ support. The tunability in the composition, size, and loading of metallic NPs as well as the $MO_x$ support composition, phase, and microporosity offer opportunities for the design of dilute alloy catalysts. $Pd_xAu_{1-x}$ RCT-$SiO_2$ catalysts with low Pd concentrations (<10 atomic %) activate $O_2$ and catalyze CO oxidation with long-term stability via atomically distributed Pd atoms at the surface.[105] CO oxidation was chosen here as a probe reaction to provide insights into the catalytically optimal composition and structure of catalyst design that leads to enhanced CO oxidation activity. The apparent activation energies observed for PdAu ($Pd_{0.02}Au_{0.98}$ and $Pd_{0.09}Au_{0.91}$) RCT-$SiO_2$ catalysts


https://doi.org/10.1021/acs.chemrev.1c00967
Chem. Rev. 2022, 122, 8758−8808

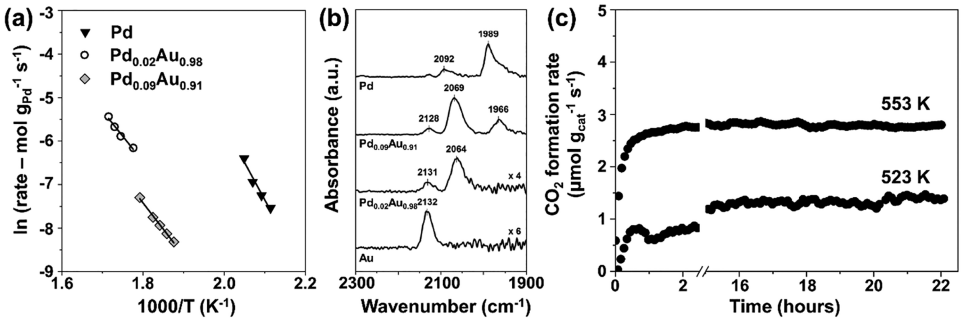


**Figure 9.** Catalytic performance of $Pd_xAu_{1-x}$ RCT-$SiO_2$ catalysts for CO oxidation and the characterization of its surface Pd distribution. (a) Apparent activation energies for Pd, $Pd_{0.02}Au_{0.98}$, and $Pd_{0.09}Au_{0.91}$ RCT-$SiO_2$. (b) CO-DRIFTS spectra of Au, $Pd_{0.02}Au_{0.98}$, $Pd_{0.09}Au_{0.91}$, and Pd RCT-$SiO_2$ after reduction at 523 K for 1 h and exposure to CO for 20 min at room temperature. (c) Time-on-stream measurements for CO oxidation over $Pd_{0.09}Au_{0.91}$ RCT-$SiO_2$. Adapted from ref 105. Copyright 2019 American Chemical Society.

are close to those observed for pure Pd, and thus the reaction on Pd sites appears to drive the kinetics for the oxidation of CO (Figure 9a). Pd K-edge EXAFS data indicate that Pd distribution within the Au host for $Pd_{0.09}Au_{0.91}$ is mostly uniform with $N_{PdAu}$ = 12.0 ± 0.9. However, it is difficult to obtain the $N_{AuPd}$ values because Au−Au contribution dominates the Au $L_3$-edge EXAFS data, especially for low Pd concentration ($Pd_{0.02}Au_{0.98}$). This limitation is common for analyzing the EXAFS of dilute metal component, which has inspired the development of a ML-aided analysis method (see section 5.2.3). Minor amounts of Pd atoms are stabilized on the surface by interaction with CO and varies with the bulk concentration. Based on CO-DRIFTS measurements (Figure 9b) correlated with DFT-calculated CO adsorption structures, it was concluded that atomically distributed Pd exists at the surface of $Pd_{0.02}Au_{0.98}$ RCT-$SiO_2$ after CO exposure, while both isolated and clustered Pd appear to be present in $Pd_{0.09}Au_{0.91}$ RCT-$SiO_2$. No deactivation was observed for $Pd_{0.09}Au_{0.91}$ RCT-$SiO_2$ catalysts for more than 20 h under CO oxidation reaction conditions at 523 K (Figure 9c). The resistance to sintering is the result of NPs partially anchored in the matrix as well as the RCT architecture of the $MO_x$ support.[138]

*3.2.1.4. Reaction Pathway over Reducible Oxide Supports: Mars−van Krevelen.* An alternative reaction pathway of CO oxidation proceeds via the Mars−van Krevelen mechanism,[139] which involves the release of lattice oxygen from reducible oxide supports during oxidation reaction to generate oxygen vacancies, which are then filled by molecular oxygen. The mobility of lattice oxygen in the oxide support has a positive effect on the CO oxidation activity of Au and Pd catalysts.[140−143] Similarly, the surface lattice oxygen at the perimeter of Au NPs supported on $TiO_2$ serves as the active oxygen species to react with CO and is later replenished by gas-phase $O_2$. This is demonstrated in both temporal analysis of products (TAP) reactor measurements and microreactors operated at atmospheric pressure.[144,145] A Mars−van Krevelen-type mechanism has also been reported for single-atom Au catalysts supported on reducible oxides, including $Au_1/FeO_x$ and $Au_1/CeO_2$.[146,147] Adsorption of $O_2$ on an oxygen vacancy near the single-atom catalyst forms an intermediate with CO, which facilitates $O_2$ dissociation and improves CO oxidation activity. On the contrary, single-atom $Pd_1/CeO_2$ goes through a Langmuir−Hinshelwood-type mechanism, where the reaction only proceeds when CO and $O_2$ are coadsorbed.[148] In this case, single Pd atoms stabilized in the form of PdO and $PdO_2$ give very low activation barriers for CO oxidation, where metallic Pd is inactive due to CO poisoning.

**3.2.2. Alcohol Oxidation.** Au-based catalysts have been shown to be highly selective for oxygen-assisted self-and cross-coupling of alcohols, as well as cross-coupling of amines with alcohols or aldehydes. Although Au surfaces are active for selective oxidation reactions, pure Au does not activate molecular $O_2$ efficiently. This could be improved via the addition of a dopant metal to facilitate $O_2$ dissociation or with the presence of a $MO_x$ support. The general mechanism for oxidative coupling of alcohols involves the activation of the O−H bond in the alcohol by adsorbed atomic oxygen to form an adsorbed alkoxy intermediate and the subsequent C−H bond activation to yield an aldehyde, which reacts further with the adsorbed alkoxy. Fundamental understanding of these processes provides an insight into optimizing the cross-coupling selectivity/yield on Au-based catalysts.

*3.2.2.1. Alcohol Oxidation Mechanism.* A major inspiration for the work described in this review originated from the discovery that O atoms adsorbed on the surfaces of Cu, Ag, and Au promote novel, selective reactions of gas-phase acids, meaning molecules with reasonably acidic C−H, N−H, or O−H bonds.[19] These unique, single atom O sites behave as a Brønsted base and extract acidic protons from such molecules to create the conjugate base of the acid bound to the surface (Scheme 2). Typical examples are the creation of adsorbed alkoxy from alcohols, adsorbed amides from amines, and adsorbed alkylidynes from alkynes. Because neither Cu, Ag, nor Au is otherwise particularly reactive, these molecules are initially selectively activated by the adsorbed O atom via reactions with low-energy barriers.[149] Further, due to the limited reactivity of these surfaces, the surface-bound intermediates typically react selectively by C−H bond cleavage from the carbon atom adjacent to the atom bound to the surface (e.g., the O, N, or C originally bound the acidic H) and selectively yield dehydrogenation products, such as aldehydes or imines.

To make matters even more interesting, these surface-bound intermediates are themselves nucleophilic because they bear a negative charge at the O, N, or C atom. Consequently, they readily attack electron-deficient centers, such as the carbonyl carbon of the coadsorbed aldehydes or imines that formed, leading to coupling and cross-coupling reactions that can be utilized to produce mono- or mixed esters (from mixed alcohols) and amides (from alcohols and amines) (Scheme 2).[19] These coupling reactions are indeed fascinating, but


https://doi.org/10.1021/acs.chemrev.1c00967
Chem. Rev. 2022, 122, 8758−8808

**Scheme 2. Elementary Steps in the Catalytic Cycle for Oxygen-Assisted Self-Coupling Methanol to Methyl Formate**[a]

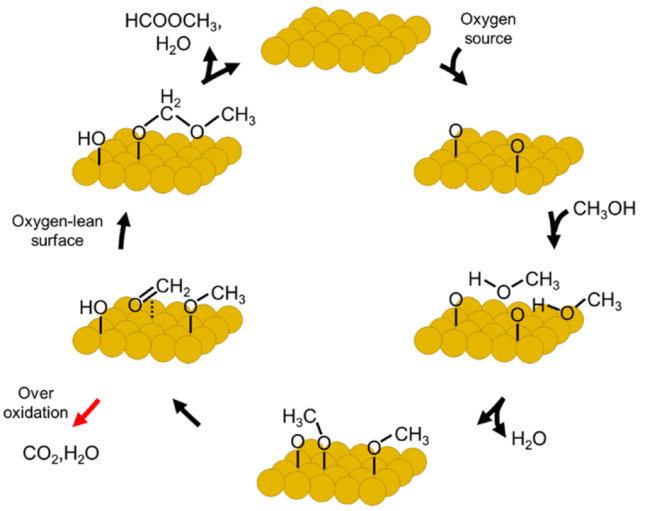


[a]Adsorbed oxygen atoms initiate the reaction cycle, which is propagated by dehydrogenation of adsorbed methoxy and the nucleophilic reaction between formaldehyde and methoxy to form the adsorbed hemiacetal alcoholate. Reprinted with permission from ref 150. Copyright 2021 Elsevier, Inc.

because Au does not dissociate $O_2$, they cannot be effectively carried out catalytically with pure Au catalysts. Moreover, for other reasons, neither Cu nor Ag is suitable for selective production of these coupled products. Thus, a catalytic material that preserves the selectivity of pure Au but provides adsorbed atomic O is ideal for promoting these oxidative coupling reactions.

*3.2.2.2. Alcohol Oxidation over Support-Free Au-Based Materials.* As described previously in this review (section 2.3), npAu is produced by leaching excess Ag from a bulk AuAg alloy. The process results in the inclusion of a low percentage of Ag in the npAu. Although the ability of pure Ag to activate $O_2$ is low, it is *finite*, so the possibility of creating atomic oxygen on the surfaces of npAu at high pressures of $O_2$ appeared possible.

In a breakout experiment, pursuant to the principles described in section 3.2.2.1, npAu was shown to produce methyl formate in a flowing stream of methanol and $O_2$ below 373 K with 60% conversion and above 90% selectivity.[73] The activation of $O_2$ was attributed to the presence of Ag,[125] and the selectivity was assigned to the surface chemistry of Au (Scheme 1). The hypothesis was then born that one could, in principle, use a binary combination of metal atoms to effect selective reactions, where the more reactive metal atom activates one key reactant and the selective reactions followed on the less reactive metal.

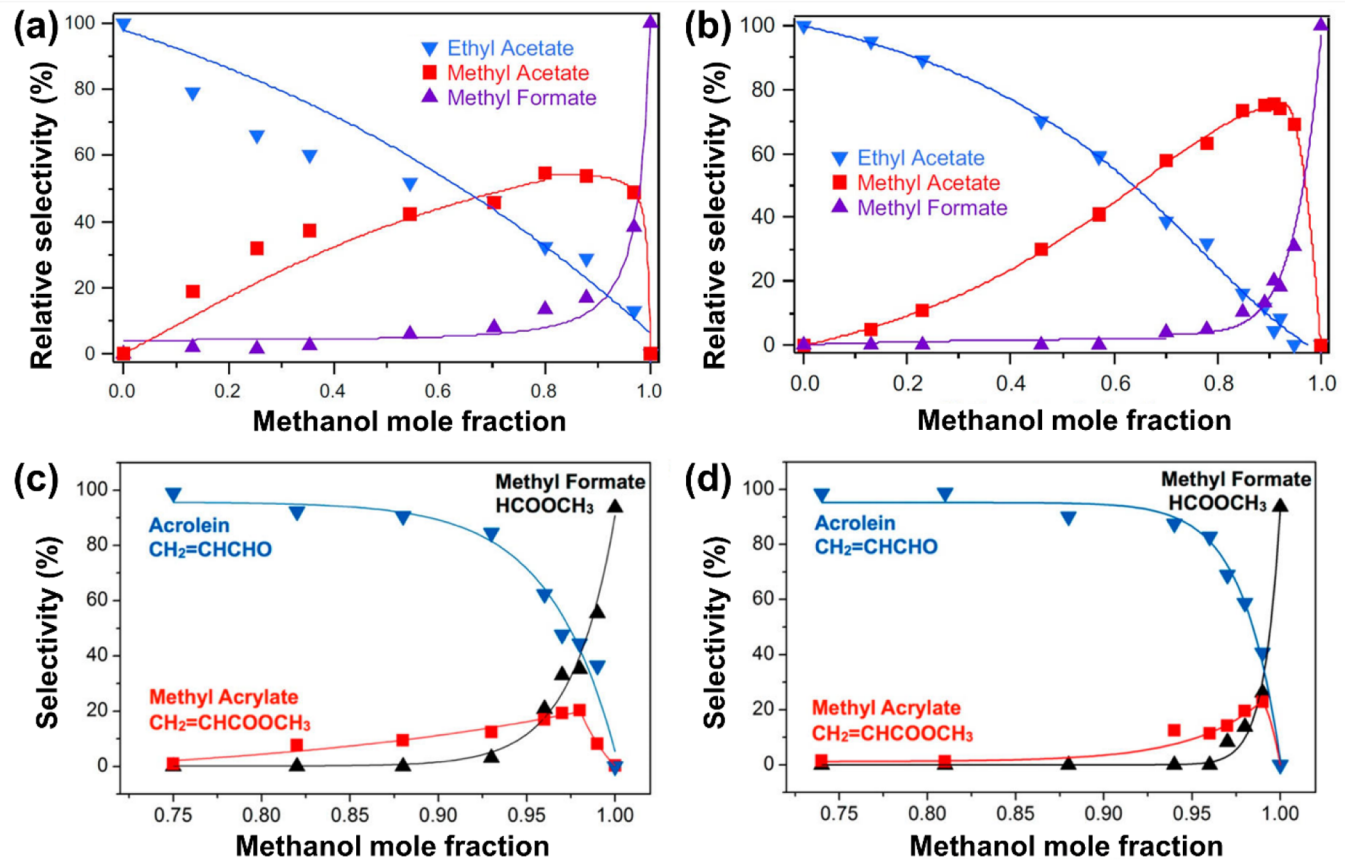


**Figure 10.** Selectivity of the products of oxygen-assisted cross-coupling of alcohols on Au varies asymmetrically with the concentrations of the reactants. The distribution of esters formed by oxygen-assisted reactions of methanol with ethanol (a,b) and allyl alcohol (c,d) on Au(110) (a,c) and under flow reactor conditions (b,d). The optimal concentration for cross-coupling to form the mixed ester greatly exceeds equimolar level due to the greater stability of the adsorbed alkoxy of the higher molecular weight species. Adapted with permission from refs (a,b) 77 and (c,d) 78. Copyrights 2015 Elsevier Inc. and 2016 American Chemical Society.


https://doi.org/10.1021/acs.chemrev.1c00967
Chem. Rev. 2022, 122, 8758−8808

Table 3. Reaction Rates over the $Pd_{0.03}Au_{0.97}$ RCT-$SiO_2$,[150] $Ag_{0.1}Au_{0.9}$ RCT-$SiO_2$, and $npAg_{0.03}Au_{0.97}$[31] under Oxidative Reaction Conditions[a]

| | | | consumption rate of $CH_3OH$ | | production rate of $HCOOCH_3$ | |
|---|---|---|---|---|---|---|
| catalysts | $HCOOCH_3$ distribution (%) | selectivity to $HCOOCH_3$ (%) | ($\mu$mol $mg^{-1}$ $s^{-1}$) | ($\mu$mol $mg_{minority}^{-1}$ $s^{-1}$) | ($\mu$mol $mg^{-1}$ $s^{-1}$) | ($\mu$mol $mg_{minority}^{-1}$ $s^{-1}$) |
| $Pd_{0.03}Au_{0.97}$ | 55.5 | 71.4 | 0.54 | 29 | 0.19 | 10 |
| $Ag_{0.1}Au_{0.9}$ | 90.0 | 94.7 | 0.23 | 3.9 | 0.11 | 1.8 |
| $npAg_{0.03}Au_{0.97}$ | 98.0 | 99.0 | 0.06 | 3.3 | 0.03 | 1.6 |

[a]Conversion of methanol ($CH_3OH$) and selectivity to methyl formate ($HCOOCH_3$) over the $Pd_{0.03}Au_{0.97}$ RCT-$SiO_2$ catalyst was found to be 94.2 and 71.4%, respectively. Reaction conditions: 6% methanol, 20% $O_2$, balanced in He, 50 sccm total, at 423 K.

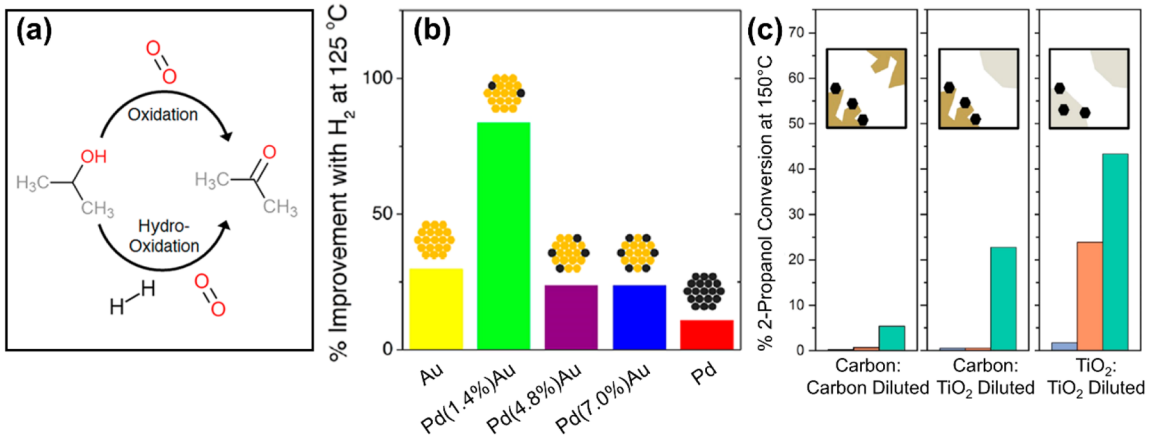


**Figure 11.** (a) Oxidation pathways of 2-propanol to acetone with reaction conditions involving only $O_2$ (oxidation, top path) or a combination of $H_2$ and $O_2$ (hydro-oxidation, bottom path). (b) Comparison of percent improvement in acetone yield between hydro-oxidation and oxidation conditions at 398 K over $TiO_2$-supported catalysts. (c) Comparison of 2-propanol conversion over catalysts containing no particles (blue), Au NPs (orange), and $Pd_{0.15}Au_{0.85}$ NPs (green) on different supports at 423 K. Adapted from refs (a,b) 9 and (c) 30. Copyrights 2018 and 2020 American Chemical Society.

Subsequently, a variety of oxygen-assisted coupling and cross-coupling reactions on npAu and other Au-based dilute alloy catalysts were studied in catalytic flow reactors[76−78] and on single-crystal Au surfaces and shown to form coupled products with high selectivity. For example, the oxygen-assisted reaction of mixtures of methanol and ethanol on the single-crystal Au surfaces show preferential self-coupling of the ethanol at low concentration of methanol, progressing to increasing amounts of cross-coupling as the methanol concentration in the reactant mixture is increased (Figure 10a). The veritable absence of methyl formate in even a modest excess of the higher molecular weight species is due to the significantly higher thermal stability of the ethoxy intermediate than the adsorbed methoxy, so the dominant coupling pathway in the mixture is the reaction of acetaldehyde with adsorbed ethoxy (Scheme 2). An analogous pattern of reactivity is seen with coupling of methanol and allyl alcohol (Figure 10c). These patterns of selectivity were also observed for reactions of methanol and ethanol over the npAu catalyst under flow reactor conditions at 425 K (Figure 10b,d).[77] Quite notably, the optimal concentration of methanol in the reactant mixture necessary to maximize the yield of cross-coupling product is not 50%, which would be expected if the relative surface concentrations of the two alkoxy species were reflective of the relative reactant concentrations. The origin of this effect is discussed in section 3.2.3. This general pattern is typical of these types of coupling reactions catalyzed in the vapor phase.[151]

Because the extent of these coupling reactions is directly related to the rate of activation of $O_2$ by the more reactive minority metal, replacement of Ag in the binary alloy catalyst with a more reactive metal could conceivably increase the activity of the catalyst. Furthermore, in general, these nanoporous metals do not make the best use of the precious metals, as much of the Au in the nanoporous material resides in the bulk of the material. Unfortunately, supported NPs of Au tend to sinter under reaction conditions, and, as dilute alloys of Au are needed for these reactions, they would be expected to sinter, as well. In order to avoid this issue, supported, dilute binary alloy NP catalysts were synthesized using a special templating procedure, as reviewed in section 2.4.

*3.2.2.3. Alcohol Oxidation over Supported Au-Based Materials.* More recently, $Ag_xAu_{1-x}$ and $Pd_xAu_{1-x}$ NPs anchored in the RCT-$SiO_2$ have been examined for methanol self-coupling.[31,150] The catalysts do not sinter appreciably even after extended use. These new catalyst architectures make significantly better use of the metal than npAgAu alloy catalysts, while retaining a clear predictive relationship between their surface reactivity with that of single-crystal Au surfaces. Furthermore, the activity of the $Pd_{0.03}Au_{0.97}$ RCT-$SiO_2$ catalyst per unit weight of active metal exceeded that of a $Ag_{0.10}Au_{0.90}$ RCT-$SiO_2$ catalyst by nearly 10-fold (Table 3). The indication is that the Pd-based catalyst is significantly more effective in activating $O_2$ than the Ag-based catalyst, thus promoting a higher turnover rate.

Dilute PdAu alloys supported on $TiO_2$ synthesized via colloidal methods have shown improved hydro-oxidation of 2-propanol to acetone (Figure 11).[9] Selective oxidation activity on Au can be enhanced under hydro-oxidation conditions,


https://doi.org/10.1021/acs.chemrev.1c00967
Chem. Rev. 2022, 122, 8758−8808

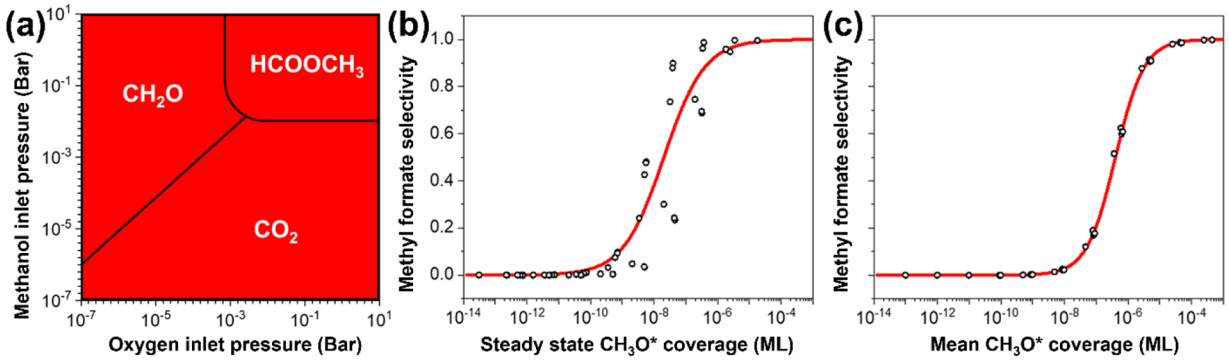


**Figure 12.** (a) Selectivity phase diagram for the methanol self-coupling reaction at 383 K, indicating the regions where either formaldehyde ($CH_2O$), methyl formate ($HCOOCH_3$), or $CO_2$ is the major product (>50% selectivity). Reactor conditions were approximately 0.1 bar of both methanol and $O_2$; the microkinetic analysis based on single-crystal source date accurately predicted reactor selectivity. (b,c) Surface concentration of adsorbed methoxy determines the selectivity for methyl formate production from the self-coupling of methanol over a wide range of reactant conditions. (b) Steady-state methoxy coverage versus selectivity to methyl formate from plug flow cofeed simulation, with $O_2$ and methanol pressures varied from $10^{-5}$ to $10^{-1}$ bar at 423 K. (c) Mean methoxy ($CH_3O^*$) coverage recorded during Knudsen pulses versus selectivity to methyl formate taken from simulation of the Knudsen pulse data with mean methanol pressure varying between $10^{-7}$ and 10 bar, with fixed oxygen coverages of $10^{-1}$ to $10^{-7}$ monolayers at 423 K. Solid red lines represent the best fit. Adapted from ref 155. Copyright 2019 American Chemical Society.

with $H_2$ assisting the formation of oxidizing species, similar to the case of propylene epoxidation.[152,153] Here, the presence of isolated Pd facilitates $H_2$ dissociation, while the Au/oxide interface promotes the formation of hydroperoxy intermediates. The formation of selective oxidizing species is probed by measuring the difference in acetone yield between oxidation and hydro-oxidation conditions (Figure 11a). The $Pd_{0.014}Au_{0.986}/TiO_2$ catalyst showed the greatest increase in activity due to its lower activity under oxidizing conditions, whereas high Pd content alloys behave similarly to pure Pd with a less active hydro-oxidation pathway (Figure 11b). A follow-up study further demonstrates the mobility of $H_2O_2$ intermediates formed under hydro-oxidation reactions and that metal PdAu NPs are capable of producing the same species without the presence of metal oxide interface (Figure 11c).[30] $PdAu/TiO_2$ catalysts remained active for hydro-oxidation of 2-propanol to acetone regardless of the choice of support, either on $TiO_2$ or carbon diluted with $TiO_2$ supports, indicating that similar reactive species are formed without the presence of metal oxide interface. In the case of $Pd_{0.15}Au_{0.85}/C$ diluted with $TiO_2$, $H_2O_2$ is generated on PdAu NPs and travels through the gas phase to $TiO_2$, where selective alcohol oxidation occurs.

A very critical issue in catalysis research is how to link the knowledge of kinetics and mechanism obtained on single-crystal surfaces with the performance of real catalysts under flow reactor conditions.[18] In principle, a direct connection can be obtained using the rate constants for each elementary step in the mechanism determined on the single-crystal model surfaces in a microkinetic model of the functioning catalyst in the reactor.[154] This connection requires that the functional state of the catalyst surface be very similar under operating conditions. Au single crystals and dilute binary alloy Au catalysts satisfy this criterion, so it is possible to use the elementary steps and rate constants determined for Scheme 2 to bridge the gap between low-pressure, single-crystal studies and the reactor performance of npAu catalysts.[155]

Most of the rate constants for the elementary steps pictured in Scheme 2 were determined in the single-crystal studies.[156,157] Two key rate constants, those for $O_2$ dissociation and for reaction of methanol with adsorbed O to form methoxy and water, were measured directly on the actual npAu catalyst with a Knudsen pulse, low-pressure technique over a temperature range that spanned the temperature used in the catalytic reactor.[158] The remainder of the rate constants could be estimated by a combination of DFT and elementary transition state theory (TST).[18] With these rate constants, it was possible to make semiquantitative predictions of both the selectivity and conversion of the npAu catalyst under reactor conditions using microkinetic analysis. Indeed, such results yielded generally correct trends in the selectivity with changes in reactant partial pressures and temperature, but quantitative agreement was not achieved.[159]

In order to attain *predictive* accuracy, the rate constants determined in the single-crystal surfaces were adjusted to fit the performance of the npAu catalyst by reacting small Knudsen pulses of methanol with O atoms preadsorbed on the npAu catalyst itself, monitoring the time evolution of products as the O was reacted away.[18] The resultant information allowed regression of the rate constants determined from the single-crystal experiments to yield an adjusted set of values for the catalytic material itself. When these regressed rate constants were used in the microkinetic analysis, excellent quantitative agreement with the conversion and selectivities observed under reactor conditions was achieved. In short, scaling of the reactivity from single-crystal studies in ultrahigh vacuum to reactor conditions at atmospheric pressure was accomplished. Further analysis revealed separated regions of reactant partial pressures favoring methyl formate, formaldehyde and $CO_2$ (Figure 12a).[155] Significantly, high selectivity to methyl formate was predicted under reactor conditions, whereas high selectivity to formaldehyde was predicted under the conditions of the low-pressure Knudsen pulse flow, in agreement with experiment. Furthermore, the analysis showed that reaction conditions which favored a high surface concentration of adsorbed methoxy was key intermediate to determining the high selectivity for methyl formate production (Figure 12b,c).

**3.2.3. Fundamental Studies of Oxidation Reactions on Au- and Cu-Based Materials.** Au-based materials can catalyze a variety of selective oxidation reactions,[160] and sections 3.2.1 and 3.2.2 have provided several examples of reactor studies of CO and alcohol oxidation reactions. As a


https://doi.org/10.1021/acs.chemrev.1c00967
Chem. Rev. 2022, 122, 8758−8808

complement to reactor studies of nanostructured catalysts, surface science and DFT studies can provide strong, fundamental insights on these reactions. The correspondence between reactor studies and fundamental studies can be particularly strong for Au-based materials because Au surfaces are relatively inert and therefore may be less crowded under reaction conditions than more reactive materials. This can allow a close correspondence in the state of the surface between fundamental studies and catalytic reactor studies.

*3.2.3.1. Fundamental Studies of the Effect of van der Waals Interactions on Intermediate Stability and Reaction Selectivity.* For oxidative coupling on Au, the highest amounts of cross-coupling products do not necessarily occur at a 1:1 molar ratio of the two reactants, as described in section 3.2.2. For example, the highest yield of the cross-coupling product between methanol and ethanol on Au(111) occurs at roughly 80% methanol and 20% ethanol, qualitatively similar to the result on npAu catalysts (Figure 10).[151] In fact, selectivity in cross-coupling reactions is controlled by surface coverage of the relevant intermediates and not by the gas-phase concentration of the reactants, and the ratio of surface coverages often differs from the gas-phase molar ratio (Figure 13),[77] due to differences in surface stability. To carefully probe

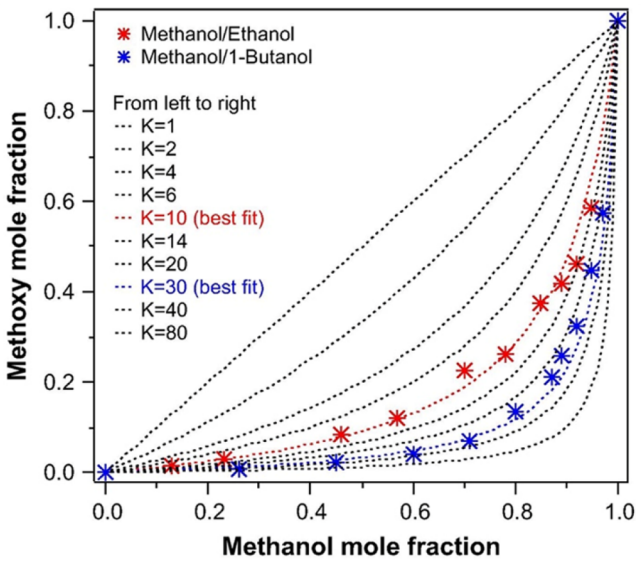


**Figure 13.** Surface coverage of methoxy as a function of the methanol mole fraction in the gas phase when Au(110) is exposed to a mixture of methanol and ethanol or 1-butanol. The points are data from experiments, and the lines represent ratios derived from different equilibrium constants. The surface coverage ratio is not the same as the gas-phase molar ratio, due to differences in surface stability between alkoxy groups. Adapted with permission from ref 77. Copyright 2015 Elsevier Inc.

the factors that control surface stability of crucial intermediates on metal surfaces, several studies measured relative stabilities using competition and displacement experiments on well-defined surfaces as well as DFT calculations, as will be discussed in the next few paragraphs. For Au surfaces, O was first dosed onto the surface at a low coverage (0.05 ML), and then two alcohol species were dosed either sequentially or together. By subsequently measuring signature desorption products, the coverage of each species can be determined. Comparison to DFT calculations allows further understanding of trends and atomic-scale details. However, a detailed, quantitative comparison of energetics can be difficult due to entropic effects, such that qualitative trends are generally the focus of comparison.

For alcohol cross-coupling on Au surfaces, the surface coverage is controlled by the stability of the alkoxy intermediates, which is influenced by van der Waals interactions. Indeed, DFT calculations that do not include van der Waals interactions predict nearly identical binding strength for most alkoxy groups, in clear disagreement with experiment.[151] When the calculations do include van der Waals interactions, the correct stability hierarchy is reproduced (Table 4). Therefore, van der Waals interactions—though

**Table 4. Experimental and Computational Binding Hierarchy on Au Surfaces[151]**

| | DFT reaction energy (eV)[b] | | | |
|---|---|---|---|---|
| experimental binding hierarchy[a] | Au(111), PBE | Au(111), PBE+vdW$^{surf}$ | Au(110), PBE | Au(110), PBE+vdW$^{surf}$ |
| methoxy | 0.18 | 0.28 | 0.18 | 0.40 |
| ethoxy | 0.21 | 0.44 | 0.21 | 0.50 |
| 1-propoxy | 0.22 | 0.55 | 0.22 | 0.58 |
| 2-propoxy | 0.21 | 0.59 | 0.21 | 0.66 |
| allyloxy | 0.22 | 0.66 | 0.24 | 0.68 |
| methallyloxy | 0.22 | 0.73 | 0.27 | 0.75 |
| benzyl alkoxy | 0.20 | 0.84 | 0.20 | 0.92 |

[a]Least stable to most stable. [b]Calculated as the negative of $2XH_{(g)} + O_{(ads)} \rightarrow 2X_{(ads)} + H_2O_{(g)}$, such that a higher absolute value is more stable.

often considered weak—can strongly influence overall catalytic selectivity.[151,161,162] van der Waals interactions can also somewhat influence the adsorption geometry of adsorbed species.[151] Based on the hierarchy of stability, it was determined that longer alkyl chains, unsaturated C=C bonds, aromatic rings, and bidentate adsorption lead to stronger binding of alkoxy groups.[151] Changing H to F in a molecule tends to make adsorption weaker or have no effect, depending on the surface structure.[162] Both experiment and theory show similar trends for Au(111) and Au(110), suggesting that there is little structure sensitivity, although absolute binding energies differ between these two surfaces.[151,162]

A combined computational and experimental study of alkoxy groups on Cu(110) found similar trends as the Au studies.[161] On Cu(110), preadsorbed O is not needed for the experiments, as alcohols are activated at defect sites. Similar to the Au surfaces, on Cu(110), van der Waals interactions are crucial in controlling the relative stability of alkoxy groups, and on both Au and Cu surfaces, each $CH_2$ group adds roughly 0.1 eV of stability.

For carboxylates on Au, adsorbate−surface van der Waals interactions are not as important. There is some stabilization of longer alkyl chains, but the effect is small.[163] Instead, stability depends on the group that binds to the surface and adsorbate−adsorbate interactions.[163] Specifically, carboxylates form dense islands on Au(110), which lifts the 1 × 2 reconstruction that occurs on pristine Au(110).[163,164] In these islands, adsorbate−adsorbate van der Waals interactions increasingly stabilize larger carboxylates. Indeed, DFT calculations of isolated carboxylates without van der Waals interactions do not obtain the correct stability hierarchy, but calculations of close-packed


https://doi.org/10.1021/acs.chemrev.1c00967
Chem. Rev. 2022, 122, 8758−8808

molecules that include van der Waals interactions reproduce most of the experimental trends.

For some sets of homologous molecules, gas-phase acidities correlate with binding strengths, likely because polarizability correlates with the gas-phase acidity and the strength of van der Waals interactions.[151,163] This can provide a simple, useful predictor for binding strength in these cases. However, the correlation between acidity and binding can break down when considering a wider array of molecules altogether.[162] For example, this correlation does not hold when considering molecules where H has been replaced with F.[163]

Even for small molecules like $CO_2$, van der Waals interactions can be important. DFT calculations that do not include van der Waals interactions predict that $CO_2$ has an adsorption energy of approximately 0 eV on Cu(111), at variance with TPD experiments suggest an adsorption energy of approximately 0.25 eV (Figure 14).[165] DFT calculations that include van der Waals interactions predict an adsorption energy similar to that found from TPD, with particularly close agreement for PBE-D2 and optB86b-vdW. More generally, different methods for correcting DFT calculations for van der Waals interactions can give fairly different energetics.[166]

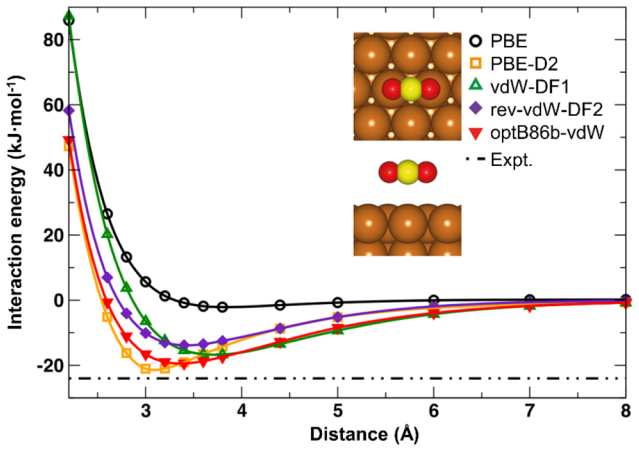


**Figure 14.** DFT-calculated interaction energy of $CO_2$ on Cu(111) as a function of the surface-molecule distance using different functionals. The experimentally derived adsorption energy from TPD is shown as the dot-dash line. Adapted with permission from ref 165. Copyright 2017 American Institute of Physics.

While van der Waals interactions will have the largest fractional contribution to adsorption on more inert metals, such as coinage metals, these interactions can still be critical on more reactive metals. For example, DFT calculations suggest that van der Waals interactions can be important for formic acid dehydrogenation on Pt(111).[167,168] DFT calculations also suggest that van der Waals interactions can have significantly different effects on different reaction pathways—specifically, O−H versus C−H bond breaking in methanol.[169] However, careful comparison using many functionals suggests that this is an artifact of optimized van der Waals functionals.[168]

In addition to the extended surfaces discussed above, van der Waals interactions have also been studied on small clusters. Propene adsorption has been studied on pure and Y-doped Au clusters with 9 to 15 atoms, where the van der Waals interactions ranged from 0.08 to 0.22 eV without a clear dependence on the size of the cluster.[167] This contribution is somewhat smaller than what has been observed for similarly sized molecules on extended Au surfaces. Whether this is due to the binding through the double bond or the small cluster size is unclear as of yet.

Therefore, van der Waals interactions can play a crucial role in catalytic reactions, especially for cases that involve chemically similar species of varying sizes. Related work in other fields, such as tribology, has also highlighted the importance of van der Waals interactions.[166,170,171]

*3.2.3.2. Fundamental Studies of the Surface Structure and Active Site of Au-Based Materials.* Metallic Au cannot dissociate $O_2$ except under extreme conditions;[172] however, Au-based materials can be effective oxidation catalysts using $O_2$. As discussed in section 3.2.2, npAu can catalyze methanol oxidative coupling with high activity and 100% selectivity.[73] Reactor studies suggest that residual Ag (typically 1−3%) in the material[62,74,127] and the step sites on the surface may be important,[127] but the specific role of each in $O_2$ dissociation, and the structure of the active site, is difficult to elucidate using reactor studies of nanostructured materials. Therefore, fundamental studies have been performed to gain some insight into the active site for $O_2$ dissociation on AgAu alloys such as npAgAu. Studies on stepped pure Au surfaces were also performed to specifically show the role of the surface structure.

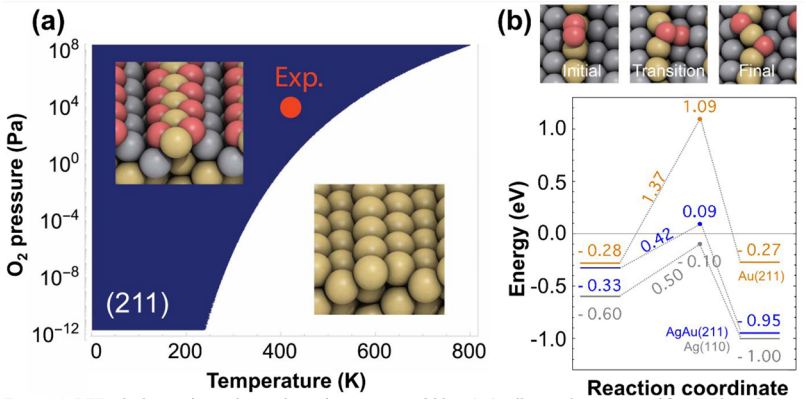


**Figure 15.** DFT calculations for predicting the surface structure of dilute AgAu alloys in the presence of $O_2$. (a) Phase diagram of the surface structure of dilute AgAu alloys for the (211) facet. The red dot marks typical experimental conditions for catalytic studies on npAgAu. (b) $O_2$ dissociation pathway and energetics on the thermodynamically stable AgAu(211) structure, compared to Au(211) and Ag(110). Adapted from ref 125. Copyright 2016 American Chemical Society.



https://doi.org/10.1021/acs.chemrev.1c00967
Chem. Rev. 2022, 122, 8758−8808

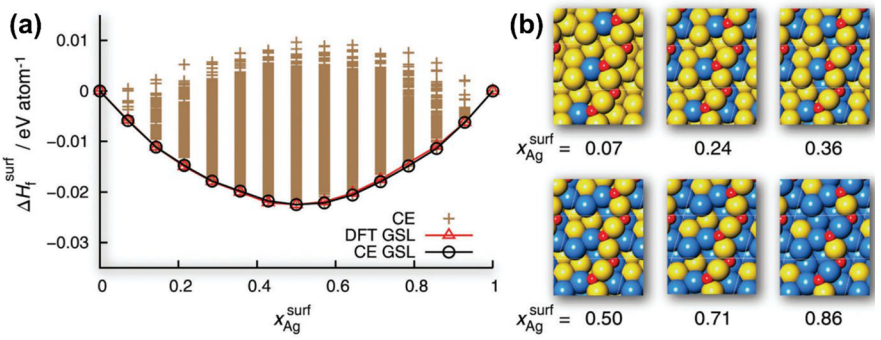


**Figure 16.** (a) Surface stability of many AgAu(321) structures at different Ag concentrations. (b) Most stable structures at several different Ag concentrations. Adapted with permission from ref 176. Copyright 2016 Royal Society of Chemistry.

To shed light onto the nature of the active site for $O_2$ dissociation on dilute AgAu alloys, DFT-based thermodynamic studies were performed to predict the surface structure of dilute AgAu alloys in the presence of $O_2$.[125] These studies predicted that terraces are Au-terminated, with Ag in the subsurface. In contrast, step sites are predicted to have Ag at the surface—specifically, the atoms next to the step atoms are predicted to be Ag, whereas all other atoms are Au (Figure 15a). These AgAu step sites have a low $O_2$ dissociation barrier (Figure 15b), in qualitative agreement with the experimentally measured barrier on npAu.[158] Subsequent experimental studies have supported the finding that reaction conditions induce Ag segregation to the surface[173] and have shown that adding Ag to Au(111) results in no oxidation activity, but adding Ag to curved Au surfaces with steps results in activity.[174] DFT studies also suggest that subsequent oxidation steps after $O_2$ dissociation occur on or near step sites, primarily because O spillover onto pure Au terraces is unfavorable.[175]

Comprehensive computational studies employing DFT, cluster expansion, and ab initio MD have found similar conclusions for AgAu(321) as were found for AgAu(211).[176] Without O, the surface is predicted to be pure Au. Adsorbed O forms zigzag chains, and when these chains are present, the most stable surface structures generally have Ag in the surface next to the step atoms, whereas the step atoms typically remain Au (Figure 16).

A crucial difference between steps and terraces for Au-based materials is the structure and energetics of adsorbed O. On terraces at low and moderate coverage, O occupies face-centered cubic (fcc) hollow sites, and O−O interactions are generally repulsive. On step sites, O forms zigzag chains, with attractive interactions between the O atoms. These chains have been observed directly using STM on Au(110)[177] and Au(511).[178] On Au(110), which exhibits a missing-row reconstruction, oxidation happens preferentially along the step direction, and the reaction rate increases significantly at a low overall O coverage.[179] Both of these effects are due to the specific structure and stability of O chains, including strain effects. The more strongly bound and more tightly packed O at steps also stabilizes Ag there based on DFT calculations.[125] As a more extreme example of oxygen-induced segregation, a $Ag_{0.7}Au_{0.3}$ alloy exposed to $O_3$ results in dramatic Ag segregation, leaving a Ag-depleted nanoporous region.[180]

When the major findings are taken together, there appears to be an interplay for AgAu oxidation catalysts under steady-state conditions: surface O is needed to stabilize Ag on the surface, and surface Ag is needed to dissociate $O_2$. This appears to also require step sites.[125,181] This is consistent with catalytic studies that show that as-prepared npAu is not always active for oxidation catalysis, but samples pretreated with $O_3$ are consistently active for alcohol coupling reactions.[55]

However, there is some potentially conflicting evidence concerning the behavior of Ag in dilute AgAu alloys under various conditions. For example, transient reactor experiments find that as-prepared $npAg_{0.01}Au_{0.99}$ can dissociate $O_2$ at a limited number of localized sites, without first exposing the material to oxidizing species.[158] These sites may be metastable or may be stabilized by other species present during sample preparation. Further, some studies of $npAg_{0.03}Au_{0.97}$ suggest that Ag is present in the near-surface region under reducing conditions, although in much lower amounts than under oxidizing conditions.[62] This may indicate that Ag prefers to reside in the second layer in the absence of adsorbates, which is what DFT calculations predict, or that kinetic limitations prevent Ag from diffusing away from the near-surface region. Additionally, some work has suggested that alcohols may be able to facilitate $O_2$ dissociation such that $O_2$ activation could occur on some pure Au steps.[182] Overall, the atomically precise structure of Ag in these materials under oxidation conditions has not been directly confirmed by experiment.

Au alloys can also be used for oxidative C−C coupling, based on surface science studies.[29] Specifically, when methyl iodide is exposed to a Au(111) surface embedded with Pd, ethane is formed. DFT studies suggest that Pd atoms at undercoordinated sites on the surface are needed for the coupling to occur, again highlighting the importance of undercoordinated sites (such as step sites).

### 3.3. Anhydrous Aldehyde Production

**3.3.1. Ethanol to Acetaldehyde on Cu-Based and Au-Based Catalysts.** The current industrial process for aldehyde production from alcohols relies on oxidative dehydrogenation of the alcohols; however, the formation of water−aldehyde mixtures poses separation problems and thus reduces the energy efficiency of this process.[183,184] For non-oxidative dehydrogenation of alcohols, $H_2$ gas is produced as a byproduct and is valuable as an energy carrier. The oxygen-free condition will also suppress overoxidation to form carboxylic acids.[185] Moreover, as ethanol can be produced from biomass fermentation with increased availability and reduced cost, it serves as an alternative and renewable feedstock for the production of fine chemicals.[186,187]

*3.3.1.1. Ethanol to Acetaldehyde on Cu-Based Catalysts.* Ethanol dehydrogenation to acetaldehyde can be achieved over copper chromite ($CuO{\cdot}CuCr_2O_4$) catalysts with selectivity above 95%.[188] The reaction steps involve initial cleavage of the


https://doi.org/10.1021/acs.chemrev.1c00967
Chem. Rev. 2022, 122, 8758−8808

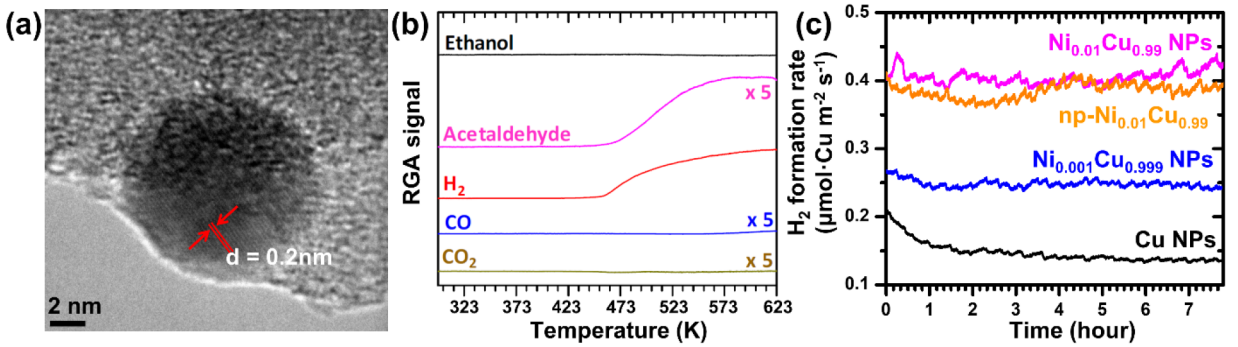


**Figure 17.** Selective non-oxidative dehydrogenation of ethanol to acetaldehyde and $H_2$ on highly dilute NiCu alloys. (a) HRTEM image of $Ni_{0.01}Cu_{0.99}$ SAAs/$SiO_2$. (b) TPRS of ethanol on $Ni_{0.01}Cu_{0.99}$ SAAs/$SiO_2$. Reaction conditions: 100 mg of catalyst, 6% ethanol balanced in He, He flow rate 10 sccm. (c) Stability tests of Cu NPs, np$Ni_{0.01}Cu_{0.99}$, and $SiO_2$-supported $Ni_xCu_{1-x}$ SAAs ($x$ = 0.001−0.01) in ethanol dehydrogenation reaction at 523 K. The reaction rates are normalized by the surface area of Cu in the catalyst. Adapted with permission from ref 47. Copyright 2017 Elsevier B.V.

O−H bond to form alkoxide and hydrogen intermediates, followed by C−H bond scission to produce an aldehyde and by hydrogen recombination to form $H_2$. This was revealed by a combination of surface science experiments and DFT calculations performed on oxygen-free, highly defective Cu surfaces.[189] Because Cu is more reactive than Ag and Au but less reactive than most other transition metals, Cu-based materials can often activate alcohols without adsorbed oxygen atoms, without decomposing or combusting them beyond the desired aldehydes. Cu supported on $SiO_2$ and $Al_2O_3$ prepared by incipient wetness impregnation showed above 85% selectivity toward acetaldehyde for the ethanol dehydrogenation reaction occurring at 473−523 K.[190,191] A mixture of $Cu^+/Cu^0$ that is formed on the catalyst surface during reduction pretreatment is proposed to be the active site, based on CO-DRIFTS analysis and time-resolved XANES studies. On the other hand, Cu supported on high surface area graphite has also shown close to 100% selectivity to acetaldehyde for ethanol dehydrogenation reaction performed at 423−573 K.[192] However, Cu-based catalysts are often unstable and tend to sinter extensively under reaction conditions.[193] More recently, a 4-fold enhancement in ethanol dehydrogenation activity with greater than 95% selectivity to acetaldehyde at 473 K over Cu NPs was closely correlated with the appearance of surface defect sites.[194] This enhancement was extended to the dehydrogenation of longer chain alcohols. The oxygen-induced surface reconstruction and roughening without altering Cu dispersion and the oxidation state was observed via in situ TEM and XAFS measurements. This is consistent with temperature-programmed reaction spectroscopy (TPRS) and STM studies that showed the step sites on a roughened Cu(111) surface are the active sites for alcohol dehydrogenation.[189] Reactor studies summarized here have shown that dehydrogenation of ethanol (or longer chain alcohols) for aldehyde formation over Cu catalysts occurs at ∼423−573 K; however, it is important to note that dehydrogenating a $C_1$ alcohol (methanol) to formaldehyde often requires a promoter or extremely high temperatures.[183] This difference is further discussed in section 3.3.2 by taking into account the effect of van der Waals interactions.

It has been demonstrated that the presence of atomically dispersed Ni in Cu-based materials could lead to 100% selectivity of acetaldehyde and $H_2$ in non-oxidative ethanol dehydrogenation while greatly suppressing catalyst sintering (Figure 17).[47,106] For instance, a low loading of Ni (0.1−3%) can be introduced to $SiO_2$-supported Cu NPs by galvanic exchange,[47] where atomically dispersed Ni appears on the near surface layer of Cu (Figure 17a). Reduction pretreatment of $Ni_{0.01}Cu_{0.99}$ SAAs/$SiO_2$ at 623 K brought Ni atoms to the subsurface, which was confirmed by the decrease in surface atomic ratio of Ni/Cu from XPS, and remained in place during reaction conditions. A nearly 100% selectivity for ethanol dehydrogenation to acetaldehyde up to 623 K was observed based on TPRS measurements over $Ni_{0.01}Cu_{0.99}$ SAAs/$SiO_2$ (Figure 17b). The catalysts are stable after 8 h in ethanol dehydrogenation reaction conditions at 523 and 573 K, whereas monometallic Cu NPs deactivate quickly (Figure 17c). This clearly demonstrates that the addition of Ni atoms into the Cu surfaces prevented the Cu NPs from coarsening.

Unsupported npNiCu materials were also compared in the study mentioned above and showed similar intrinsic catalytic activity to the $Ni_{0.01}Cu_{0.99}$ SAAs/$SiO_2$. The rate-limiting step for ethanol dehydrogenation over dilute NiCu catalysts has been identified as a C−H bond cleavage step via in situ DRIFTS observations of ethoxy and acetaldehyde species, which is the same as the rate-limiting step on pure npCu.[106] The reaction mechanism is also consistent with surface science experiments and DFT calculations performed on Cu step sites (section 3.3.2). In the current study, isolated Ni atoms lower the activation barrier for C−H bond scission and thus promote ethanol dehydrogenation. The high activity and near-100% selectivity of np$Ni_{0.01}Cu_{0.99}$ are independent of catalyst pretreatment conditions ($O_2$ or $H_2$).[69] However, $H_2$-treated np$Ni_{0.01}Cu_{0.99}$ suffers from deactivation within ∼40 h on stream as a result of the formation of Ni-rich metallic particles on the surface under reduction conditions and carbon deposition during ethanol exposure. In contrast, $O_2$ treatment stabilizes the catalyst by keeping it in a metastable $Ni^{2+}$ state covered by a surface overlayer of copper oxide, where most of the Ni is trapped in its oxidized state and thus improves long-term stability. A more recent example of ethanol dehydrogenation over NiCu dilute alloy catalysts with 0.04−0.18% of Ni is to drive the reaction by focused solar light and achieve a high solar-to-fuel conversion efficiency as a result of the synergistic effects of photothermal heating and hot carrier generation through the excitation of surface plasmon resonance of Cu followed by migration to Ni atoms.[89]


https://doi.org/10.1021/acs.chemrev.1c00967
Chem. Rev. 2022, 122, 8758−8808

Other minority metals have also shown a positive impact on the ethanol dehydrogenation performance. For instance, the presence of isolated Pd and Pt in $Pd_{0.01}Cu_{0.99}$ and $Pt_{0.01}Cu_{0.99}$ SAAs/$SiO_2$ lowers the reaction barrier for hydrogen atom recombination and desorption but has a negligible promotion effect on its activity compared with monometallic Cu NPs based on DRIFTS measurements. This is different from $Ni_{0.01}Cu_{0.99}$ SAAs/$SiO_2$, where the addition of Ni improves the reactivity of Cu.[106] Comparing the three different Cu-based SAAs discussed so far, the trend in apparent activation energy for Cu-based SAAs/$SiO_2$ decreases in the order of Pd to Pt to Ni (Figure 18). The role of Pt proposed for $Pt_{0.01}Cu_{0.99}$ SAAs/

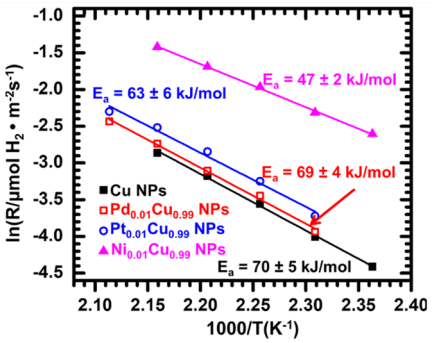


**Figure 18.** Comparison of Cu-based SAAs with different minority metals for anhydrous acetaldehyde production. Arrhenius-type plots of the reaction rate in ethanol dehydrogenation, normalized by the surface area of Cu over metallic Cu NPs, $Pd_{0.01}Cu_{0.99}$, $Pt_{0.01}Cu_{0.99}$, and $Ni_{0.01}Cu_{0.99}$ SAAs/$SiO_2$. Adapted with permission from ref 106. Copyright 2018 Elsevier B.V.

$SiO_2$ is in good agreement with a separate flow reactor study based on TPRS measurements of water-catalyzed methanol dehydrogenation. Both $SiO_2$-supported $Pt_{0.01}Cu_{0.99}$ SAAs and Cu NPs are not active in methanol dehydrogenation to formaldehyde unless there is water present, and the addition of isolated Pt atoms promotes the reactivity of Cu.[107] The study of $Pt_{0.01}Cu_{0.99}$ SAAs/$SiO_2$ for alcohol dehydrogenation also suggests that ethanol dehydrogenation can proceed without the presence of water, while methanol remains inactive.[106,107] This is consistent with surface science experiments and DFT calculations, as described in section 3.3.2. With water facilitating the formation of methoxy species, it further promotes C−H bond activation and thus formaldehyde formation.

However, the minority component does not always have a significant impact on the catalytic performance. For instance, npCu prepared by different etching solutions allows control of the morphology and, more specifically, the step-edge densities. Typically, the residual impurities left behind during the dealloying process contribute to the catalytic performance, as in the case of npNiCu for ethanol dehydrogenation and npAgAu for CO oxidation.[122] However, for the ethanol dehydrogenation reaction over npZnCu occurring at 453−503 K, it was not sensitive to residual Zn amount or the nanoscale ligament morphology in npCu based on the comparison of apparent activation energies calculated under steady-state conditions.[52]

*3.3.1.2. Ethanol to Acetaldehyde on Au-Based Catalysts.* Supported Au materials have also been studied for non-oxidative dehydrogenation of ethanol to acetaldehyde. For instance, a size dependency study of Au/$SiO_2$ revealed an optimum conversion of 90% and above 95% acetaldehyde selectivity over ∼6 nm Au NPs.[195] The surface step sites are proposed to be the active sites for non-oxidative dehydrogenation, where the rate-limiting step involves C−H bond scission.[195] The activity and selectivity of $C_2$−$C_4$ alcohol dehydrogenation over Au NPs on various oxide supports showed a strong dependency on the support acidity.[185] The most promising result is with amphoteric supports, such as hydrotalcite (HT), and the activity of Au/HT increases in the order of ethanol to 1-propanol to 1-butanol, with selectivity all above 80%.[185] It was proposed that an alkoxide intermediate forms over the basic support, and the rate-limiting step involving C−H bond scission occurs over coordinately unsaturated Au sites based on kinetic isotope effect studies.[185] The presence of isolated Ni atoms in $SiO_2$-supported NiAu SAAs increases the catalyst activity for alcohol dehydrogenation while preserving the selectivity of monometallic Au, which activates O−H and C−H bonds but not the C−C bond.[60] The apparent activation energy for non-oxidative dehydrogenation of ethanol decreased from 96 ± 3 kJ/mol for $SiO_2$-supported Au NPs to 59 ± 5 kJ/mol for np$Ni_{0.001}Au_{0.999}$. Atomically dispersed Ni in $Ni_{0.005}Au_{0.995}$ SAAs/$SiO_2$ showed 100% selectivity to acetaldehyde and $H_2$, which behaves similarly to the $Ni_{0.01}Cu_{0.99}$ SAAs discussed previously. Although both catalysts showed similar catalytic performance, the active structure is different. In $Ni_{0.005}Au_{0.995}$ SAAs/$SiO_2$, the catalyst is activated by the reactant where reduction pretreatment brings Ni atoms to the subsurface and the presence of ethanol brings Ni back to the surface. This is different from $Ni_{0.01}Cu_{0.99}$ SAAs/$SiO_2$, where Ni was brought to the subsurface by catalyst pretreatment and remained there during reaction. The presence of Ni also slows down the coarsening kinetics of the NiAu catalyst, allowing for prolonged use under reaction conditions without any apparent drop in activity. The dynamic behaviors of NiCu and NiAu catalyst surfaces are further discussed in section 4.2

**3.3.2. Fundamental Studies of Anhydrous Aldehyde Production.** As a complement to the reactor studies of anhydrous aldehyde production discussed in section 3.3.1, surface science and DFT studies of well-defined model systems can bring more detailed insight into mechanisms, energetics, and the role of structure. These studies have elucidated differences between steps and terraces, the role of alloy sites, and differences between alcohols.

*3.3.2.1. Effect of Surface Structure and Alloy Sites.* Fundamental studies strongly suggest that Cu terraces are essentially inactive for alcohol dehydrogenation.[189,196] DFT studies of alcohols on Cu(111) terraces predict that alcohol desorption is favored over reaction by 0.39 eV for methanol and 0.26 eV for ethanol. Ethanol−ethanol interactions do not facilitate dehydrogenation on flat Cu(111), so higher alcohol coverages will not change this conclusion. A possible confounding factor is the fact that water can act as a cocatalyst for alcohol dehydrogenation on Cu(111) (see section 3.3.2.2), but for the experimental work described here, conditions were carefully controlled such that water has no impact on the activity.

In contrast to Cu terraces, Cu steps can be active for alcohol dehydrogenation.[189,196,197] For example, a significant fraction of methanol dosed at high coverage on Cu(210) at 100 K is converted to formaldehyde.[197] On Cu(111) single crystals, the density of active sites for alcohol activation is similar to the density of step sites. Similarly, STM studies show that step


https://doi.org/10.1021/acs.chemrev.1c00967
Chem. Rev. 2022, 122, 8758−8808

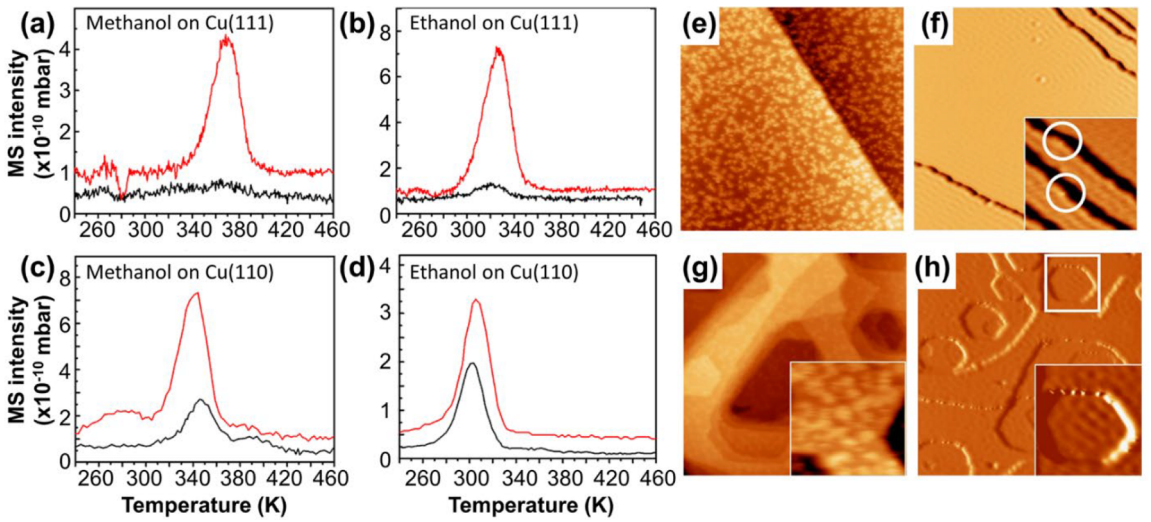


**Figure 19.** Surface structure dependence of the dry dehydrogenation of alcohols on Cu single crystals. (a–d) TPD traces of aldehyde desorption from alcohols dosed onto flat (black) and sputtered (red) Cu surfaces. Roughened surfaces produce a much greater yield of aldehydes. (a) Methanol and (b) ethanol on Cu(111), dosed at 180 K for saturation. (c) Methanol and (d) ethanol on Cu(110), dosed at 200 K for saturation. (e–h) STM images (50 nm × 50 nm) of Cu(111) surface exposed to ethanol. White circles in (f) highlight ethoxy adsorbed at Cu(111) steps. The inset in (g) shows ethanol adsorbed on a small terrace of Cu(111). The inset in (h) highlights adsorbed ethoxy intermediates on Cu steps and kinks. Adapted from ref 189. Copyright 2017 American Chemical Society.

sites on Cu(111) are the active site for alcohol dehydrogenation. Sputtering Cu(111) and Cu(110) single crystals results in activity toward alcohol dehydrogenation much higher than that observed on flatter, annealed surfaces (Figure 19).[189] These experiments showed 100% selectivity toward aldehydes and the same yields for several cycles. Cu(110) steps had higher activity than Cu(111), perhaps due to the more open structure of this surface.[189] The higher yields on sputtered surfaces are attributed to the lower initial alcohol coverages, as adsorbed clusters of alcohols do not fit as well on sputtered surfaces.

Steps are more active than terraces due to both stronger binding and lower reaction barriers. For step sites on Cu(111),[196] DFT studies show that it is more favorable for alcohols to react than desorb by roughly −0.25 to −0.5 eV. Both STM and DFT studies show that alcohols are more strongly bound at steps than terraces, with DFT calculations showing a difference of roughly −0.3 eV.[189,196] These DFT calculations also show that the O−H activation energy decreases from roughly 0.9 eV on terraces to roughly 0.5 to 0.6 eV on steps. Therefore, the alcohols are more strongly bound and have lower reaction barriers on steps. Indeed, all adsorbates in the reaction are more stable at steps than terraces. Alcohols are more stable at kink sites than step sites, but DFT calculations suggest that these sites do not facilitate reaction due to higher barriers.[189,196]

Through a combination of surface science experiments and DFT calculations, strong insight was gained into the reaction mechanism and energetics of alcohol dehydrogenation on Cu step sites. The first step is rupture of the O−H bond, while the reactivity is controlled by the subsequent C−H bond breaking step.[189] More specifically, DFT results suggest that the reaction rate is controlled by the energy difference between the adsorbed alkoxy (the most stable state) and the gas-phase aldehyde.[196] Whereas aldehyde desorption has the largest single barrier along the pathway, this step alone cannot explain the observed kinetics. Using the energy difference between the alkoxy and the aldehyde with a simple kinetic model in the Redhead formalism gives a predicted desorption temperature of roughly 350 K for desorption of acetaldehyde when ethanol is exposed to Cu(111), in good agreement with the experimental value of roughly 325 K.[189] This kinetic scheme also allowed comparison between DFT-calculated (or extrapolated) energetics and experimental desorption temperatures for several $C_1$ to $C_4$ alcohols on Cu surfaces.[196] A strong correlation was found in which the DFT tended to predict desorption temperatures around 41 K higher than the experimental values.

The DFT studies gave further insights that are not directly testable with current experiments.[196] First, van der Waals interactions and zero-point energies were found to be important for correctly calculating the energetics. Based on the DFT results, it was hypothesized that Cu(111) terraces can dehydrogenate 1-butanol and longer alcohols because they will be bound strongly enough to the surface to allow reaction. Furthermore, recombining H* to $H_2$ would force aldehydes to stay as aldehydes instead of allowing them to rehydrogenate, which would make them desorb at a lower temperature.

Introducing Pt as a minority metal that binds alcohols stronger than Cu(111) can have a positive impact on its ethanol dehydrogenation reactivity. The Pt site interacts more strongly with ethanol and lowers the barrier for O−H scission, promoting activation of the alcohol, which occurs below 160 K. Importantly, Cu sites interact more strongly with ethoxy than the Pt site, which promotes spillover of the ethoxy intermediate.[107,198] DFT calculations show that O−H bond scission is favored over ethanol desorption on the PtCu site, but desorption is favored on a Cu site.

Fundamental studies of PdAu(111) alloys for ethanol conversion have found that these alloys can also form acetaldehyde.[199,200] These studies also showed the critical importance of ensemble size. Whereas smaller Pd concentrations can produce acetaldehyde, ethanol decomposition becomes more prevalent at higher surface concentrations of Pd. DFT calculations suggest that the $Pd_2Au(111)$ surface is particularly active because reaction barriers are fairly low, but


https://doi.org/10.1021/acs.chemrev.1c00967
Chem. Rev. 2022, 122, 8758−8808

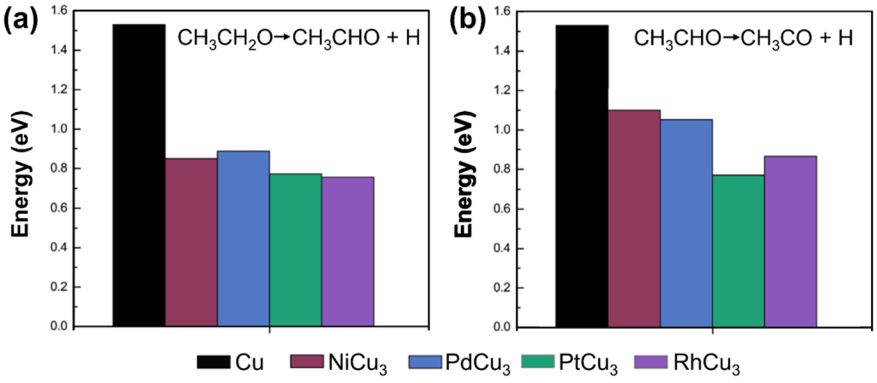


**Figure 20.** DFT-calculated activation barriers for (a) ethoxy dehydrogenation and (b) acetaldehyde dehydrogenation on the (211) facet of different Cu alloys. Reproduced with permission from ref 202. Copyright 2018 Springer New York LLC.

H and C are not too strongly bound, which leads to fast $H_2$ evolution and prevents coking.

Additionally, other Cu-, Ag-, and Au-based alloys have been suggested as effective catalysts for alcohol dehydrogenation, especially dilute alloys, based on computational studies.[201,202] Many of these alloys promote dehydrogenation of the $\alpha$ C−H bond over the O−H bond. For the (211) facet of $Cu_3M$ alloys (M = Ni, Pd, Pt, Rh), Pt and Rh were found to give the lowest dehydrogenation barriers (Figure 20), and $Cu_3Pt$ was predicted to be the most active based on microkinetic modeling.[202]

TPD and DFT studies of ethanol on Ag surfaces have also shown that adsorption is slightly stronger at steps and kinks than on terraces.[203] The measured differences for Ag are 0.03 and 0.07 eV for steps and kinks, respectively, which appear to be somewhat smaller than the differences on Cu.

*3.3.2.2. Effects of Chain Length and Adsorbate−Adsorbate Interactions.* Reactor experiments have shown that Cu catalysts can dehydrogenate ethanol to acetaldehyde at ∼473 to 573 K (section 3.3.1),[204] but dehydrogenating methanol to formaldehyde requires a promoter or extremely high temperatures.[183,205] To provide insight into this difference, DFT studies with van der Waals corrections were performed to compare dehydrogenation of $C_1$−$C_4$ alcohols on Cu(110).[206] These studies found that the initial O−H activation barrier was similar for all alcohols. However, the subsequent C−H activation barrier was found to be 0.93 eV for methoxy, much higher than the barrier of 0.55 to 0.58 eV for the other alcohols. As a result, these barriers suggest that methoxy groups prefer to re-form methanol and desorb rather than forming formaldehyde, whereas aldehyde formation is kinetically favored for longer chain alcohols. The calculated barrier for methanol is quite similar to the experimentally measured barrier of 0.91 eV, and similarly close agreement is found for the methanol adsorption energy.

Kinetic modeling confirmed that formaldehyde production is much slower than production of longer chain alcohols. The longer alcohols have similar rates, with 1-butanol having a somewhat lower rate due to stronger adsorption of butyraldehyde. Based on the kinetic model, stabilizing the transition state (TS) and/or final state for C−H bond scission should increase the rate. On Cu(111) single crystals, experiments show that ethanol dehydrogenates more easily than methanol.[189] The estimated barrier was roughly 0.1 eV lower for ethanol than for methanol, whereas DFT calculations on a stepped Cu(111) surface found a somewhat smaller difference of around 0.06 eV for the rate-controlling energy difference.[196]

Water can greatly increase the rate of anhydrous methanol dehydrogenation on Cu-based materials, such as dilute PtCu alloys.[107] At low temperature, steam reforming does not occur on these materials. Relatedly, ethanol−ethanol interactions can be stabilizing on Cu surfaces,[107,196] where ethanol−ethanol hydrogen bonding is roughly −0.3 eV on a Cu(111) terrace and roughly −0.1 eV on steps. Ethanol−ethoxy hydrogen bonding is weaker with −0.06 eV on terraces and +0.02 to +0.05 eV on steps. For an ethanol−ethoxy pair at a (111) step, a H atom is shared between the two molecules, hopping between the two O atoms approximately every 150 fs. This may have consequences for alcohol−alkoxy replacement reactions.

### 3.4. Selective Hydrogenation of Alkynes

**3.4.1. Selective Hydrogenation of Alkynes on Pd Catalysts.** Selective hydrogenation of carbon−carbon multiple bonds is a key step for purification in upgrading light alkanes via steam cracking processes as trace amounts of alkynes can be detrimental to the downstream polymerization processes.[207,208] In large-scale applications, hydrogenation of acetylene and diene impurities in alkene feedstocks is achieved via Pd-based catalysts.[209] The reaction mechanism for the hydrogenation of alkynes is often referred to as the Horiuti−Polanyi mechanism, where $H_2$ is dissociated and added sequentially to molecularly adsorbed alkyne followed by desorption of the product. Typically, the difference in the heat of adsorption of alkyne versus alkene governs the selectivity. Weakening the alkene adsorption will turn the selectivity to favor its formation while binding alkynes strongly will result in higher activity.[210] Pd is active for hydrogenation but often suffers from overhydrogenation of alkynes to alkanes, especially at high conversions. It is, however, possible to achieve selective hydrogenation of alkynes to alkenes over Pd catalysts where the population of hydrogen or carbon on the subsurface Pd sites governs the selectivity.[211−213] The catalyst support also plays a role in tuning the selectivity. For instance, carbon-supported Pd has been reported to be more selective than oxide supports toward ethylene formation for the hydrogenation of acetylene in excess ethylene, due to an increased electron density on Pd that results from the presence of Pd−C bonding as evidenced by XANES and EXAFS characterizations.[214]

**3.4.2. Alkyne Hydrogenation on Ag- and Au-Based Materials.** The addition of a second metal is another strategy to modify the electronic structure of Pd atoms and reduce the


https://doi.org/10.1021/acs.chemrev.1c00967
Chem. Rev. 2022, 122, 8758−8808

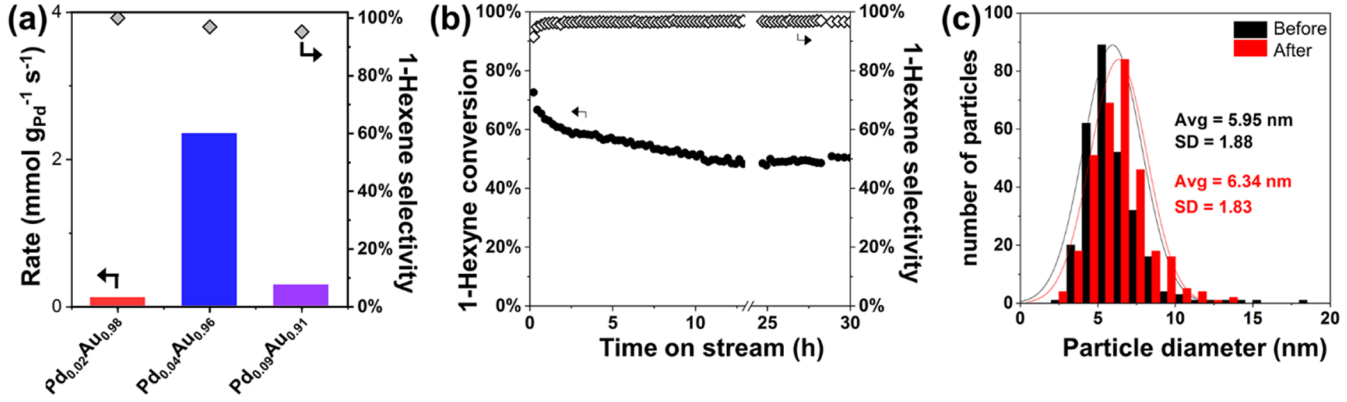


**Figure 21.** Catalytic performance and characterization of $Pd_xAu_{1-x}$ RCT-$SiO_2$ catalysts for selectivity hydrogenation of 1-hexyne. (a) Rate of 1-hexyne conversion (box) and the selectivity for 1-hexene (diamond open) over $Pd_xAu_{1-x}$ ($x$ = 0.02, 0.04, 0.09) RCT-$SiO_2$ catalysts at 323 K. (b) Time-on-stream of 1-hexyne conversion (circle solid) and 1-hexene selectivity (diamond open) over $Pd_{0.04}Au_{0.96}$ RCT-$SiO_2$ catalysts. (c) Average particle size of $Pd_{0.04}Au_{0.96}$ RCT-$SiO_2$ catalysts calculated based on TEM analysis before and after 1-hexyne hydrogenation reaction. Adapted from ref 112. Copyright 2020 American Chemical Society.

binding energies of adsorbates to Pd surface, thereby improving the selectivity toward alkenes.[210] PdAg alloy is widely used for industrial alkyne partial hydrogenation with the addition of Ag changing the stability of adsorbed acetylene and ethylene; this effect is comparable to that of subsurface carbon on Pd based on theoretical studies.[3,215] The improvements in selectivity of acetylene to ethylene have been attributed to both geometric and electronic effects between Pd and Ag in dilute PdAg alloys.[3,80] For example, high activity and selectivity in partial hydrogenation of acetylene was demonstrated over a wide range of temperatures for a series of Ag-alloyed Pd single atom catalysts.[3] The selectivity further increased with increasing reduction temperature, and under optimum conditions, long-term stability of over 24 h time-on-stream was achieved over $Pd_{0.01}Ag_{0.99}/SiO_2$ catalysts. Isolated, electron-rich Pd atoms formed via charge transfer from Ag to Pd was observed from XPS and XANES and proposed to be the reason for enhancement in ethylene selectivity.[3] In a separate study, acetylene hydrogenation reaction over PdAg catalysts was compared to PdCu alloys supported on $SiO_2$ and $TiO_2$.[80] While $Pd_{0.64}Ag_{0.36}/TiO_2$ catalysts give the highest turnover frequency (TOF) with 97% selectivity to ethylene, $Pd_{0.02}Cu_{0.98}$ $TiO_2$ catalysts show the highest rate per Pd basis with more than 99% selectivity measured. Although the Pd concentrations are very different in these two catalysts, CO Fourier transform infrared (CO-FTIR) spectroscopy showed the presence of primarily isolated Pd species in both cases, which have been reported to be the active sites for high ethylene selectivity.[216,217] The choice of support also affects the distribution of Pd, characterized by CO chemisorption, EXAFS, and IR. For PdAg, the stronger interaction between Pd and $TiO_2$ results in subsurface Pd, whereas on the $SiO_2$ support, Pd remained on the surface.[80]

Au catalysts are another example where overhydrogenation reaction is limited.[218,219] However, they are often not active at low temperatures and suffer from deactivation.[219−221] Promoting Au catalysts with Pd by forming PdAu alloys has shown improved selectivity with similar activity as monometallic Pd.[111,219,222] This is the result of improved hydrogen activation kinetics—often the rate-determining step—by the formation of surface Pd on PdAu under reaction condition, which was characterized by the DRIFTS studies.[82,134] A similar conclusion was reported based on the increase in ethylene selectivity over Au@Pd core−shell structure with a high dispersion of Pd.[223]

Efforts have been made to introduce single-atom Pd on Au to enhance activity while maintaining the high selectivity to alkenes. For instance, single-atom Pd in PdAu/$SiO_2$ catalysts showed higher selectivity in the hydrogenation of acetylene to ethylene compared to catalysts containing higher Pd loadings.[111] The presence of isolated Pd sites promotes the formation of adsorbed $\pi$-species over dissociation adsorption of ethylene and thus a superior selectivity to ethylene, which is confirmed by in situ DRIFTS and EXAFS combined with microcalorimetry results.[111]

PdAu RCT-$SiO_2$ catalysts with a dilute ratio of Pd (2−9%) in Au showed 90% selectivity to 1-hexene at 80% conversion of 1-hexyne for gas-phase reaction.[104,112] The $Pd_{0.04}Au_{0.96}$ RCT-$SiO_2$ catalysts yielded the highest rate of 1-hexyne hydrogenation compared to that of any other Pd compositions with above 97% selectivity to 1-hexene (Figure 21a). The catalytic performance remains stable after more than 30 h of operation at 363 K (Figure 21b) with no change in the average particle size based on postreaction TEM analysis (Figure 21c), demonstrating the high stability and resistance to sintering of the RCT catalysts. The long-term stability is also achievable under CO oxidation reaction conditions.[105]

The structures of $Pd_{0.04}Au_{0.96}$ RCT-$SiO_2$ catalysts are sensitive to pretreatment conditions, which results in changes in its catalytic performance.[104] For instance, the activity of $Pd_{0.04}Au_{0.96}$ RCT-$SiO_2$ catalysts for 1-hexyne hydrogenation increased from 20 to 30% with increasing $O_2$ pretreatment temperature from 323 to 673 K, whereas selectivity to 1-hexene maintained around 96% over all temperatures. The increase in activity is attributed to the stabilization of Pd on the surface by Pd−O bond formation, based on the EXAFS spectra collected after $O_2$ pretreatment at 673 K. Pretreating the same catalyst in $H_2$ at high temperature facilitates Pd dissolution into the bulk and thus diminishes catalyst activity to <5% 1-hexyne conversion. The catalyst can be partially reactivated by pretreatment in CO even at room temperature, which is attributed to adsorbate-induced stabilization of surface Pd. The dynamic restructuring of the catalyst surface in response to the pretreatments are concluded from correlations between theoretical calculations and experimental results. Specifically, a shorter Pd−Pd distance in EXAFS fitting of samples after $O_2$


https://doi.org/10.1021/acs.chemrev.1c00967
Chem. Rev. 2022, 122, 8758−8808

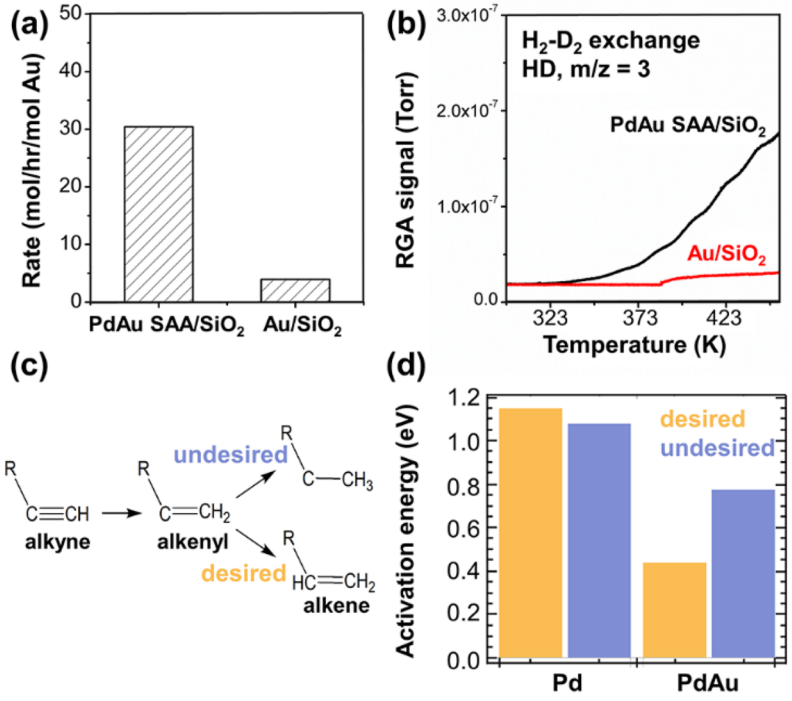


**Figure 22.** $Pd_{0.004}Au_{0.996}$ NP/$SiO_2$ catalysts for liquid-phase selective hydrogenation of 1-hexyne. (a) Initial reaction for hydrogenation of 1-hexyne normalized by the amount of Au and (b) $H_2$–$D_2$ exchange over Au/$SiO_2$ and $Pd_{0.004}Au_{0.996}$ NP/$SiO_2$ catalysts. (c) Schematic of alkyne hydrogenation pathways and (d) DFT calculations of the activation energy of desired and undesired hydrogenation pathways over Pd(111) and PdAu(111) SAA surfaces. Adapted with permission from refs (a,b) 109 and (c,d) 110. Copyrights 2017 Royal Society of Chemistry and 2019 American Chemical Society.

or CO pretreatment was observed compared to those treated in $H_2$ pretreatment. No change in NP size and morphology based on in situ TEM characterization in $O_2$ or $H_2$ further supports the redistribution of Pd atoms within single particles. With the rate-limiting step being the addition of the second hydrogen to the half-hydrogenated intermediate, the high selectivity is the result of higher stability of the half-hydrogenated intermediate of alkyne over the half-hydrogenated alkene. The reaction mechanism was determined based on experimentally calculated reaction order and DFT calculations.[112] Based on DFT calculations of adsorption energies, it was shown that acetylene and ethylene bind more strongly on Pd(111) than on dilute Pd/Au(111).[112] A similar mechanism has also been reported for hydrogenation of acetylene to ethylene over single-atom Pd on Au or Ag NPs, where the presence of alloyed Pd single-atom structure successfully weakens the adsorption of ethylene.[3,111]

A different mechanism for improved alkene selectivity was proposed in the study of PdAu NPs for liquid-phase hydrogenation reaction.[100,110] $Pd_{0.004}Au_{0.996}$ NP/$SiO_2$ showed a 10 times higher activity for hydrogenating 1-hexyne compared to that for monometallic Au in the liquid-phase reaction (Figure 22a).[100] This was achieved by facilitating $H_2$ dissociation with isolated Pd atoms, where the rate-limiting step being $H_2$ activation. $Pd_{0.004}Au_{0.996}$ NP/$SiO_2$ showed much higher HD production rate than Au/$SiO_2$ in $H_2$–$D_2$ exchange experiments, which supports the presence of single Pd atoms on the surface of Au NPs effectively catalyze the $H_2$ activation (Figure 22b). The similar apparent activation energy observed for PdAu NPs and monometallic Au also indicates the reaction pathways are identical and qualitatively different from monometallic Pd.[110] The atomistic insight provided by DFT calculations suggests that the selectivity was governed by the second step of hydrogenation, and a high selectivity can be achieved by $Pd_{0.004}Au_{0.996}$ NP/$SiO_2$, where the reactive surface atom attracts both the hydrogen atom and the most reactive atom in the intermediate (Figure 22c,d).[110] In TPD studies over PdAu(111) SAA surface, both reactant and product have almost identical binding strengths. This led to favoring the selective over nonselective reaction pathway and provides clear evidence supporting the proposed mechanism. Different from $Pd_{0.04}Au_{0.96}$ RCT-$SiO_2$ catalysts, where differential binding strength of the reactant and products governs selectivity, product and reactant have almost identical binding strengths on $Pd_{0.004}Au_{0.996}$ NP/$SiO_2$. This suggests the selectivity of $Pd_{0.004}Au_{0.996}$ NP/$SiO_2$ is the result of changes in the favorability of the selective versus nonselective reaction pathway.

**3.4.3. Alkyne Hydrogenation on Cu-Based Materials.** Different from the PdAu SAAs introduced previously, high selectivity of partial hydrogenation of alkynes and dienes has also been reported in PdCu and PtCu SAAs where a bifunctional mechanism dominates.[5,35,87,224] One of the earliest example was demonstrated over PdCu and PtCu model SAA surfaces via STM and $H_2$-TPD experiments for facile $H_2$ dissociation and recombination, even at cryogenic temperatures.[14,224] Hydrogen spillover onto Cu, where Cu imparts selective hydrogenation of acetylene on 0.01 ML PtCu(111) alloy surface.[23] Cu is intrinsically selective for hydrogenation reactions because of the relatively low-energy barrier of alkene desorption compared to the hydrogenation barrier of alkenes. Substituting Au with Cu also provides a route to reduce catalysts cost. Based on TPRS results, the low-temperature pathway for ethene formation showed >95% selectivity on 0.01 ML PtCu(111), whereas extensive decomposition happens on 1 ML Pd/Cu(111).[23] In addition


https://doi.org/10.1021/acs.chemrev.1c00967
Chem. Rev. 2022, 122, 8758−8808

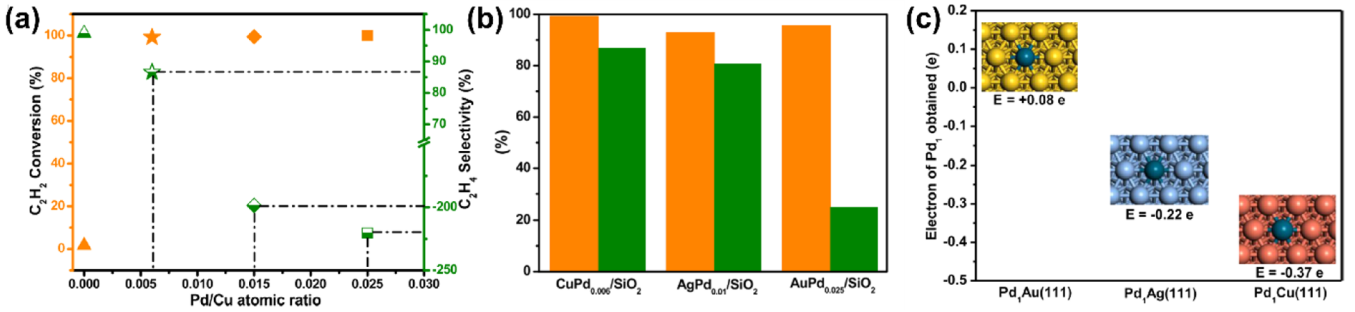


**Figure 23.** Acetylene conversion (orange) and ethylene selectivity (green) at 433 K (a) as a function of the Pd/Cu atomic ratio and (b) over $SiO_2$ supported $Pd_{0.006}Cu$, $Pd_{0.01}Ag$, and $Pd_{0.025}Au$. (c) DFT calculations of electron states of isolated Pd atoms alloying into Au(111), Ag(111), and Cu(111) surfaces. Adapted from ref 108. Copyright 2017 American Chemical Society.

to the model systems, the bifunctional concept has been translated to NP catalysts. For example, PdCu SAAs/$Al_2O_3$ with 0.18 atomic % Pd is active for the hydrogenation of phenylacetylene to styrene at ambient temperature with 94% selectivity at all conversions.[87] $H_2$ dissociates on single-atom Pd sites followed by spillover onto the Cu host metal where selective product forms and desorbs prior to complete hydrogenation. The incorporation of Pd atoms into the subsurface layer of Cu(111) has also been proposed as the active site that can effectively reduce the $H_2$ dissociation barrier based on simulated XPS and theoretical calculations.[225] In this case, the high catalytic activity is the result of enhanced surface−adsorbate interactions by subsurface Pd atoms modifying the Pd-doped Cu surfaces.

Another example of single-atom Pd on Cu (Pd/Cu = 0.006) supported on $SiO_2$ showed 85% selectivity to ethylene at 100% acetylene conversion with the same bifunctional nature.[108] By exploring different Pd/Cu atomic ratios (Figure 23a), the decrease in Pd/Cu ratio results in increased isolated Pd atom sites and thus the improved selectivity to ethylene. This improvement is mainly the result of weakened adsorption of ethylene, which was confirmed via microcalorimetric measurements and DFT calculations. This work also compared across Cu, Ag, and Au as the host metal with single-atom Pd dopant, and all three showed similar apparent activation energies and ethylene adsorption strengths, suggesting the ability for acetylene activation was almost equal among the group IB metals.[108] The selectivity to ethylene decreased going from $Pd_{0.006}Cu$ to $Pd_{0.01}Ag$ to $Pd_{0.025}Au/SiO_2$ (Figure 23b), which correlates well with the amount of electron transfer from group IB metals to Pd based on DFT calculations, XANES, and XPS results.[3,108] Electrons transfer from a host metal to Pd for PdCu or PdAg catalysts, whereas it is the opposite direction for PdAu (Figure 23c); this is consistent with the order of their electronegativity.

Evidence of hydrogen spillover has been demonstrated in PdCu dilute alloy catalysts.[114,226,227] PdCu alloys with dilute Pd in Cu showed combined intrinsic properties of its monometallic components for the hydrogenation of acetylene and propyne. The catalyst can be activated and used at moderate temperatures (~373 K) with performance strongly dependent on the Pd/Cu ratio.[114,226,227] At close to 100% conversion of acetylene, over 80% selectivity to ethylene over $Pd_{0.02}Cu_{0.98}/Al_2O_3$ was attributed to small Pd clusters formed at both the surface and subsurface region over a Cu-rich surface, which promotes $H_2$ dissociation as shown via CO-FTIR characterization.[226] Furthermore, the hydrogenation activity can be improved by CO-induced Pd surface segregation; however, at a higher Pd/Cu atomic ratio ($Pd_{0.1}Cu_{0.9}/Al_2O_3$), the increase in surface Pd dimers due to CO-induced segregation shifted selectivity toward ethane production.[113]

## 4. DYNAMIC BEHAVIOR DURING CATALYSIS

### 4.1. Overview

Dynamic changes in the surface structure and composition as well as adsorbate migration between reactive ensembles are fundamental to the catalytic behavior of dilute alloys. The atomic-scale arrangement of an alloy surface depends on the reactant composition and temperature and can thus be modified through pretreatment and reaction conditions. The reactive minority metal(s) can be substantially enriched at the surface by pretreatment conditions to provide a thermodynamic driving force for surface segregation. Once at the surface, the reactive metal can be trapped in metastable states even in absence of the original trigger, thereby providing sites needed to initiate catalytic chemistry. Reactive intermediates must then migrate between the minority and host metals to undergo selective transformations. Recent research has provided fundamental insights for understanding the dynamic behavior of dilute alloy catalysts and its role in mediating catalytic chemistry.

This section will focus on two main themes of dynamic behavior during catalysis: 1) determining how alloy surface structure and composition change in response to gas-phase composition and temperature and identifying reaction conditions that retain the optimal catalyst structure, and 2) elucidating the mechanisms for adsorbate migration between coexisting surface phases and its coupling to reaction kinetics and surface restructuring.

### 4.2. Dynamic Materials Behavior: Support-Free Nanoporous Materials

Adsorbate-triggered dynamic changes of morphology and surface composition can dramatically affect activity and selectivity as well as long-term stability of catalyst materials. For instance, the high surface area morphology of nanoporous metals is not thermodynamically stable with respect to coarsening.[228] Adsorbate-induced changes of the surface mobility can thus directly affect the coarsening kinetics and long-term stability of nanoporous alloy catalysts. The actual surface composition, on the other hand, can reflect the thermodynamically stable surface composition or, at low enough temperatures, be kinetically trapped in a metastable state. Thus, adsorbate-induced changes in both the thermodynamically stable surface composition and the diffusion kinetics


https://doi.org/10.1021/acs.chemrev.1c00967
Chem. Rev. 2022, 122, 8758−8808

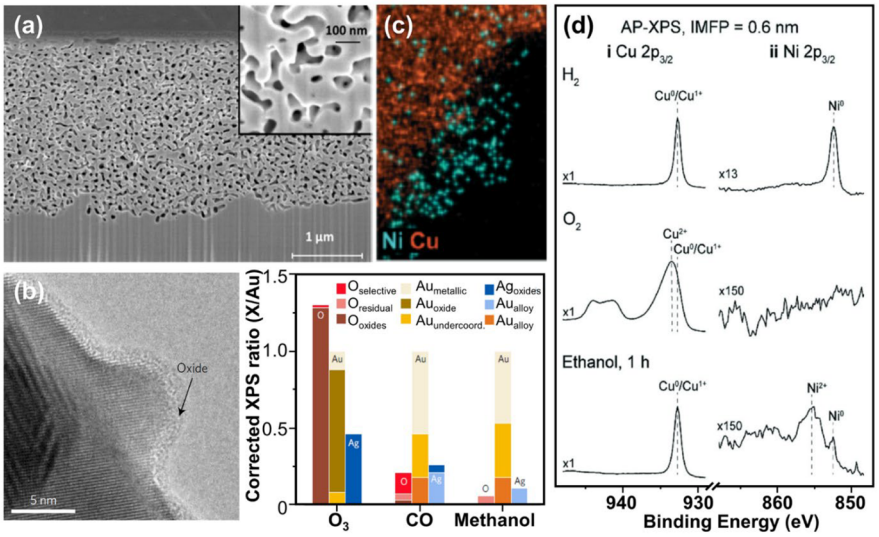


**Figure 24.** (a) Focused ion beam/X-SEM showing $O_3$-induced 3D nanoporosity formation in $npAg_{0.7}Au_{0.3}$. Inset in (a) shows a higher-magnification image. (b) Formation of a 1−2 nm thick Ag-rich surface oxide layer on npAu upon $O_3$ exposure (left) and changes of the surface composition upon $O_3$ exposure as well as consequent reduction with CO and methanol (right). (c) STEM-EDS map of an $O_2$-stabilized npNiCu catalyst confirming that Ni is also present in the form of a dilute NiCu alloy in addition to oxidized Ni-rich particles at the surface. (d) Ambient pressure XPS (AP-XPS) data revealing the compositional and chemical-state changes of npNiCu during $H_2$ and $O_2$ pretreatments as well as during ethanol-to-acetaldehyde conversion. Adapted with permission from refs (a) 180, (b) 62, and (c,d) 69. Copyrights 2017 American Chemical Society, 2017 Springer Nature, and 2020 Royal Society of Chemistry.

can trigger compositional changes ranging from local place exchange between different surface and subsurface alloy components to large-scale mass transport leading to the formation of thick surface oxide layers or large-scale surface segregation phenomena. An extreme example is the dry oxidation of $npAg_{0.7}Au_{0.3}$ alloys by $O_3$ at 423 K (Figure 24a,b) that dramatically changes both the morphology and surface composition by oxygen-triggered Ag outward diffusion to the gas/alloy interface and consequent formation of nanoporosity in the Ag depleted near-surface volume.[180] Adsorbate-induced changes in surface stress can further contribute to changes in the catalytic properties of nanometer-sized ligaments as they can trigger lattice strain up to several permille.[28]

In most cases, the morphological and compositional changes induced by surface chemistry are subtle but nevertheless of critical importance for catalyst activity and selectivity. For example, while as-dealloyed npAu (with dilute amount of Ag) is highly active toward CO oxidation, it is only after activation with $O_3$ that npAu shows high selectivity toward oxidative coupling of alcohols while becoming inactive for CO oxidation (catalytic studies over npAu is reviewed in section 3.2).[55] Advanced in situ environmental TEM (ETEM) and AP-XPS have been used to explore the complex restructuring and compositional changes that occur along the path to catalytic activity for selective alcohol oxidation.[62,74] In short, $O_3$ exposure at 423 K leads to the formation of a 1 nm thick Ag-rich surface oxide layer with about 10 times the average Ag concentration of npAu (Figure 24a). In contrast to the $npAg_{0.7}Au_{0.3}$ alloy example discussed above, npAu no longer reacts with $O_3$ once the 1 nm thick Ag-rich surface oxide layer has been formed. The oxygen of this oxide layer is highly reactive toward both CO oxidation and alcohol combustion. While some of the Ag realloys into the bulk of the ligaments during reduction of the Ag-rich surface oxide layer by either CO or alcohol exposure, the surface of the npAu ligaments remains enriched in Ag and becomes covered with disordered Ag-containing NPs which crystallize upon further alcohol exposure. The formation of the AgAu surface alloy together with the increase in the concentration of undercoordinated Ag and Au surface atoms caused by the formation and growth of the crystalline NPs seem to be responsible for stabilization of a distinct oxygen species which provides the high selectivity toward partial oxidation of alcohols. Similar effects have been observed during the oxidation of PdAg single-crystal model surfaces, in which oxygen exposure at ∼373 K leads to Pd dewetting and formation of ∼1 nm tall Pd particles on the planar Ag surface.[229]

No specific activation procedure is necessary for the more reactive NiAu dilute alloy catalysts for non-oxidative dehydrogenation of ethanol as this catalyst is activated by the interaction with the reactant ethanol at temperatures as low as 423 K. Ni segregation to the surface is induced by ethanol, whereas it prefers to occupy subsurface sites on the clean surface under $H_2$-rich conditions.[60] The presence of Ni also slows down the coarsening kinetics of the NiAu catalyst allowing for prolonged use under reaction conditions without an apparent drop in activity.

Although npNiCu dilute alloys show good long-term stability for non-oxidative ethanol dehydrogenation at lower reactant flow (conversion) rates,[47] $O_2$ pretreatment is necessary to stabilize the catalyst activity at higher reactant flow rates.[69] Here, $O_2$ pretreatment at 523 K leads to the formation of a $Cu^{2+}$ oxide surface layer that completely buries the more reactive Ni component. Subsequent ethanol exposure under reaction conditions (523 K) reduces the copper oxide overlayer, while Ni remains in a kinetically trapped $Ni^{2+}$ subsurface state thus preventing the Ni cluster formation which has been linked to catalyst deactivation through carbon deposition. Using $H_2$ pretreatment instead leads to rapid deactivation (Figure 24c and d). The catalytic studies of NiAu and NiCu dilute catalysts can be found in section 3.3.1. It is


https://doi.org/10.1021/acs.chemrev.1c00967
Chem. Rev. 2022, 122, 8758−8808

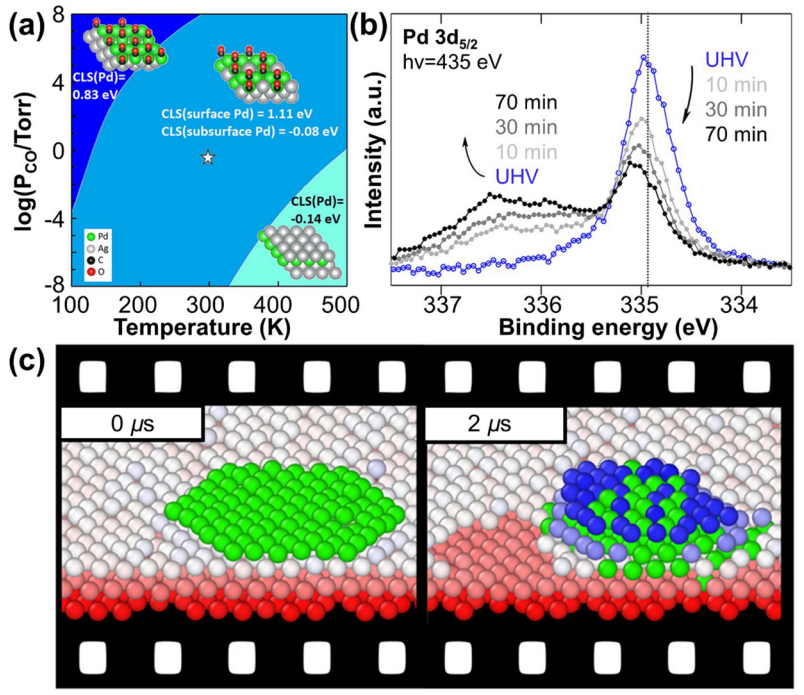


**Figure 25.** (a) DFT was used to generate a surface stability diagram of Pd/Ag(111) as a function of CO pressure and temperature. (b) Surface-sensitive Pd $3d_{5/2}$ photoelectron spectra acquired as a function of exposure time to 1 Torr $O_2$ at 400 K show the development of a broad shoulder at higher binding energy assigned to oxidized Pd that has been segregated to the surface. (c) Frames of MD simulation showing the evolution of a $Pd_{91}$ island on Ag(111) at 500 K over 2 $\mu$s. Adapted from refs (a,b) 25 and (c) 238. Copyrights 2019 and 2020 American Chemical Society.

important to note that similar, but more localized compositional changes have been observed in $Pd_{0.04}Au_{0.96}$ RCT-$SiO_2$ catalysts[104] where exposure to $H_2$, $O_2$, and CO alters the Pd content in the NP surface and thus the hydrogenation activity of the catalyst.

### 4.3. Dynamic Behavior of Catalyst Surfaces: Fundamental Studies of Au- and Ag-Based Bimetallic Surfaces

Surface science and theoretical models can provide unparalleled fundamental insights into dynamic phenomena that occur on dilute alloy surfaces and their effects on surface reactivity. Material rearrangement and reactive species migration at bimetallic surfaces have been examined in detail using model PdAu, PdAg, and PtAg surfaces. Bimetallic surfaces were among the first to establish fundamental understanding of dynamic behavior and the principles established generally translate to dilute alloy systems of interest. The composition and structure of bimetallic surfaces under reaction conditions are a result of a balance between the surface free energy of the system and the kinetics for material rearrangement. Further, the structure and coverages of reactive species can mediate the migration of intermediates across phase interfaces and directly contribute to the surface reactions. Material rearrangement and reactive species migration were demonstrated not only to occur concurrently but also to directly impact one another, thus highlighting the need for fundamental model studies to understand complex catalyst behavior toward improving catalyst design.

#### 4.3.1. Material Rearrangement at Bimetallic Surfaces.

Surface segregation can play a decisive role in the performance of dilute alloy catalysts based on coinage metals. Under vacuum conditions, thermodynamics favors surface enrichment by the coinage metal component because their surface free energies are lower than those of the late transition metals typically utilized in these catalysts, including Pd, Pt, Rh, Ir, Ru, and Ni.[230] In contrast, surface segregation of the transition metal dopant is thermodynamically preferred in the presence of reactive gases due to the stronger adsorbate bonding that can be achieved. Although kinetic barriers can hinder surface segregation, coinage metals have high atomic mobility that enable their surfaces to efficiently restructure at the moderate temperatures at which these dilute alloy catalysts are employed.

Model studies with PdAu alloys were among the first to establish fundamental principles for understanding surface segregation in other dilute alloys of coinage metals. The exposure of strongly interacting species, such as CO[231−233] and $O_2$,[234] on PdAu bulk alloys drives the segregation of Pd to the surface when there are no kinetic limitations for restructuring. At room temperature, the partial pressure of CO impingent on AuPd(100) controls the segregation of Pd to the surface, with higher CO pressures enhancing the Pd enrichment of the surface.[231] The surface segregation of Pd by CO is not observed below ∼200 K, suggesting that Pd diffusion to the surface becomes kinetically limited at sufficiently low temperature.[232] The surface site distribution of Pd in PdAu bulk alloys is dependent on both the CO pressure ($10^{-7}$−10 Torr) and temperature (100−650 K) as determined by IR spectroscopy and STM measurements, where low pressure and temperature predominantly induce the formation of isolated Pd atoms while ensembles with contiguous Pd sites develop at higher pressure and temperature.[232,233] Isolated Pd atoms also tend to distribute randomly on clean PdAu(111), with larger $Pd_n$ ensembles developing at higher Pd coverages.[235,236] More facile $H_2$ activation and greater stabilization of adsorbed H atoms is achieved with increasing $Pd_n$ ensemble size; Pd tetramers are the smallest ensemble capable of activating $H_2$ in UHV.[236] The presence of contiguous Pd sites is also necessary for the dissociation of $O_2$, which directly controls the rate of


https://doi.org/10.1021/acs.chemrev.1c00967
Chem. Rev. 2022, 122, 8758−8808

CO oxidation.[232,237] This is evident in both reactor and surface science studies of the CO oxidation reaction (section 3.2.1). The exposure of $O_2$ to $Au_{0.3}Pd_{0.7}(110)$ at room temperature also can induce the segregation of Pd to the surface.[234] The demonstration of these surface phenomena on PdAu surfaces provides a foundation for understanding structural rearrangements on PdAg and PtAg surfaces.

In the absence of adsorbates, there is a strong thermodynamic driving force for PdAg alloys to form a Ag-terminated surface although metastable structures can exist when there is insufficient thermal energy for rearrangement.[25,238] The energetic driving force for Ag termination is to minimize the surface free energy of the system, where bare Pd and Ag have surface free energies of 2.05 and 1.25 J $m^{-2}$, respectively.[230] Investigations with PdAg surfaces confirm the tendency for Ag to enrich the surface of crystalline PdAg alloys and further demonstrate that the Pd and Ag atoms tend to disperse within the surface layer.[239−242] The formation of well-mixed PdAg surface alloys is thermodynamically favored but requires thermal energy to overcome kinetic barriers for intermixing, enabling metastable structures to be formed at low temperature. For instance, the deposition of submonolayer coverages of Pd on Ag(111) at 300 K predominantly forms single-layer Pd islands as determined by a combination of surface science experiments and DFT calculations.[25,238] A mild thermal treatment provides sufficient energy to form Ag-terminated double-layer structures and neighboring Ag vacancy pits, as predicted by DFT calculations.[25,238]

Similar to PdAu introduced above, exposure of the Ag-terminated double-layer PdAg structure to both CO and $O_2$ induces the segregation of Pd to the surface.[25] DFT calculations predict phase diagrams of the most stable structures in CO and $O_2$ gas environments, where increasing gas pressure favors Pd-terminated structures while increasing temperature favors Ag-terminated structures (Figure 25a).[25,242,243] In fact, under sufficiently $O_2$-rich conditions, a single-layer Pd oxide becomes thermodynamically favored on PdAg(111) surfaces and forms under relatively mild conditions.[242,243] Likewise, surface oxidation of the $Pd_{0.75}Ag_{0.25}(100)$ bulk alloy generates an ordered, single-layer Pd oxide in addition to a Ag-rich interfacial region in the subsurface.[242,243] The partial pressure of CO can also drive the segregation of Pt in a PtCu alloy surface.[244] However, the thermodynamically preferred structures may not be accessible under experimentally relevant time scales due to kinetic limitations for structural rearrangement as demonstrated by the gradual surface segregation of Pd in a PdAg alloy observed during exposure to $O_2$ (Figure 25b).[25] Therefore, it is critical to understand the kinetics for structural changes in addition to the thermodynamically preferred structures.

The kinetics of elementary restructuring events control whether thermodynamic minimum energy structures or kinetically trapped metastable structures are observed under reaction conditions.[238,245] Advanced MD simulations of a single-layer $Pd_{91}$ island on Ag(111) at 500 K demonstrate that the system rapidly reaches an apparent quasi-equilibrium structure composed of a double-layer island that has a Ag-rich surface, in agreement with experiments (Figure 25c).[238] However, at elevated temperatures, layer-by-layer dissolution of Pd into the bulk occurs while Pd atoms periodically visit the surface as single-atom Pd sites.[238] The evolution of thermodynamically stable and sufficiently long-lived metastable structures can be understood by advanced dynamics simulations coupled with experiments which inform the most relevant structures under reaction conditions.

Surface temperature can also contribute to the kinetics of dilute alloy surfaces. For instance, the surface structure of PtAg alloys can be modulated by the surface temperature during alloying, which controls the dispersion of Pt in Ag by tuning the kinetics for Pt−Ag direct exchange on terraces and at step edges.[4] Near-room temperature deposition of dilute Pt on Ag(111) leads to the preferential formation of Pt aggregates as islands due to insufficient thermal energy for surface alloying. Depositing Pt at elevated temperatures enhances the dispersion of Pt in Ag as well as the concentration of isolated Pt alloy sites. Surface alloying at elevated temperatures occurs primarily by widening the PtAg alloy brim at the step edges; however, at 480 K, extensive alloying occurs directly into the Ag terraces. The kinetics for Pt−Ag exchange can be tuned by surface temperature to control the dispersion of Pt in Ag for kinetically trapped surface configurations.

**4.3.2. Reactive Species Migration across Bimetallic Interfaces.** The surface migration of reactive species is critical to realizing unique reactivity and selectivity in bimetallic alloy materials. Hydrogen atom migration between the host and dopant sites of dilute alloy surfaces and across domain interfaces (metal/metal, metal/oxide) is particularly important due to its role in supplying hydrogen atoms for selective hydrogenation reactions.[14,87,252,224,229,246−251] For example, on dilute alloys, selective hydrogenation can be accomplished by hydrogen atom spillover onto the host metal surface to enable the activation and subsequent hydrogenation of the co-reactant on a dopant site.[7] Employing surface science and theoretical models can provide a detailed understanding of the energetics and kinetics of reactive species migration on alloy surfaces. These investigations establish fundamental principles to guide the understanding and prediction of phenomena in dilute alloy catalyst systems.

Hydrogen spillover on dilute alloys generally requires a mechanism by which hydrogen atoms can overcome a thermochemical energy barrier that arises from stronger binding of hydrogen on the dopant site compared with the coinage metal surface. In the absence of other adsorbates, hydrogen migration away from isolated dopant sites can be driven by the entropic gain that results from dispersion onto the host surface. Indeed, hydrogen atom spillover is facile on several dilute alloys employed in catalytic applications (see examples reviewed in section 3.4.3), suggesting that the differences in H binding energy on the dopant versus host metal in these systems are small enough to allow hydrogen release onto to the host surface.[253]

The coadsorption of hydrogen with a more strongly binding species can also induce hydrogen spillover onto the host surface.[249,251] In this case, thermodynamics favors configurations in which the strongly binding species adsorbs on dopant sites while hydrogen atoms disperse onto the host surface. Lastly, hydrogen spillover can also be mediated by the local H coverage. On PdAg surfaces, hydrogen migration away from isolated Pd sites is inefficient below ∼200 K,[254] suggesting that entropic gain is insufficient to overcome the reaction endothermicity. However, hydrogen migration from contiguous Pd domains to Ag becomes accessible when a dense phase of hydrogen atoms forms on Pd and a substantial hydrogen atom concentration can accumulate on both metals.[255] DFT shows that increasing the H coverage on the Pd lowers the hydrogen binding energy and renders hydrogen


https://doi.org/10.1021/acs.chemrev.1c00967
Chem. Rev. 2022, 122, 8758−8808

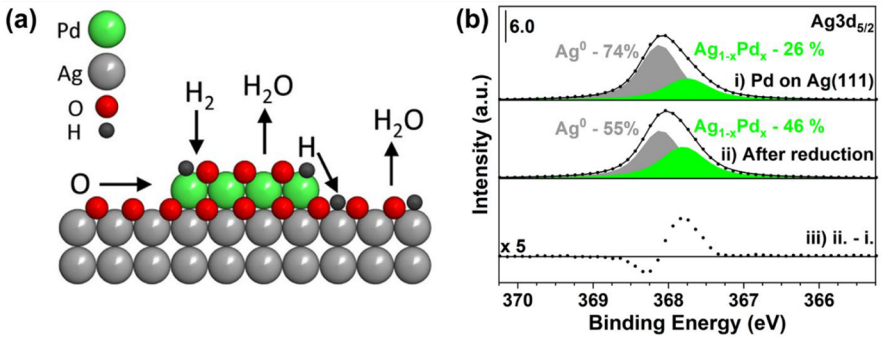


**Figure 26.** (a) Representation of cooperative mechanisms for reduction of an oxidized Pd/Ag(111) surface by $H_2$, including hydrogen and oxygen atom migration. (b) Pd−Ag intermixing occurs after reduction of $PdO_x$ on Ag(111), as evidenced by the increased $Ag_{1-x}Pd_x$ alloy peak in the Ag $3d_{5/2}$ region (green) using AP-XPS. Adapted with permission from refs (a) 229 and (b) 258. Copyrights 2020 The Authors and 2020 American Chemical Society.

migration to the Ag surface thermodynamically and kinetically feasible. These studies establish fundamental mechanisms governing hydrogen spillover on dilute alloys and reveal a sensitive dependence on reaction conditions and surface structure.

Species that bind strongly to the dopant metal can undergo reverse spillover, wherein adsorbates migrate from the host surface to the dopant and typically induce aggregation of the dopant atoms. The reverse spillover of oxygen can be particularly important in oxidation reactions promoted by Ag and Au-based alloys. Recent work demonstrates that oxygen atom migration from Ag to Pd occurs efficiently,[254] which is driven by the greater oxophilicity of Pd.[256−258] Autoxidation of Pd clusters occurs facilely during Pd deposition onto oxidized Ag(111) surfaces at 300 K, generating local O coverages on Pd that depend on the Pd domain size and the properties of the initial $AgO_x$ layer.[256−258] Further, the oxidation of large, single-layer Pd islands on metallic Ag(111) with near-ambient pressure of $O_2$ at elevated temperature causes Pd to dewet the surface, forming multilayer Pd particles with a surface $PdO_x$ termination, whereas Ag forms a surface $AgO_x$.[229,258] The oxidation and structure of Pd and Ag domains of a PdAg oxide surface are intimately connected as a result of facile oxygen transport between the two metals. This illustrates the importance of understanding the complex interplay between reactive species migration and the structure and concentration of surface species and their impact on catalytic chemistry.

**4.3.3. Dynamic Coupling of Material Evolution and Species Migration and Its Effect on Reactivity.** The dynamical coupling of material evolution and reactive species migration is rarely considered; however, the concomitance of these phenomena can significantly influence surface reactivity. A clear demonstration of the coupling of material evolution and reactive species migration is observed by examining the reaction of both $H_2$ and CO with oxidized PdAg surfaces. In both cases, the reactivity is significantly modified, highlighting the need to understand the coexistence of these phenomena and inclusion of these effects when modeling surface chemistry on bimetallic surfaces.

The reactivity of $AgO_x$ with $H_2$ at 300 K is dramatically enhanced on PdAg oxide surfaces by reactive species migration that involves Pd−Ag intermixing.[229,258,259] $PdO_x$ readily dissociates $H_2$ which reacts with oxygen atoms to evolve water,[260] while Ag surfaces have a significant barrier which prevents $H_2$ dissociation and the accumulation of hydrogen atoms.[261,262] The $AgO_x$ structure that forms during oxidation of a PdAg surface reacts with $H_2$ at a rate that is $10^4$ times larger than the reaction rate on pure $AgO_x$, due to hydrogen atom migration from Pd to Ag as well as oxygen atom migration from Ag to Pd (Figure 26a).[229] Similarly, an enhancement in the reaction rate of a $CuO_x$ phase with $H_2$ on a PtCu oxide surface compared with pure $CuO_x$ has been observed.[263] The surface reaction is accompanied by Pd−Ag intermixing which slows the reduction rate of $PdO_x$ for the PdAg oxide surface compared to pure $PdO_x$ (Figure 26b).[229] Smaller, well-distributed Pd domains have a higher rate of $AgO_x$ reduction due to (1) an increased Pd−Ag interface for enhanced reactive species migration, (2) lower spatial requirement for species migration, and (3) higher concentration of undercoordinated Pd sites for $H_2$ dissociation, possibly at the Pd island edges.[258] Alternating between oxidizing and reaction conditions causes drastic composition changes by Pd dewetting and PdAg alloying which slightly affects the reactivity of $PdO_x$ while maintaining a nearly constant reactivity of $AgO_x$ with $H_2$.[259] These studies demonstrate that the migration of reactive species across a Pd−Ag interface leads to a dramatic change in surface reactivity and that the evolution of the structure of the PdAg surface is affected by the surface reaction. The overall reaction rate is highly sensitive to the nature of the Pd−Ag interface and the structure and dispersion of Pd domains.

The reactivity of PdAg oxide surfaces with CO is significantly affected by oxygen atom migration from $AgO_x$ to Pd which is controlled by the structure and contact of the Pd and Ag phases.[257] Pure $PdO_x$ as well as oxygen-covered, metallic Pd readily oxidize CO to $CO_2$ at mild temperatures (∼100−500 K), where oxygen transport from less reactive $PdO_x$ phases can enhance the reactivity of a more reactive metallic phase.[264−267] A similar mechanism is reported on $AgO_x$.[268] Reduction of a $Pd_5O_4$ layer by CO occurs more slowly on $Pd_{0.75}Ag_{0.25}(100)$ compared with Pd(100) because the reemergence of surface Ag atoms during reduction suppresses CO adsorption as well as diffusion to oxidized domains.[243] Understanding the interaction of the metallic and oxide phases for a catalyst surface with minority reactive metal dispersed on a selective metal is important for bimetallic catalyst design for CO oxidation (see section 3.2.1 for catalytic studies). The reaction of CO adsorbed at 100 K with a partially oxidized, PdAg surface yields efficient production of $CO_2$, whereas minimal reactivity is observed for the $AgO_x$ surface in the absence of Pd.[257] Oxygen atom transfer occurs via both the buried PdAg oxide interface and diffusion across the $AgO_x$


https://doi.org/10.1021/acs.chemrev.1c00967
Chem. Rev. 2022, 122, 8758−8808

surface to the Pd domains.[257] A heterogeneous distribution of oxygen atoms on Pd is generated, where preferential oxygen binding to the edges of Pd islands enhances the CO oxidation activity of Pd clusters of decreasing size. The interplay between the oxygen-rich Pd edges and the CO-enriched Pd interior facilitates efficient CO oxidation. In summary, the initial oxygen transfer determines the local distribution of oxygen on the Pd phases which in turn controls the CO oxidation activity of the PdAg surface. Similar oxygen transfer processes may be broadly important in oxidation catalysis by dilute alloys.

## 5. ADVANCES IN METHODOLOGY

### 5.1. Overview

Understanding the evolution of structure and composition of catalysts and their relationship to catalytic function is the key and central challenge to advance the understanding of dilute alloy catalysts. The challenges stem from the dilute nature of the minor species in the metal alloys, the restricted geometry of the nanostructures, and the multi-length scale and multi-time scale evolution on the surface of catalysts. To overcome these challenges and to investigate the catalyst structures and compositions, including their evolution under reactive conditions, new tools and advanced methods are required.

In this section, new experimental and theoretical techniques developed for dilute alloy catalysts are reviewed. Experimental tools include in situ atomic-scale imaging using electron microscopy and structural determination using X-ray absorption spectroscopy combined with ML. Theoretical tools include ML methods and automation that accelerate MD simulations and enable the modeling of catalyst restructuring over microsecond time scales.

### 5.2. Novel Strategies of X-ray Absorption Spectroscopy for Dilute Alloy Catalysts

XAFS spectroscopy is an element-specific technique for probing local structural, electronic, and dynamic properties in a wide range of materials,[269] from crystalline to amorphous to liquids.[270−279] It is common to extract bond lengths, coordination numbers, and electronic states (e.g., metal oxidation states) from XAFS data. These local structural parameters provide rich information pertaining to the geometry and chemistry of nanoporous or NP catalysts, such as particle sizes, shapes (sometimes), as well as compositional motifs.[280−282] Following the changes of these parameters over pretreatments and reactions can elucidate the important local structures for highly active and selective catalysts.

However, it can be challenging to extract structural parameters for the dilute minority species from XAFS data because the measured signal is an ensemble average, and hence all contributions are lumped into one total spectrum. For example, as described in section 2.4, one prominent method to synthesize high surface area dilute alloy catalysts employs RCT-$SiO_2$ materials, where dilute alloy NPs are supported and stabilized within a porous silicate matrix. The element of interest, the dilute minority metal, has an atomic fraction less than 5 atom % in the NPs, and the weight loading of the NPs in the RCT matrix can be as low as 2.5−10 wt %. The significant heterogeneity stemming from diverse configurational motifs as well as static and dynamic disorder poses a very significant challenge to structural refinement due to the ensemble-averaging nature of XAFS, making active site characterization impossible with conventional analytical techniques.

This challenge can be addressed by several routes. This section briefly reviews several novel solutions that are particularly suitable for dilute alloys. Because of the challenges and these recently developed solutions are common for a large class of mixed systems, examples from other dilute systems such as molten salts with metal impurities and doped ceramic oxides are also reviewed.

**5.2.1. MD-EXAFS for Resolving Unique Metal Complexes in Dilute Systems.** One route to reduce the degeneracy of different heterogeneous structural motifs is to seek guidance from first-principle calculations that can describe different structural motifs, such as using MD simulations. Ab initio molecular dynamics (AIMD) is a common method for modeling materials evolution.[283] The resulted trajectories for each motif (if their numbers can be limited to just a few unique local structural units) can then be used to construct theoretical time-resolved EXAFS spectra. The spectra of the entire simulation box are then averaged to simulate the ensemble average done in experiments. By comparing the so obtained MD-EXAFS theoretical spectrum with experiments, the heterogeneity in local motifs can be resolved using their theoretically calculated structure and dynamics information.

One example uses this method to resolve the possible metal impurities in the molten salts,[284,285] which is a multicomponent system with multiple $MX_n$ (where M is the metal (Ni or Co), X is a halogen, $n = 3−6$) complexes coexisting. To ultimately deconvolute the experimental EXAFS signal, which is the sum of the signals coming from multiple species, AIMD was used to generate simulation trajectories and reveal the highly disordered coordination environments of dilute ions. The experimental data were then fitted to a linear combination of the theoretical spectra that are constructed from these AIMD trajectories. This analysis was able to provide accurate quantification on the heterogeneous distributions of ions with different coordination states at various temperatures and melt compositions.[284,285]

**5.2.2. RMC-EXAFS for Modeling Local Environment in Dilute Alloys.** Reverse Monte Carlo (RMC) modeling, similar to the MD-EXAFS method described in the previous section, offers another way to disentangle partial contributions to the total EXAFS spectrum. During the RMC simulation, the coordinates of all atoms in the computational model are varied until the best agreement between the experimental and calculated EXAFS spectra is reached. This method was used in trivalent cation doped $CeO_2$.[286] In this example, dopant cations and oxygen vacancies are distributed in several motifs throughout the lattice, which can be hard to distinguish by conventional EXAFS fitting. RMC was used to find the most likely motif for each dopant and doping concentration whose computed spectra matches experimental EXAFS well. The optimized coordinates were used to extract detailed information about the local structure of multiple cation and anion sites, including oxygen vacancies.

**5.2.3. Neural Network Analysis for Unlocking Structural Information.** In the two methods described above, theoretical spectra that were constructed with the aid of atomistic simulations are directly used to compare with or fit to the experimental EXAFS data. ML replaces these comparison/fitting processes with more sophisticated learning frameworks. The ML methods used for XAFS analysis can be from supervised, semi-supervised, and unsupervised learning categories. In most cases, a model is designed to take input spectra (either XANES or EXAFS) and predict structural descriptors


https://doi.org/10.1021/acs.chemrev.1c00967
Chem. Rev. 2022, 122, 8758−8808

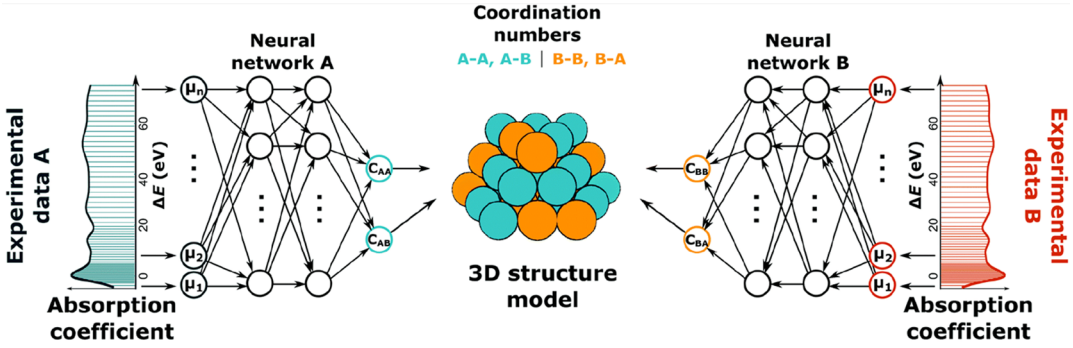


**Figure 27.** Schematic that represents the application of NN-XANES to an $A_xB_{1-x}$ bimetallic system. Partial first coordination numbers are extracted from the XANES of A and B absorbing components. The partial coordination numbers (A−A, A−B, B−B, and B−A) are used to deduce the average NP structure. Adapted with permission from ref 293. Copyright 2020 The Royal Society of Chemistry.

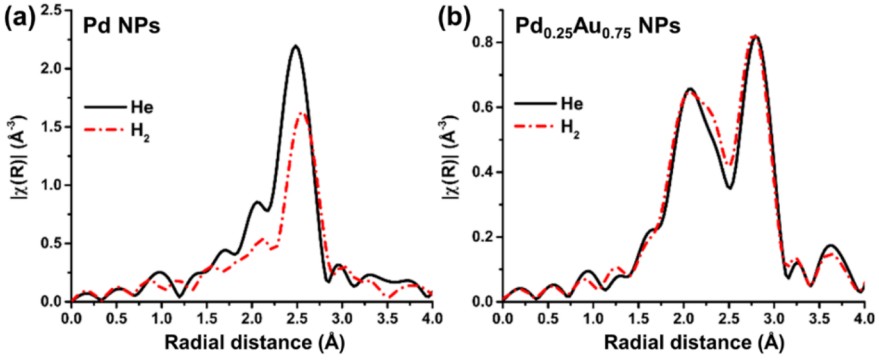


**Figure 28.** Fourier transform magnitudes of $k_2$-weighted EXAFS spectra of (a) Pd NPs and (b) $Pd_{0.25}Au_{0.75}$ RCT-$SiO_2$ under flowing He or $H_2$ at 298 K and 1 bar. Adapted with permission from ref 103. Copyright 2020 John Wiley and Sons.

or, in general, problem-specific descriptors. An inversion approach was developed by utilizing the neural network (NN) as a function that directly "inverts" the XANES spectrum to structure descriptors, including coordination numbers and distances.[287] The same method was used to invert EXAFS to the radial pair distribution function.[287] Recently, a similar inversion approach but with the more advanced self-organizing map (SOM) NNs was used to decompose and interpret the EXAFS of various technetium species as they interact with chukanovite in terms of problem-specific descriptors such as pH, redox potential, Tc loading, carbonate concentration, and contact time.[288] ML methods are also applied to enhance conventional EXAFS fitting procedures. In addition to NN-based methods, other ML methods were also explored. For example, an Extra Trees regressor algorithm was applied to enhance the ability to fit EXAFS spectra with multiple scattering paths;[289] and an evolutionary algorithm method was employed to automate EXAFS analysis, with a goal of enhancing reliability and reproducibility of results.[290]

These ML methods can provide statistical correlation among diverse configurations, more flexible analysis, and better interpretability, which is suitable for analyzing XAFS data for dilute alloys. Here, two examples are elaborated on how NN-based methods can significantly improve the analysis of XAFS data for $Pd_xAu_{1-x}$ NPs ($x$ = 0.02−0.09).

Considering a dilute alloy system composed of AB components, an ML method was developed to predict partial radial distribution function (PRDF), $g_{AB}(R)$ for A−B pairs and $g_{AA}(R)$ for A−A pairs directly from the EXAFS signal of A; similarly, $g_{BA}(R)$ for the B−A and $g_{BB}(R)$ for B−B pairs can be predicted from the EXAFS signal of B.[287,291] Absorber-specific NNs were trained to predict all four PRDFs with 250 computational PdAu NP models with different sizes, shapes, packing motifs (cuboctahedral and icosahedral), and Pd distributions. These NP structures were all equilibrated using MD simulations at different temperatures. The NNs were deployed on EXAFS data collected from the $Pd_{0.02}Au_{0.98}$ RCT-$SiO_2$ and $Pd_{0.09}Au_{0.91}$ RCT-$SiO_2$.[105] The NN-assisted EXAFS (NN-EXAFS) analysis is able to obtain the PRDF in four coordination shells, whereas this was not possible with conventional analysis. With this new information, a more detailed model was constructed, which helps to conclude the presence of surface segregation of Pd atoms in these NPs.[292]

Similarly, another NN method was developed to predict partial first coordination numbers using XANES spectra of PdAu alloy as input (Figure 27).[293] Because high-quality XANES data is easier to measure than high-quality EXAFS data in challenging conditions of high temperature, low weight loading, and reactor configuration constraints, this NN method has been used to analyze the structural information on $Pd_{0.03}Au_{0.97}$ RCT-$SiO_2$ catalyst using XANES spectra collected in situ under different gas treatments. The analysis results are consistent with the previous hypothesis that the $H_2$ treatment induces Pd dissolution into the subsurface, decreasing the number of Pd atoms on the surface.[104,245,294] The PdAu RCT-$SiO_2$ studied here is reviewed in section 3.4.2 for its catalytic performance.

**5.2.4. Novel Detection Method of Contiguous Pd Regions in PdAu Alloys.** For alloys containing Pd as one component, it is possible to discriminate between different structural motifs, notably, those in which Pd segregates to form


https://doi.org/10.1021/acs.chemrev.1c00967
Chem. Rev. 2022, 122, 8758−8808

contiguous, Pd-rich regions or homogeneously disperses in Au.[103] The key idea is that bulk Pd[295] and Pd NPs[296−298] are known to form a $\beta$-phase hydride under $H_2$ treatment. Previous EXAFS studies showed that Pd−Pd bond length increased as the octahedral fcc sites were occupied by hydrogen.[297,298] In PdAu NPs, Pd hydride also forms under $H_2$ treatment.[103] Importantly, the bond length expansion between Pd and its nearest neighbors can occur only at contiguous, 3D Pd regions but not the alloyed PdAu regions nor the low dimensional (e.g., 2D) Pd regions. Furthermore, the EXAFS measurement of Pd−Pd distance can probe contiguous Pd regions quantitatively by measuring the relative interatomic distance ($R$) change upon $H_2$ treatment compared to the baseline value under He, $(R_{H_2} - R_{He})/R_{He}$.[103]

EXAFS data were measured for Pd NPs and a $Pd_{0.25}Au_{0.75}$ RCT-$SiO_2$ system under He and $H_2$ treatment. The Pd−Pd interatomic distance in Pd NPs is consistent with the hydride formation observed in the literature.[297,298] The spectra of $Pd_{0.25}Au_{0.75}$ NPs varied upon $H_2$ treatment (Figure 28) and the quantitative fitting shows a slight increase in Pd−Pd interatomic distances. Even though the change in interatomic distance was near the limit of detectability by the conventional EXAFS fitting, the existence of contiguous Pd regions was confirmed, which is also corroborated with other experimental evidence from STEM energy-dispersive X-ray spectroscopy (STEM-EDS) and CO-DRIFTS measurements. In conclusion, this EXAFS-based method could be used as a probe of Pd hydride formation in Pd alloys with other metals and, as a result, provide insights into the nature of the distribution (homogeneous or heterogeneous) of Pd within the host metal structure.

### 5.3. Transmission Electron Microscopy Technique for Bimetallic Catalysts

TEM is particularly suitable to characterize metallic nanostructures for catalysis.[299] Combined with spectroscopy methods such as EDS or EELS, high-resolution images obtained with TEM can provide an insight into the chemistry of materials at the atomic level. Additionally, in situ TEM studies can complement traditional ex situ TEM studies to analyze materials under reaction conditions, which can image and chemically characterize a metallic catalyst in contact with reactants such as $H_2$, $O_2$, or $N_2$ under a range of temperatures. This is critical to elucidate the crucial localized features for the control and design of highly active and selective catalysts.

**5.3.1. Ex Situ Transmission Electron Microscopy for Bimetallic Catalysts.** Dark-field imaging and EDS can be used to elucidate the compositional profile of bimetallic alloy NPs. For example, dark-field STEM images of $Pd_xAu_{1-x}$ NPs[104] can show the Pd segregation zones, which are less bright. The brightness contrast is the result of the signal detected by a dark-field detector being proportional to $Z^{1.6}$ ($Z$ = 46 for Pd and 79 for Au). The quantification analysis of the EDS data can also reveal whether the Pd segregated zone is constituted of 100%. For $Pd_{0.25}Au_{0.75}$ NPs (Figure 29), Pd segregates to the edge of the particle with a Pd content of 40−45 atom %, higher than the bulk composition of 25 atom %. Similar segregation is also observed for $Pd_{0.09}Au_{0.91}$ NPs. For $Pd_{0.04}Au_{0.96}$ NPs, no Pd-rich regions were detected. However, Pd-rich regions may still exist, even though they are not detectable due to insufficient signal. The absence of large Pd clusters in $Pd_{0.04}Au_{0.96}$ NPs suggests that Pd atoms are better

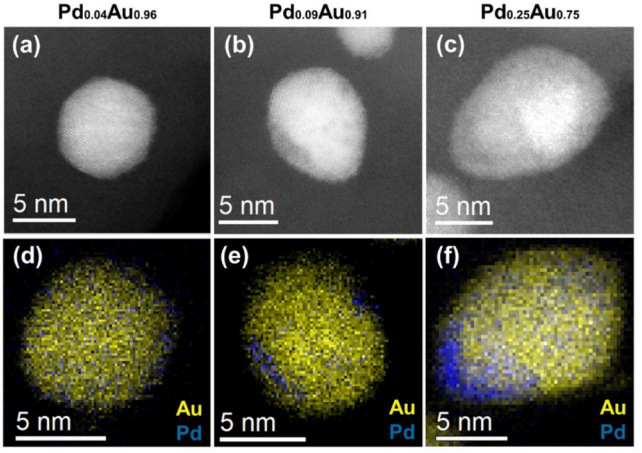


**Figure 29.** Presence of Pd-rich regions in $Pd_xAu_{1-x}$ RCT-$SiO_2$ was observed for $Pd_{0.25}Au_{0.75}$ and $Pd_{0.09}Au_{0.91}$ NPs but not in $Pd_{0.04}Au_{0.96}$ NPs. The control of the Pd distribution within individual particles is crucial to optimize the selectivity and the activity of the particles. (a−c) Dark-field STEM images of $Pd_{0.04}Au_{0.96}$, $Pd_{0.09}Au_{0.91}$, and $Pd_{0.25}Au_{0.75}$ NPs and (d−f) corresponding EDS maps, respectively.

dispersed across the surface, which contributes to the high activity and selectivity of these samples.

**5.3.2. In Situ Transmission Electron Microscopy for Bimetallic Catalysts.** In situ studies of bimetallic catalysts can complement ex situ ones to understand dynamical phenomena during reactions, such as restructuring.[103,300,301] Indeed, restructuring events can occur during reactions where an ex situ measurement cannot detect.[302]

Two methods are available to perform in situ TEM analysis: First is a dedicated ETEM where the part of the column surrounding the sample is kept under pressure, while the rest of the column is maintained under normal vacuum conditions with differential pumping. The typical maximum pressure available with an ETEM is 1 Torr but can be higher, depending on the number of pumps in the system.[303] With this setup, ETEM can be used to directly observe catalyst restructuring, such as oxidation of Cu and reduction of $Cu_2O$[304] as well as oxidation of dilute alloys of $Ni_{0.05}Cr_{0.95}$ NPs.[305] The second option is an ETEM holder (Figure 30).[302] This holder contains samples enclosed in a small microreactor, with electron-transparent windows, multiple gas inlets, and an outlet. The 50 nm electron transparent windows made of amorphous $Si_3N_4$ can sustain the pressure difference between the inside of the microreactor and the surrounding vacuum of the TEM column. The temperature can be controlled up to 1273 K, and the pressure inside the microreactor can go up to 2 atm. Examples of using the ETEM holder include studies of the crystal growth of NiCr NPs with 5−15% of Cr[306] and NP oxidation of NiFe[307] and $Ni_2Co$[308] bulk alloys.

In situ TEM with an environmental holder was used to characterize $Pd_{0.04}Au_{0.96}$ RCT-$SiO_2$ catalysts, as this specific system showed excellent catalytic properties (also reviewed in sections3.2.1 and 3.4.1). The catalyst was treated with $O_2$ at 673 K, then $H_2$ at 773 K, and finally $O_2$ at 673 K. TEM images (Figure 31) show that the particle morphology did not change during the experiment. Only several particles initially very close to each other merged at the end of the process via the center of mass migration, but the amount of merged particles is negligible. The interaction between particles and the RCT support prevents particle migration and coalescence. Because


https://doi.org/10.1021/acs.chemrev.1c00967
Chem. Rev. 2022, 122, 8758−8808

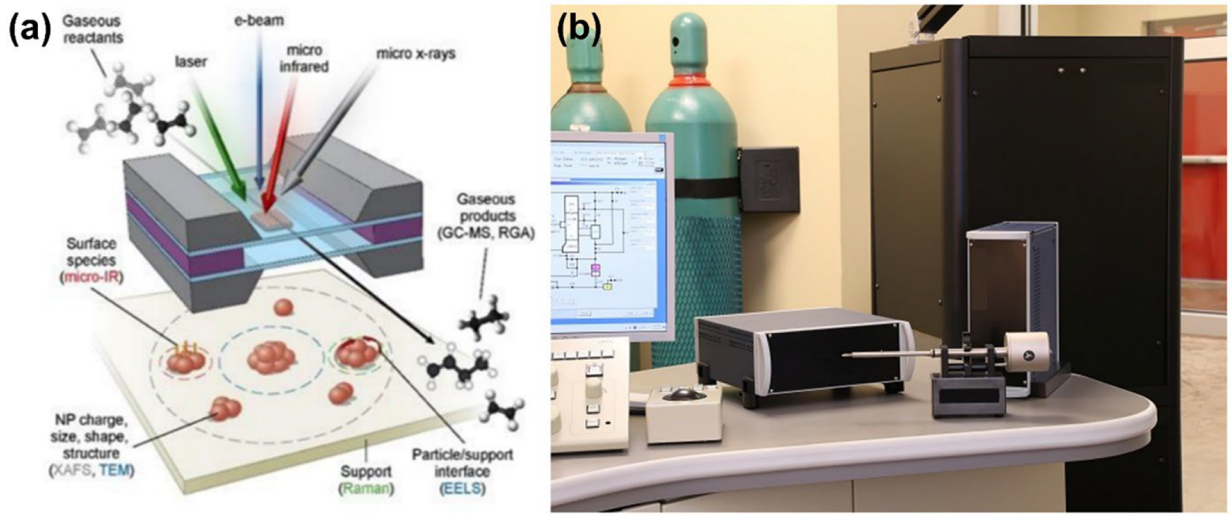


**Figure 30.** General principles of ETEM holders for in situ studies. (a) Cartoon showing how the sample is sandwiched between two electron-transparent windows and can be heated with an integrated microcoil. Small inlets and an outlet make the flow of gas possible. This approach is feasible for electron-based characterization techniques such as TEM but can also be applied to bulk approaches such as X-ray absorption spectroscopy. (b) Picture of a dedicated in situ holder for a gas-heating experiment. A software and a gas system regulate the flow of gases going through the holder. The inlet and outlet are at the bottom of the holder and can be connected to gas lines. Image in (a) is reprinted with permission from ref 309. Image in (b) used with permission from Hummingbird Scientific. Copyrights 2015 The Authors and 2022 Hummingbird Scientific.

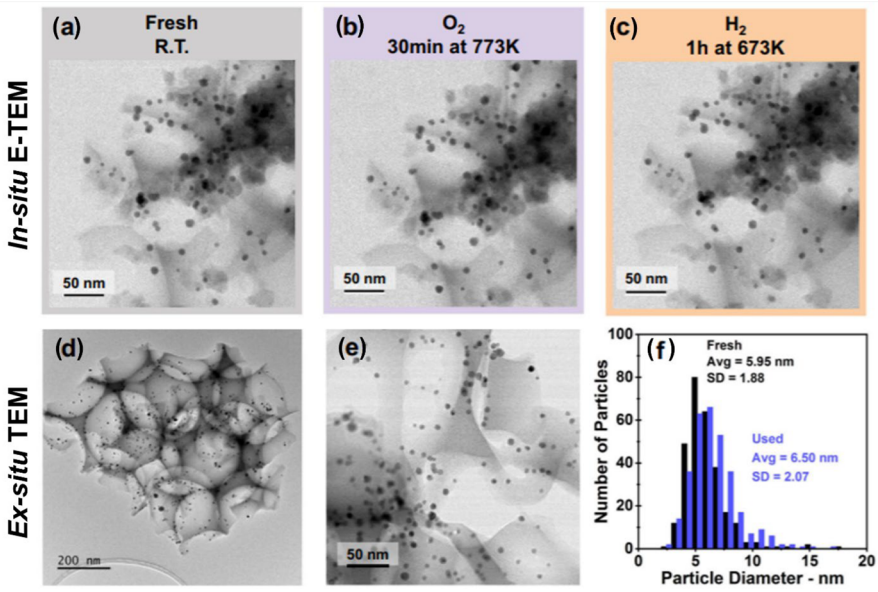


**Figure 31.** In situ TEM results compared with ex situ results; all images were taken in bright-field STEM mode. (a) Fresh $Pd_{0.04}Au_{0.96}$ RCT-$SiO_2$ at room temperature. (b) Sample after a 30 min exposure to $H_2$ at 773 K with a flow rate of 4 sccm. (c) Sample after 1 h exposure to $O_2$ at 673 K with a flow rate of 4 sccm. (d,e) Images of samples analyzed for ex situ studies. (f) Size distribution of $Pd_{0.04}Au_{0.96}$ NPs before and after treatment was obtained using images collected with ex situ TEM. The results are consistent with those collected with in situ analysis, showing the particle migration and coalescence is happening at a smaller scale. Adapted with permission from ref 104. Copyright 2020 The Authors.

of the unchanged particle morphology, internal restructuring, i.e., Pd atoms redistribute within particles, can be the only cause of the catalytic performance drop after $H_2$ treatment. However, EDS analysis performed in situ did not reveal dramatic shifts, indicating a very subtle change of the Pd distribution.

### 5.4. Machine learning Accelerated Molecular Dynamics

Computational modeling techniques have advanced the atomistic understanding of heterogeneous catalysis, correlating electronic structure to surface reactivity,[310,311] interpreting microscopic and spectroscopic observations,[312] and predicting kinetics of reaction networks.[18,313,314] Methods based on the explicit quantum mechanical treatment of electronic structures, such as DFT calculations, are critically important since they can accurately describe the forming and breaking of bonds in catalytic reactions.

However, modeling dilute alloy catalysts is still an untrivial task due to the complexity of these systems. As discussed in section 2.4, typical dilute alloy catalysts are supported NPs, where catalytically active structural motifs, such as edges,


https://doi.org/10.1021/acs.chemrev.1c00967
Chem. Rev. 2022, 122, 8758−8808

corners, and surface islands, are several nanometers in extent. At the same time, as discussed in section 4, the catalytic activity can be altered by slow surface restructuring under different pretreatments and chemical reaction conditions. Directly modeling these larger structures and slow events with AIMD is prohibitive due to AIMD's poor scaling and high computational cost. For this reason, AIMD simulations are often limited to fast reactions on small periodic surfaces[315,316] or small nanoclusters[317−319] at high temperatures.

**5.4.1. Cluster Expansions and Classical Interatomic Potentials.** Initially, cluster expansions (CE) and classical interatomic potentials were used to replace DFT for faster calculations. Both methods rely only on the information about atomic positions and do not directly consider the electronic structure. Due to their local nature, the cost of these methods scales linearly with the number of atoms, as opposed to the cubic scaling of DFT, resulting in an overall acceleration of several orders of magnitude. For example, combined with Monte Carlo, CE predicted oxygen-induced Ag segregation on AgAu surfaces[176] (also discussed in section 3.2.3), CO-induced Pd segregation on PdAu surfaces,[320] and acetylene-induced reverse segregation on PdAg surfaces.[321] Reactive force fields, such as ReaxFF[322] and COMB,[323] can model some catalytic reactions, including oxidation and dissociation of small molecules on Pt,[324,325] Cu,[326,327] Pd,[328] Ni,[329] and Fe[330] metals and their oxide surfaces.

However, the accuracy and transferability of these parametric models are limited due to their restricted analytical expressiveness. Unlike DFT, which treats electronic degrees of freedom explicitly and is thus transferable across different systems, there is no guarantee that a CE model or an interatomic potential developed for one set of reaction intermediates and bonding chemistry can work well in other scenarios that are not considered in the model construction.

**5.4.2. Machine-Learned Interatomic Potentials.** The advent of ML for developing interatomic potentials opens new possibilities in the realm of catalysis. Machine-learned interatomic potentials (MLIPs) are much more flexible than classical interatomic potentials. Additionally, they can model complex reaction pathways with many distinct bonding chemistries. With over a decade of development, noteworthy examples of MLIPs include the high-dimensional neural network (HDNN),[331−334] Gaussian approximation potential (GAP),[335] Schnet,[336] moment tensor potential (MTP),[337] spectral neighbor analysis potential (SNAP),[338] mapped force field (MFF),[339] and DeepMD,[340] in addition to recently developed fast learning of atomistic rare events (FLARE)[341−343] and neural equivariant interatomic potential (NequIP).[344]

A growing number of MLIPs have been developed to model Au-, Ag-, and Cu-based alloys. Table 5 lists several alloys discussed in sections 2−4. It is worth noting that MLIPs also have transferability issues: MLIPs that do not incorporate physical information are usually limited to specific compositions and phases. For example, potentials trained on bulk alloy data may not model NPs accurately, nor vice versa. This transferability challenge is exacerbated by the need to include the reactant and product molecules as well as the rare and often a priori unknown intermediate configuration in the training set to ensure accuracy across the catalytically relevant reaction path. Except for the CuAu potential,[345] which can model CuAu NPs in water, all MLIPs in Table 5 focus on predicting NPs or bulk alloys in vacuum, while most MLIPs that can study chemical reactions at gas/solid or liquid/solid interfaces are often limited to a single metal instead of metal alloys.[334,344,346−352]

**Table 5. List of ML Potentials Developed for Alloys**

| alloys | year | type of MLIP[a] | training set |
|---|---|---|---|
| CuZn | 2021[353] | HDNN | bulk, surface and cluster structures at up to 1400 K |
| CuNi | 2019[354] | MTP[a] | fcc, bcc, and hcp bulk |
| CuPd | 2019[355] | MTP | bcc, hcp, and fcc bulk |
| CuPt | 2019[356] | MFF | active learning on NPs |
| CuAu | 2014,[357] 2015[345] | HDNN | fcc bulk, surface, and clusters in vacuum and in water |
| PdAg | 2018[358] | NN-EA | clusters |
| | 2020[238] | FLARE | active learning on melted surface |
| | 2021[359] | GAP, MTP | fcc and bcc bulk structures and liquid-like structures at up to 3360 K |
| AgAu | 2017[360] | ANN | NPs |
| | 2021[361] | DeepMD | fcc bulk, low index surfaces, amorphous and nanoparticle at 100−1500 K |
| PdAu | 2017[235] | HDNN | fcc(111) surface |
| CuPdAg | 2019[362] | HDNN | bulk fcc and NPs |
| PtNiCu | 2018[363] | HDNN | NPs |

[a]This study includes multiple MLIPs including MBTR + KRR, MBTR + DNN, SOAP + GP, MTP (+polynomial reg), and it also trained on nine other alloys (AgCu, AlFe, AlMg, AlNi, AlTi, CoNi, CuFe, CuNi, FeV, and NbNi).

Training a robust MLIP requires DFT calculations that are representative of the reaction pathways of interest. However, efficiently exploring the landscape of these pathways and selecting configurations that are relevant for training and benchmarking the ML model accuracy is difficult. Among the examples listed in Table 5, the training data were obtained from (1) enumeration by automated workflow or evolutionary algorithms,[346,353−355,358] (2) AIMD trajectories,[359,361] and (3) active learning.[238,356] One example of an MLIP that uses active learning is FLARE.[341−343,364] Its prediction of forces for each atomic configuration is accompanied by the variance, or uncertainty of the model prediction, which enables active learning of the potential energy surface on the fly during the time evolution of the MD simulation. When the model encounters a configuration outside its training set, such as a rare transition event, causing uncertainty to exceed a certain threshold, DFT calculations are autonomously performed to acquire accurate forces and augment its training set. This approach was successfully employed to train models and perform large-scale MD of the restructuring of PdAg dilute alloy catalysts[238] reviewed in section 4.3.1, as well as the reactive simulation of $H_2$ splitting and recombination of the Pt(111) surface.[365] For the former example of active learning on PdAg, this model uses only two- and three-body terms to compare atomic environments and can be turned into a very efficient model that can simulate a million atoms on a single GPU.[342]

**5.4.3. Automated Mechanism Extraction from Molecular Dynamics.** MLIPs are beginning to enable quantum-accurate simulations of reactive dynamics over microseconds, long enough to capture catalyst restructuring at gas−solid or liquid−solid interfaces and to understand microscopic mechanisms governing catalysis and material degradation. The large amount of data captured by long MD trajectories


https://doi.org/10.1021/acs.chemrev.1c00967
Chem. Rev. 2022, 122, 8758−8808

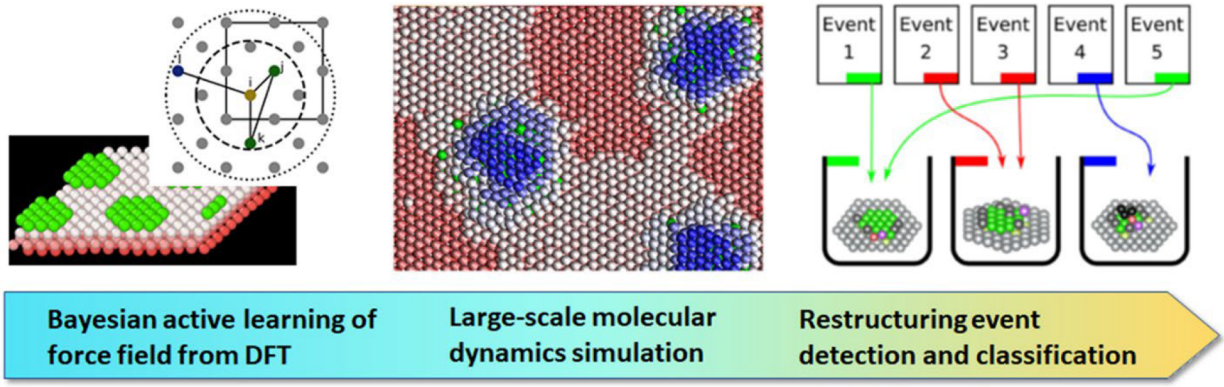


**Figure 32.** Automated workflow to discover restructuring events on surfaces of PdAg dilute metal alloy from MD with MLIPs.

brings additional challenges to data management and postprocessing, especially automated extraction of rare events and reaction mechanisms.

Unambiguously determining the initial and final states of rare transition events and categorizing them is a research frontier.[366] In the example of surface segregation in binary alloys discussed in section 4.3.1, high-temperature MD simulations were used to explore the energy landscape and restructuring events of bimetallic PdAg surfaces. By isolating restructuring events in classical force field simulations of a single-component Ag surface and estimating the reaction barriers using DFT, new predominant classes of mechanisms controlling rearrangement at step edges were found.[245] A more complex bimetallic system was later modeled with more accurate GP MLIPs, and reactive events were analyzed by an automated workflow.[238] Furthermore, Ag encapsulation of the Pd island, prior to the layer-by-layer Pd dissolution, was observed in a microsecond-long simulation of thousands of atoms (Figure 32).

## 6. CONCLUSION AND OUTLOOK

### Bridging between Model Systems and Catalytic Systems

The research described herein is sharply focused on the development of design principles for dilute alloy catalysts that can be used in more energy-efficient chemical synthesis. Because of the complexity of heterogeneous catalytic processes, a comprehensive approach that integrates experiment and theory is required. The approach described in this review integrates fundamental studies at low pressure using well-defined single crystals, first-principles theory on model systems, and kinetic studies of dilute alloy catalysts under catalytic conditions. The ability to advance understanding of other catalytic processes using fundamental theoretical and experimental studies has been exemplified by several groups,[367,368] further establishing the validity of this approach. This methodology provides valuable insights into the key factors that determine reaction selectivity, as demonstrated for several different dilute alloy systems. For example, the mechanisms and rate constants determined for selective alcohol oxidation on Au single crystals and anhydrous aldehyde production on Cu single crystals provided a framework for predicting performance of Au- and Cu-based dilute alloy catalysts.

A major breakthrough was the ability to quantitatively model changes in the selectivity for alcohol oxidation over npAgAu alloys.[159] Transient kinetic measurements performed for methanol oxidation catalyzed by npAgAu at operational temperatures provided a critical bridge to the model studies at low pressure and low temperature, enabling prediction of changes in selectivity over several orders of magnitude of pressure and several hundred degrees of temperature. Furthermore, scaling relationships obtained from DFT measurements successfully predicted selectivity for oxidation of higher chain alcohols.[17] This set of studies clearly illustrates the predictive power of molecular-level understanding of the reaction network for catalytic processes.

The ability to accurately model selective oxidation reactions on Au-based materials relied on several important factors. First, the surface concentrations of reactants must be similar under lower pressure and temperature to those achieved under catalytic conditions. Hence, the reactions of interest must occur at sufficiently low temperature (with a low enough barrier) that reactants have a sufficient surface lifetime for reaction to occur. Selective hydrogenation reactions on the PdAu and PdAg alloys are an example of a more challenging system because the binding of hydrogen atoms on these materials is relatively weak, leading to desorption below room temperature at low pressure. Nevertheless, DFT models provide insight into reaction mechanisms and key kinetic steps as a complement to reactor studies, which can guide the understanding and prediction of the function of dilute alloy catalysts.

A second critical factor that is important for connecting fundamental studies to catalytic performance is that the state of the surfaces must be the same both for the models and the working catalysts. Thus, if spectator species accumulate under catalytic conditions, they must also be included in any experimental or theoretical models. The fact that Au is itself relatively unreactive renders it ideal for investigations spanning vast pressure and temperature ranges. Besides the potential influence of spectators, the distribution of the reactive minority metal on the surface is also a key factor, as discussed below.

### 6.1. Understanding the Function of Dilute Alloy Catalysts

The specific focus on dilute alloy catalysts for improving reaction selectivity was motivated by the potential to use the bifunctionality of two dissimilar materials. The underlying principle is that the more reactive minority metal, e.g., Pd, Ni, Pt, or Ag would initiate the catalytic cycle, and the less reactive host, e.g., Au, Ag, or Cu, would impart selectivity. Based on the progress so far, it is clear that this concept, while valuable, is too simplistic. First of all, the distribution of the reactive minority metal on the surface is important but often difficult to


https://doi.org/10.1021/acs.chemrev.1c00967
Chem. Rev. 2022, 122, 8758−8808

control. Bonding and reactivity are generally different for single atoms, small ensembles of a few atoms, and larger islands, rendering specific knowledge of the state of the surface crucial. Furthermore, migration of intermediates across boundaries between dissimilar metals may also be challenging and may only occur under specific conditions that are not readily accessible either during catalysis or in model studies. The migration of adsorbed hydrogen atoms from Pd to Ag, discussed in section 4.3, is such an example.[255]

Control of the distribution and concentration of the minority metal atoms at the surface of the catalyst under reaction conditions is critical, as mentioned above. The reactive metal atoms must be at or near the surface to participate in reactive steps. On the other hand, the active metals are often more stable in the bulk. For example, Pd is most stable as dispersed atoms in the bulk of either Au or Ag on a pristine surface.[25,104]

Fortunately, pretreatment of the dilute alloys can be used to provide a thermodynamic driving force for segregation of the reactive metal to the surface. For example, Pd is segregated to the surface of dilute PdAu NPs via oxidation at higher temperature (573 K)[104]—an effect also previously demonstrated on single-crystal Pd/Au(111) models.[369] Similarly, segregation of Ag in the npAgAu catalysts was effected by oxidative pretreatment.[62,74] In both of these cases, the reactive state of the material was maintained under catalytic conditions by operating in a temperature regime where diffusion of the minority metal is not too rapid. A second factor is that reactants present in the ambient gas phase can stabilize the more reactive metal at the surface. Clearly, it is important to determine the distribution and structure of the active metal on the catalyst surface under reaction conditions.

The ability to synthesize well-defined and stable catalyst materials is essential to testing the underlying principles developed in fundamental work. The intrinsic behavior of dilute alloy catalysts would ideally be tested in the absence of a support material. The success of understanding the catalytic function of npAgAu is illustrative of this approach. On the other hand, not all dilute alloy catalysts of interest can be synthesized as support-free materials. Furthermore, practical catalysts generally contain an inert support material, such as a metal oxide. Advances in materials synthesis have resulted in the ability to prepare NP alloys with controlled composition and structure with homogeneity achieved at the atomic scale.[141,370−373] These materials can be incorporated into oxide or other supports and studied as catalysts. The specific creation of the RCT oxides[101,138] has been particularly successful because the synthetic method yields a very stable material that is resistant to sintering. This stability is attributed to the fact that the alloy NPs are embedded in the oxide support.

While metallic species play the most prominent role in the catalytic processes discussed above, recent work provides evidence that confinement effects at the interface between the metal and support can influence both activity and selectivity.[374−376] Confinement effects in catalysis are somewhat understood for microporous materials such as zeolites, but the interface between metals and oxides is less explored. Understanding such effects could allow tailoring these interfaces to favor specific reaction pathways, thus inducing changes in selectivity. Moreover, nanoarchitectures in which the oxide support is permeable to small molecules, such as in the case of some silicates, can benefit not only from confinement effects but also from size-selective access of reactant molecules to the active site.[374−376] This provides exciting new opportunities to carry out systematic studies comparing these interfaces for 2D silicates on metal supports and encapsulated NPs in RCT-$SiO_2$ catalysts.

### 6.2. Advancing Characterization and Modeling for Catalysts in Action

Development of cutting-edge theoretical and experimental tools is essential to understanding how to optimize the distribution of the active metal on the surface under reaction conditions. Operando tools, such as EXAFS and ambient pressure TEM, are examples of powerful experimental tools; however, very dilute alloys present challenges in sensitivity. Accordingly, new approaches to determining metal atoms distribution, such as application of ML techniques, are being developed.

The expansive configurational space of dilute metal sites in bimetallic catalysts results in a vast ensemble of candidate structures that cannot be handled by theoretical methods, even with the advent of exascale and petascale computational capabilities. One promising method is to narrow the range of candidate structures using experimental XANES and/or EXAFS spectra for obtaining their descriptors from the spectra. New directions in this area will also aim at exploring in greater detail the information content in experimental data to understand the number, and the physical meaning, of descriptors stored in the spectra. More work is needed to identify those which are directly responsible for reactivity, i.e., activity descriptors.

New computational tools are also required to understand how the components of the alloy materials distribute under various conditions. To this end, automated workflows[245] and ML techniques are under development. Accurate ML interatomic potentials[341,342,344] can replace DFT force calculations and accelerate MD by several orders of magnitude. Furthermore, dimensionality reduction and multitask learning[377] can be employed to extract data-driven collective variables that are then used to guide enhanced sampling techniques for efficient calculations of free energy barriers and transition rates of reactions.

Advances in automated training of fast accurate uncertainty-aware ML interatomic potentials (MLIPs) and data-driven discovery of low-dimensional reaction manifolds will enable new types of multiscale computational methods to study the reactive dynamics of heterogeneous catalysis systems. In this emerging direction there remain several key challenges: (1) developing fast and accurate MLIPs that break the cost-accuracy trade-off for highly diverse chemical configurations, (2) devising autonomous training and benchmarking protocols that ensure the transferability of MLIPs over different intermediate structures in the reaction network, (3) advancing autonomous algorithms for detecting and analyzing rare events in large-scale MD, (4) designing robust unsupervised and efficient algorithms for free energy landscape exploration and estimation of reaction rates.

Further advancement of these and other methods that probe surface structure, composition and rearrangement will provide insights into how to control the state of the catalyst surface to optimize selectivity using reaction conditions and materials properties. These same methods will be broadly applicable to understanding complex materials relevant to other applications, such as electrocatalysis and energy storage.


https://doi.org/10.1021/acs.chemrev.1c00967
Chem. Rev. 2022, 122, 8758−8808

### 6.3. Challenges

Significant advances in understanding of catalytic processes at a molecular scale have clearly been made; however, several challenges remain. One of the most significant challenges is the need to accelerate the development of new and efficient catalytic processes through a more rapid cycle of prediction-synthesis-characterization-testing.

Rapid screening of specific alloy configurations and compositions can be performed for simple elementary steps, e.g., $H_2$, $O_2$, or C−H dissociation. These initial steps can be modeled for specific ensembles and for simple steps using DFT. On the other hand, modeling a complex reaction network without input from experiment is currently very challenging. Furthermore, accurate modeling of the state of the surface under reaction conditions is not possible from first-principles only.

Rapid controlled synthesis of specific alloy catalyst materials is also challenging, often requiring specialized synthetic methods and detailed experimental characterization. Once a material is made, catalytic testing is required under different conditions and using specific pretreatment protocols. Detailed understanding of these phenomena is time-intensive; hence, efficient approaches are needed.

One potential approach is to test the efficacy of initial elementary steps, e.g., $H_2$, $O_2$, or C−H dissociation, on low surface area, unsupported thin film alloys. Indeed, it is even possible to investigate alloys with gradients of composition as a means of screening composition effects.[378] This approach could be coupled with investigation of pretreatment and reaction conditions and with spectroscopic methods to provide more rapid evaluation and comparison to theoretical predictions. The use of thin films is compatible with fundamental studies of elementary steps using temperature-programmed methods and with the use of surface-sensitive spectroscopic probes. While the challenge of making well-controlled catalysts will remain, this more rapid screening would provide guidance on the most promising compositions.

Computational challenges lie in the need for improved kinetic modeling that spans the multitude of length and time scales relevant to heterogeneous catalytic processes. As described above, enhanced sampling techniques for efficient calculation of free energy barriers and transition rates of reactions is crucial.

Significant progress in understanding how dilute alloy catalysts can be used to enhance the selectivity of key synthetic reactions has been made. Insights at the molecular scale provide predictive power over a wide range of conditions. Even so, advancement in methods to probe structure−reactivity relationships and rapidly screen specific systems is required. The bifunctionality of dilute alloy catalysts, where the reactive minor metal initiates the catalytic cycle while the host metal imparts selectivity, can improve the activity, selectivity and stability in oxidation and hydrogenation reactions. However, the complexity of the structure under pretreatment and/or reaction conditions along with the migration of reactive species still needs careful consideration. The challenges brought by the dilute nature of materials of interest has stimulated the advancement of new experimental and theoretical methodologies to understand the evolution of structure and composition of catalysts and their relationship to catalytic function. The integrated theoretical−computational−experimental approach has been shown able to "bridge the divide" between fundamental knowledge and design of catalytic processes in complex dilute alloy systems spanning vast pressure and temperature ranges. This comprehensive approach provides a framework for generalization to other related catalytic processes and a new paradigm for catalyst discovery.

## AUTHOR INFORMATION


### Corresponding Authors

**Philippe Sautet** − *Department of Chemical and Biomolecular Engineering, University of California, Los Angeles, Los Angeles, California 90095, United States; Department of Chemistry and Biochemistry, University of California, Los Angeles, Los Angeles, California 90095, United States;* orcid.org/0000-0002-8444-3348; Email: sautet@ucla.edu

**Cynthia M. Friend** − *Department of Chemistry and Chemical Biology, Harvard University, Cambridge, Massachusetts 02138, United States; John A. Paulson School of Engineering and Applied Sciences, Harvard University, Cambridge, Massachusetts 02138, United States;* orcid.org/0000-0002-8673-9046; Email: friend@fas.harvard.edu

### Authors

**Jennifer D. Lee** − *Department of Chemistry and Chemical Biology, Harvard University, Cambridge, Massachusetts 02138, United States;* orcid.org/0000-0003-2644-3507

**Jeffrey B. Miller** − *Department of Chemistry and Chemical Biology, Harvard University, Cambridge, Massachusetts 02138, United States;* orcid.org/0000-0002-2041-3684

**Anna V. Shneidman** − *John A. Paulson School of Engineering and Applied Sciences, Harvard University, Cambridge, Massachusetts 02138, United States*

**Lixin Sun** − *John A. Paulson School of Engineering and Applied Sciences, Harvard University, Cambridge, Massachusetts 02138, United States;* orcid.org/0000-0002-7971-5222

**Jason F. Weaver** − *Department of Chemical Engineering, University of Florida, Gainesville, Florida 32611, United States;* orcid.org/0000-0002-6777-4727

**Joanna Aizenberg** − *Department of Chemistry and Chemical Biology, Harvard University, Cambridge, Massachusetts 02138, United States; John A. Paulson School of Engineering and Applied Sciences and Wyss Institute for Biologically Inspired Engineering, Harvard University, Cambridge, Massachusetts 02138, United States;* orcid.org/0000-0002-2343-8705

**Juergen Biener** − *Nanoscale Synthesis and Characterization Laboratory, Lawrence Livermore National Laboratory, Livermore, California 94550, United States;* orcid.org/0000-0002-3722-3924

**J. Anibal Boscoboinik** − *Center for Functional Nanomaterials, Brookhaven National Laboratory, Upton, New York 11973, United States;* orcid.org/0000-0002-5090-7079

**Alexandre C. Foucher** − *Department of Materials Science and Engineering, University of Pennsylvania, Philadelphia, Pennsylvania 19104, United States;* orcid.org/0000-0001-5042-4002

**Anatoly I. Frenkel** − *Department of Materials Science and Chemical Engineering, Stony Brook University, Stony Brook, New York 11794, United States; Division of Chemistry, Brookhaven National Laboratory, Upton, New York 11973, United States;* orcid.org/0000-0002-5451-1207




https://doi.org/10.1021/acs.chemrev.1c00967
Chem. Rev. 2022, 122, 8758−8808

**Jessi E. S. van der Hoeven** − *Department of Chemistry and Chemical Biology, Harvard University, Cambridge, Massachusetts 02138, United States; John A. Paulson School of Engineering and Applied Sciences, Harvard University, Cambridge, Massachusetts 02138, United States;* orcid.org/0000-0001-9832-289X

**Boris Kozinsky** − *John A. Paulson School of Engineering and Applied Sciences, Harvard University, Cambridge, Massachusetts 02138, United States;* orcid.org/0000-0002-0638-539X

**Nicholas Marcella** − *Department of Materials Science and Chemical Engineering, Stony Brook University, Stony Brook, New York 11794, United States;* orcid.org/0000-0002-2224-532X

**Matthew M. Montemore** − *Department of Chemical and Biomolecular Engineering, Tulane University, New Orleans, Louisiana 70118, United States;* orcid.org/0000-0002-4157-1745

**Hio Tong Ngan** − *Department of Chemical and Biomolecular Engineering, University of California, Los Angeles, Los Angeles, California 90095, United States*

**Christopher R. O'Connor** − *Department of Chemistry and Chemical Biology, Harvard University, Cambridge, Massachusetts 02138, United States;* orcid.org/0000-0002-9224-9342

**Cameron J. Owen** − *Department of Chemistry and Chemical Biology, Harvard University, Cambridge, Massachusetts 02138, United States; John A. Paulson School of Engineering and Applied Sciences, Harvard University, Cambridge, Massachusetts 02138, United States;* orcid.org/0000-0002-2543-7415

**Dario J. Stacchiola** − *Center for Functional Nanomaterials, Brookhaven National Laboratory, Upton, New York 11973, United States;* orcid.org/0000-0001-5494-3205

**Eric A. Stach** − *Department of Materials Science and Engineering, University of Pennsylvania, Philadelphia, Pennsylvania 19104, United States;* orcid.org/0000-0002-3366-2153

**Robert J. Madix** − *John A. Paulson School of Engineering and Applied Sciences, Harvard University, Cambridge, Massachusetts 02138, United States;* orcid.org/0000-0002-3132-2382

Complete contact information is available at: https://pubs.acs.org/10.1021/acs.chemrev.1c00967

## Notes

The authors declare no competing financial interest.

## Biographies

Jennifer D. Lee is currently a postdoctoral fellow working with Professor Cynthia M. Friend and Professor Robert J. Madix in the Department of Chemistry and Chemical Biology at Harvard University. Lee received her Ph.D. in Chemistry from the University of Pennsylvania in 2020, under the supervision of Professor Christopher B. Murray. Her research is focused on the design of atomically precise, nanostructured materials for efficient and sustainable catalysis, with a current focus on Cu-based materials for selective hydrogenation and oxidation reactions.

Jeffrey B. Miller is currently the executive director of the IMASC Energy Frontier Research Center. He received a Ph.D. in Applied Physics from Harvard University, and an M.Phil. in Statistics from Cambridge University in the UK. He has worked on exotic quasiparticle states of matter as an early member of Microsoft's "Station Q" quantum computing project and has helped bring innovative solar and energy storage technologies to the market at various startup ventures.

Anna V. Shneidman is a postdoctoral fellow in the John A. Paulson School of Engineering and Applied Sciences at Harvard University in the group of Professor Joanna Aizenberg. She received her Ph.D. in Chemical Physics at Harvard University in May 2016 for her thesis work on nanoscale optics in the laboratory of Professor Marko Lončar. Among other topics, she developed a high-throughput method for on-chip photonics using roll-to-roll processing of polymers during this time. Anna is now studying self-assembled inverse opal structures for photonic, catalytic, and photocatalytic applications.

Lixin Sun is a postdoctoral researcher working at Harvard John A. Paulson School of Engineering and Applied Sciences, working with the group of Prof. Boris Kozinsky. She received her BS in Physics from Peking University and her Ph.D. in Nuclear Science and Engineering from Massachusetts Institute of Technology. Her research focuses on applying and developing novel and highly accurate atomistic simulation methods to discover functional materials for next-generation catalysis and energy technology. Her thesis work elucidated the atomistic mechanisms of ion transport and surface reactivity on microstructures in solid-state mixed ionic−electronic conducting materials. This scientific groundwork led to design rules for solid oxide fuel cells, redox-based resistive memories, and oxide-based catalysts. She currently focuses on developing machine learning algorithms that can significantly accelerate the modeling of long-time-scale evolution in metal catalysts.

Jason F. Weaver is currently the Dow Chemical Company Foundation Term Professor of Chemical Engineering and an Affiliate Professor of Chemistry at University of Florida. He received a Ph.D. in Chemical Engineering at Stanford University in 1998. His research focuses on advancing the molecular-level understanding of surface chemical reactions through application of ultrahigh vacuum and in situ surface analysis methods as well as molecular simulations. Specific topics of focus include the growth and surface chemistry of late transition-metal oxides and rare earth oxide films, dilute alloys and the oxidation chemistry of small molecules particularly alkanes. He is a Fellow of the American Vacuum Society and has published over 115 peer-reviewed articles.

Joanna Aizenberg is the Amy Smith Berylson Professor of Materials Science, Professor of Chemistry and Chemical Biology at Harvard University. She received her MS degree in Chemistry from Moscow State University and the Ph.D. degree in Structural Biology from the Weizmann Institute of Science. After a postdoc at Harvard and nearly a decade at Bell Laboratories, Aizenberg joined Harvard University, where she is conducting research aimed at understanding some of the basic principles of biological architecture and the economy with which nature solves complex problems in the design of multifunctional, adaptive materials. These biological principles are then used as guidance in developing new, bioinspired synthetic routes and nanofabrication strategies that would lead to advanced materials and devices, with broad implications in fields ranging from architecture to catalysis and from energy efficiency to medicine. Aizenberg is elected to the National Academy of Sciences, National Academy of Engineering, American Academy of Arts and Sciences, American Philosophical Society, American Association for the Advancement of Science; and she is a Fellow of the American Physical Society, Materials Research Society and External Member of the Max Planck Society. Aizenberg's select awards include MRS



https://doi.org/10.1021/acs.chemrev.1c00967
Chem. Rev. 2022, 122, 8758−8808

Medal, Kavli Innovations in Chemistry Leader Award, ACS; Fred Kavli Distinguished Lectureship in Nanoscience, MRS; Ronald Breslow Award for the Achievement in Biomimetic Chemistry, ACS; Harvard's Ledlie Prize. She has >280 publications, >80 issued patents, and is a founder of four start-up companies.

Juergen Biener is a staff scientist at the Lawrence Livermore National Laboratory (LLNL), and his research interest lies at the intersection of surface chemistry, physics and mechanics of nanostructured materials. Juergen Biener received his diploma degree in Chemistry from the Ludwig-Maximilians-Universität in Munich in 1989. He continued his doctoral research in the field of plasma-wall interactions at the Max-Planck-Institute of Plasma Physics (IPP) in Garching and received his Ph.D. in physics in 1994. From 1997 to 2000, he worked with Bob Madix at Stanford University on metal oxide catalysts, and in 2000 he returned to the IPP to continue his research on plasma-wall interactions. In 2003, he joined the Center for Imaging and Mesoscale Structures at Harvard University where started to work on gold catalysis, and then later that year he became a founding member of LLNL's Nanoscale Synthesis and Characterization Laboratory. At LLNL, he works on development, surface engineering, and integration of mesoporous materials for energy related applications including inertial confinement fusion, electrical energy storage, actuation and catalysis. He made many important contributions advancing our knowledge of interfacial properties of mesoporous materials and has an extensive background in materials development and surface characterization, coatings, and mechanical testing. He has published over 250 peer reviewed papers and 50 patents.

J. Anibal Boscoboinik is a Materials Scientist at the Center for Functional Nanomaterials at Brookhaven National Laboratory and an Adjunct Professor at Stony Brook University. He obtained his Ph.D. (2010) at the University of Wisconsin Milwaukee and was an Alexander von Humboldt Research Fellow at the Fritz-Haber Institute of the Max-Planck Society in Berlin (2011−2013). His work focuses on surface science studies using and advancing in situ spectroscopies, focusing on the synthesis and analysis of nonconventional 2D materials and confinement effects within them and at the interface with their supports.

Alexandre C. Foucher received a combined BS/MS in Mechanical and Industrial Engineering at Arts et Métiers ParisTech, France, in 2017. He also completed in parallel a Master of Materials Science and Nanoengineering at Rice University. He is now a Ph.D. candidate in materials science and engineering at University of Pennsylvania in Philadelphia. His research focuses on in situ diagnostics using transmission electron microscopy in order to understand structural changes in novel materials.

Anatoly Frenkel is a Professor in the Department of Materials Science and Chemical Engineering at the Stony Brook University and a Senior Chemist (Joint Appointment) at the Division of Chemistry, Brookhaven National Laboratory. He received MS degree from St. Petersburg University and Ph.D. degree from Tel Aviv University, all in Physics, followed by a postdoctoral appointment at the University of Washington. His research interests focus on development and applications of in situ and operando synchrotron methods to solve a wide range of materials problems, with most recent emphasis on catalysis, electromechanical materials, filtration materials, quantum dots, as well as machine learning methods for structural analysis and design of functional nanomaterials. He is a Fellow of the American Physical Society. He has published over 400 peer-reviewed articles.

Jessi E.S. van der Hoeven is currently assistant professor at Utrecht University in The Netherlands. Previously, she worked as a postdoctoral fellow in the Chemistry and Chemical Biology department and in the John A. Paulson School of Engineering and Applied Sciences at Harvard University in the groups of Professor Cynthia M. Friend and Professor Joanna Aizenberg. She received her Ph.D. degree from Utrecht University working with Professor Alfons van Blaaderen and Prof. Petra E. de Jongh. Her research focusses on the design of novel catalyst structures using colloid synthesis techniques and advanced electron microscopy to study catalyst materials in 3D and under operating conditions.

Boris Kozinsky is the Thomas D. Cabot Associate Professor of Computational Materials Science at the Harvard School of Engineering and Applied Sciences. He studied at MIT for his BS degrees in Physics, Mathematics, and Electrical Engineering and Computer Science, and received his Ph.D. degree in Physics also from MIT. He then established and led the atomistic computational materials design team at Bosch Research in Cambridge MA. In 2018, he started the Materials Intelligence Research group at Harvard that works at the intersection of fundamental materials physics, computational chemistry, and data science. His group develops and uses atomistic and electronic structure computations and machine learning for understanding and predicting quantum-level microscopic effects, particularly ionic, electronic and thermal transport and transformations in materials for energy storage and conversion. His work on the development and application of computational methods led to computation-driven design of materials in a wide range of materials systems, including 1D and 2D materials, piezoelectrics, thermoelectrics, batteries, superionic conductors, catalysts, and functional polymers.

Nicholas Marcella received his Ph.D. in materials science and engineering from Stony Brook University and is currently a visiting postdoctoral researcher with the Structure and Dynamics of Applied Nanomaterials (SDAN) group at Brookhaven National Laboratory. Nick is interested in developing new ways to unveil and analyze the complex dynamics of nanomaterials while they are active, as this information is required to fully understand, optimize, and eventually create novel materials.

Matthew M. Montemore is the Robert and Gayle Longmire Early Career Professor at Tulane University in the Department of Chemical and Biomolecular Engineering. Previously, he received his BA in physics at Grinnell College and his PhD in mechanical engineering at the University of Colorado Boulder, followed by postdoctoral studies in chemistry at Harvard University. His research interests include computational studies of catalysts and computational design of materials for energy applications.

Hio Tong Ngan received his BS in chemical engineering from the University of California, Berkeley in 2018. He is currently a Ph.D. student in the Department of Chemical and Biomolecular Engineering at UCLA, working under Professor Philippe Sautet's supervision. His research primarily focuses on using the computational approach to understand the hydrogenation mechanisms of organic molecules on single-atom alloy (SAA) catalysts.

Christopher R. O'Connor received his BS in chemistry at the University of California, Santa Barbara, in 2015. He received his A.M. and Ph.D. in chemistry and chemical biology at Harvard University in 2017 and 2020 under the guidance of Prof. Cynthia M. Friend. He is currently conducting postdoctoral research in the Physical and Computational Sciences Directorate and Institute for Integrated Catalysis at Pacific Northwest National Laboratory under the guidance of Greg Kimmel and Zdenek Dohnálek. His research interests include the behavior of model catalysts under ultrahigh vacuum and near-ambient-pressure conditions using a combination of advanced spectroscopy and microscopy.


https://doi.org/10.1021/acs.chemrev.1c00967
Chem. Rev. 2022, 122, 8758−8808

Cameron J. Owen received his Hons. BS in chemistry and BS in physics at the University of Utah in 2019. He received his M.Phil. in chemistry from Cambridge University in the UK in the Surface Science Group under the supervision of Professor Stephen J. Jenkins. His thesis considered the stability and reactivity of single-atom catalysts on a ceria support using theoretical methods. He is currently a Ph.D. student in the Department of Chemistry and Chemical Biology at Harvard University and a member of the Materials Intelligence Research Group, under the direction of Professor Boris Kozinsky. His research focuses on modeling catalytic systems on extended surfaces and nanoparticles using active machine learning approaches.

Dario J. Stacchiola is the Interface Science and Catalysis Group Leader at the Center for Functional Nanomaterials-Brookhaven National Laboratory (CFN-BNL). He obtained his BS degree (1997) at UNSL (Argentina), his Ph.D. (2002) at the University of Wisconsin Milwaukee, and was a Humboldt Research Fellow at the Fritz-Haber-Institute in Berlin (2005−2007). His research focuses on surface chemistry studies by in situ tools, in particular structure−reactivity relationships in catalysis. He is the author of over 170 peer-reviewed publications.

Eric A. Stach is the Robert D. Bent Professor of Engineering in the Department of Materials Science and Engineering at the University of Pennsylvania and Director of the Laboratory for Research on the Structure of Matter, a National Science Foundation sponsored Materials Research Science and Engineering Center. He received his BSE from Duke University, his Ph.D. in Materials Science and Engineering from the University of Virginia, and an MBA at Stony Brook University in 2018. He is a Co-founder and Chief Technology Officer of Hummingbird Scientific. He is a Fellow of the American Physical Society, Materials Research Society, and the Microscopy Society of America.

Robert J. Madix's pioneering fundamental research established the molecular foundation for elementary surface reactions on catalytic metals. Madix was the first surface scientist to undertake cutting-edge research on the surface chemistry of complex molecules on well-defined metallic surfaces. The first application of surface science studies to heterogeneous catalysis was achieved by Madix in the seminal studies of methanol oxidation to formaldehyde over Ag(110) surfaces. These seminal studies also significantly influenced the surface science community in subsequent years. These studies provided additional fundamental insight into the kinetics and mechanisms of surface reactions. Madix is the Charles Lee Powell Emeritus Professor of Chemical Engineering at Stanford University and Senior Research Fellow in the School of Applied Science & Engineering at Harvard University. He received a BS degree in chemical engineering from the University of Illinois and a Ph.D. degree in chemical engineering from the University of California, Berkeley. He is the recipient of an Alexander von Humboldt Senior Scientist Award, the Paul Emmett Award for Fundamental Studies in Heterogenous Catalysis, the Alpha Chi Sigma Award for Fundamental Research from the AIChE, the Arthur Adamson Award of ACS, the Henry J. Albert Award of the International Institute of Precious Metals, and the Gabor Somorjai Award in Catalysis of the ACS. Madix is co-Deputy Director of the IMASC Energy Frontier Research Center.

Philippe Sautet has studied at "Ecole Polytechnique" in Paris and defended his doctorate in Theoretical Chemistry at Orsay University (Paris XI) in 1989. He then joined the Centre National de la Recherche Scientifique (CNRS) at the Institute of Research on Catalysis in Lyon, where he developed and led a group devoted to the applications of theoretical chemistry to heterogeneous catalysis. He spent a sabbatical at Berkeley University. After being the director of the laboratory of Chemistry at the Ecole Normale Supérieure of Lyon for 8 years, he was the director of the "Institut de Chimie de Lyon," a cluster of chemistry laboratories in Lyon, from 2007 to 2015. Philippe Sautet is now Distinguished Professor at the Chemical and Biomolecular Engineering department and at the Chemistry and Biochemistry department of the University of California, Los Angeles (UCLA). He acts as the vice chair for graduate studies of the Chemical and Biomolecular Engineering department and is the deputy director of the IMASC Energy Frontier Research Center. He was associate editor of ACS Catalysis, an international journal published by the American Chemical Society from 2012 to 2021. His research interests are in the theory of the electronic structure at the interface between a solid surface and molecules and the modeling of elementary steps of heterogeneous catalysis. He received several awards including the silver medal of CNRS in 2007, the Paul Pascal Prize of the French Academy of Science in 2008 and the Pierre Süe Grand Prize of the French Chemical Society in 2012. He was elected at the French Academy of Science in 2010. In addition, France distinguished him in 2011 as "Chevalier de l'Ordre National du Mérite" for his action in research and research organization and in 2015 as "Chevalier de l'ordre des palmes académiques" for his teaching and action toward students.

Cynthia M. Friend is the President of the Kavli Foundation and on leave from Harvard University, where she is the T.W. Richards Professor of Chemistry. Friend joined the Harvard faculty in 1982, earned her Ph.D. in physical chemistry at the University of California, Berkeley in 1981, and received a BS in Chemistry from University of California, Davis in 1977. She was a postdoctoral fellow at Stanford University, 1981−1982. Friend's research focuses on developing solutions to important problems in energy usage and environmental chemistry. She also continues to advance diversity and excellence in scientific research and teaching through her leadership. She is the Director of the IMASC Energy Frontier Research Center at Harvard, which focuses on sustainable production of chemicals. Friend received several national and international awards for her research. She is a fellow of the National Academy of Sciences, American Academy of Arts and Sciences, the American Association of the Advancement of Science, and the American Chemical Society.

## ACKNOWLEDGMENTS

This work was supported as part of the IMASC, an Energy Frontier Research Center funded by the U.S. Department of Energy, Office of Science, Basic Energy Sciences under Award #DE-SC0012573. Work at LLNL was performed under the auspices of the U.S. Department of Energy by LLNL under Contract No. DE-AC52-07NA27344. We acknowledge Tanya Shirman and Michael Aizenberg for their help and valuable discussions.

## LIST OF ABBREVIATIONS

AIMD, ab initio molecular dynamics; AP-IRRAS, ambient pressure infrared reflection adsorption spectroscopy; AP-XPS, ambient pressure X-ray photoelectron spectroscopy; BL, bilayer; BET, Brunauer−Emmett−Teller; CE, cluster expansions; CVs, collective variables; CO-FTIR, CO Fourier transform infrared spectroscopy; DFT, density functional theory; DRIFTS, diffuse reflectance infrared Fourier transform spectroscopy; EELS, electron energy-loss spectroscopy; EDS, energy-dispersive X-ray spectroscopy; ETEM, environmental transmission electron microscope; EXAFS, extended X-ray



https://doi.org/10.1021/acs.chemrev.1c00967
Chem. Rev. 2022, 122, 8758−8808

absorption fine structure; FLARE, fast learning of atomistic rare events; GAP, Gaussian approximation potential; GP, Gaussian process; HDNN, high dimensional neural network; HREELS, high resolution electron energy loss spectroscopy; HRTEM, high resolution transmission electron microscopy; HT, hydrotalcite; IRRAS, infrared reflection−absorption spectra; IR, infrared; IPs, interatomic potentials; LSAS, latent space analysis of spectra; LEED, low-energy electron diffraction; LEEM, low-energy electron microscopy; MFF, mapped force field; ML, machine learning; MLIPs, machine-learned interatomic potentials; MD, molecular dynamics; $MO_x$, metal oxide; MTP, moment tensor potential; NPs, nanoparticles; NNs, neural networks; NN-EXAFS, neural network assisted extended X-ray absorption fine structure; NN-XANES, neural network X-ray near edge structure; NequIP, neuro equivariant interatomic potentials; NEB, nudged elastic band; PRDF, partial radial distribution function; PM-IRAS, polarization-modulation infrared reflection absorption spectroscopy; RCT, raspberry colloid templated; RMC, reverse Monte Carlo; SOM, self-organizing map; SAA, single-atom alloys; SEM, scanning electron microscopy; SNAP, spectral neighbor analysis potential; STEM, scanning transmission electron microscopy; STEM-EDS, scanning transmission electron microscopy-energy-dispersive X-ray spectroscopy; STM, scanning tunneling microscope; SMSI, strong metal−support interactions; TAP, temporal analysis of products; TPD, temperature-programmed desorption; TPRS, temperature-programmed reaction spectroscopy; TS, transition state; TST, transition state theory; TEM, transmission electron microscope; TOF, turn over frequency; UHV, ultrahigh vacuum; XAFS, X-ray absorption fine structure; XANES, X-ray absorption near edge structure; XPS, X-ray photoelectron spectroscopy; XPEEM, X-ray photoemission electron microscopy

## REFERENCES


(1) U.S. Energy Information Administration. 2018 Manufacturing Energy Consumption Survey; https://www.eia.gov/consumption/manufacturing/ (accessed 2022-03-01).

(2) European Research Institute of Catalysis. Science and Technology Roadmap on Catalysis for Europe; http://gecats.org/gecats_media/Science+and+Technology+Roadmap+on+Catalysis+for+Europe+2016.pdf (accessed 2022-03-01).

(3) Pei, G. X.; Liu, X. Y.; Wang, A.; Lee, A. F.; Isaacs, M. A.; Li, L.; Pan, X.; Yang, X.; Wang, X.; Tai, Z.; et al. Ag Alloyed Pd Single-Atom Catalysts for Efficient Selective Hydrogenation of Acetylene to Ethylene in Excess Ethylene. *ACS Catal.* **2015**, *5*, 3717−3725.

(4) Patel, D. A.; Kress, P. L.; Cramer, L. A.; Larson, A. M.; Sykes, E. C. H. Elucidating the Composition of PtAg Surface Alloys with Atomic-Scale Imaging and Spectroscopy. *J. Chem. Phys.* **2019**, *151*, 164705.

(5) Liu, J.; Lucci, F. R.; Yang, M.; Lee, S.; Marcinkowski, M. D.; Therrien, A. J.; Williams, C. T.; Sykes, E. C. H.; Flytzani-Stephanopoulos, M. Tackling CO Poisoning with Single-Atom Alloy Catalysts. *J. Am. Chem. Soc.* **2016**, *138*, 6396−6399.

(6) Darby, M. T.; Sykes, E. C. H.; Michaelides, A.; Stamatakis, M. Carbon Monoxide Poisoning Resistance and Structural Stability of Single Atom Alloys. *Top. Catal.* **2018**, *61*, 428−438.

(7) Hannagan, R. T.; Giannakakis, G.; Flytzani-Stephanopoulos, M.; Sykes, E. C. H. Single-Atom Alloy Catalysis. *Chem. Rev.* **2020**, *120*, 12044−12088.

(8) Giannakakis, G.; Flytzani-Stephanopoulos, M.; Sykes, E. C. H. Single-Atom Alloys as a Reductionist Approach to the Rational Design of Heterogeneous Catalysts. *Acc. Chem. Res.* **2019**, *52*, 237−247.

(9) Wrasman, C. J.; Boubnov, A.; Riscoe, A. R.; Hoffman, A. S.; Bare, S. R.; Cargnello, M. Synthesis of Colloidal Pd/Au Dilute Alloy Nanocrystals and Their Potential for Selective Catalytic Oxidations. *J. Am. Chem. Soc.* **2018**, *140*, 12930−12939.

(10) Cao, Y.; Chen, B.; Guerrero-Sánchez, J.; Lee, I.; Zhou, X.; Takeuchi, N.; Zaera, F. Controlling Selectivity in Unsaturated Aldehyde Hydrogenation Using Single-Site Alloy Catalysts. *ACS Catal.* **2019**, *9*, 9150−9157.

(11) Liu, L.; Corma, A. Metal Catalysts for Heterogeneous Catalysis: From Single Atoms to Nanoclusters and Nanoparticles. *Chem. Rev.* **2018**, *118*, 4981−5079.

(12) Sankar, M.; Dimitratos, N.; Miedziak, P. J.; Wells, P. P.; Kiely, C. J.; Hutchings, G. J. Designing Bimetallic Catalysts for a Green and Sustainable Future. *Chem. Soc. Rev.* **2012**, *41*, 8099−8139.

(13) Wang, A.; Li, J.; Zhang, T. Heterogeneous Single-Atom Catalysis. *Nat. Rev. Chem.* **2018**, *2*, 65−81.

(14) Tierney, H. L.; Baber, A. E.; Kitchin, J. R.; Sykes, E. C. H. Hydrogen Dissociation and Spillover on Individual Isolated Palladium Atoms. *Phys. Rev. Lett.* **2009**, *103*, 246102.

(15) Spivey, T. D.; Holewinski, A. Selective Interactions between Free-Atom-like d -States in Single-Atom Alloy Catalysts and Near-Frontier Molecular Orbitals. *J. Am. Chem. Soc.* **2021**, *143*, 11897−11902.

(16) Greiner, M. T.; Jones, T. E.; Beeg, S.; Zwiener, L.; Scherzer, M.; Girgsdies, F.; Piccinin, S.; Armbrüster, M.; Knop-Gericke, A.; Schlögl, R. Free-Atom-like d States in Single-Atom Alloy Catalysts. *Nat. Chem.* **2018**, *10*, 1008−1015.

(17) Reece, C.; Luneau, M.; Friend, C. M.; Madix, R. J. Predicting a Sharp Decline in Selectivity for Catalytic Esterification of Alcohols from van Der Waals Interactions. *Angew. Chem.* **2020**, *132*, 10956−10959.

(18) Reece, C.; Redekop, E. A.; Karakalos, S.; Friend, C. M.; Madix, R. J. Crossing the Great Divide between Single-Crystal Reactivity and Actual Catalyst Selectivity with Pressure Transients. *Nat. Catal.* **2018**, *1*, 852−859.

(19) Personick, M. L.; Madix, R. J.; Friend, C. M. Selective Oxygen-Assisted Reactions of Alcohols and Amines Catalyzed by Metallic Gold: Paradigms for the Design of Catalytic Processes. *ACS Catal.* **2017**, *7*, 965−985.

(20) Wittstock, A.; Wichmann, A.; Biener, J.; Bäumer, M. Nanoporous Gold: A New Gold Catalyst with Tunable Properties. *Faraday Discuss.* **2011**, *152*, 87−98.

(21) Biener, J.; Biener, M. M.; Madix, R. J.; Friend, C. M. Nanoporous Gold: Understanding the Origin of the Reactivity of a 21st Century Catalyst Made by Pre-Columbian Technology. *ACS Catal.* **2015**, *5*, 6263−6270.

(22) Xu, B.; Siler, C. G. F.; Madix, R. J.; Friend, C. M. Ag/Au Mixed Sites Promote Oxidative Coupling of Methanol on the Alloy Surface. *Chem. - A Eur. J.* **2014**, *20*, 4646−4652.

(23) Kyriakou, G.; Boucher, M. B.; Jewell, A. D.; Lewis, E. A.; Lawton, T. J.; Baber, A. E.; Tierney, H. L.; Flytzani-Stephanopoulos, M.; Sykes, E. C. H. Isolated Metal Atom Geometries as a Strategy for Selective Heterogeneous Hydrogenations. *Science* **2012**, *335*, 1209−1212.

(24) Yu, W.; Porosoff, M. D.; Chen, J. G. Review of Pt-Based Bimetallic Catalysis: From Model Surfaces to Supported Catalysts. *Chem. Rev.* **2012**, *112*, 5780−5817.

(25) van Spronsen, M. A.; Daunmu, K.; O'Connor, C. R.; Egle, T.; Kersell, H.; Oliver-Meseguer, J.; Salmeron, M. B.; Madix, R. J.; Sautet, P.; Friend, C. M. Dynamics of Surface Alloys: Rearrangement of Pd/Ag(111) Induced by CO and O 2. *J. Phys. Chem. C* **2019**, *123*, 8312−8323.

(26) H Sykes, E. C.; Christopher, P. Recent Advances in Single-Atom Catalysts and Single-Atom Alloys: Opportunities for Exploring the Uncharted Phase Space in-Between. *Curr. Opin. Chem. Eng.* **2020**, *29*, 67−73.




https://doi.org/10.1021/acs.chemrev.1c00967
*Chem. Rev.* 2022, 122, 8758−8808

(27) Mao, J.; Yin, J.; Pei, J.; Wang, D.; Li, Y. Single Atom Alloy: An Emerging Atomic Site Material for Catalytic Applications. *Nano Today* **2020**, *34*, 100917.
(28) Biener, J.; Wittstock, A.; Zepeda-Ruiz, L. A.; Biener, M. M.; Zielasek, V.; Kramer, D.; Viswanath, R. N.; Weissmüller, J.; Bäumer, M.; Hamza, A. V. Surface-Chemistry-Driven Actuation in Nanoporous Gold. *Nat. Mater.* **2009**, *8*, 47−51.
(29) Réocreux, R.; Uhlman, M.; Thuening, T.; Kress, P.; Hannagan, R.; Stamatakis, M.; Sykes, E. C. H. Efficient and Selective Carbon-Carbon Coupling on Coke-Resistant PdAu Single-Atom Alloys. *Chem. Commun.* **2019**, *55*, 15085−15088.
(30) Wrasman, C. J.; Riscoe, A. R.; Lee, H.; Cargnello, M. Dilute Pd/Au Alloys Replace Au/$TiO_2$ Interface for Selective Oxidation Reactions. *ACS Catal.* **2020**, *10*, 1716−1720.
(31) Shirman, T.; Lattimer, J.; Luneau, M.; Shirman, E.; Reece, C.; Aizenberg, M.; Madix, R. J.; Aizenberg, J.; Friend, C. M. New Architectures for Designed Catalysts: Selective Oxidation Using AgAu Nanoparticles on Colloid-Templated Silica. *Chem. - A Eur. J.* **2018**, *24*, 1833−1837.
(32) Hartwig, C.; Schweinar, K.; Nicholls, R.; Beeg, S.; Schlögl, R.; Greiner, M. Surface Composition of AgPd Single-Atom Alloy Catalyst in an Oxidative Environment. *J. Chem. Phys.* **2021**, *154*, 174708.
(33) Lucci, F. R.; Lawton, T. J.; Pronschinske, A.; Sykes, E. C. H. Atomic Scale Surface Structure of Pt/Cu(111) Surface Alloys. *J. Phys. Chem. C* **2014**, *118*, 3015−3022.
(34) Bellisario, D. O.; Han, J. W.; Tierney, H. L.; Baber, A. E.; Sholl, D. S.; Sykes, E. C. H. Importance of Kinetics in Surface Alloying: A Comparison of the Diffusion Pathways of Pd and Ag Atoms on Cu(111). *J. Phys. Chem. C* **2009**, *113*, 12863−12869.
(35) Lucci, F. R.; Liu, J.; Marcinkowski, M. D.; Yang, M.; Allard, L. F.; Flytzani-Stephanopoulos, M.; Sykes, E. C. H. Selective Hydrogenation of 1,3-Butadiene on Platinum-Copper Alloys at the Single-Atom Limit. *Nat. Commun.* **2015**, *6*, 8550.
(36) Van Petegem, S.; Brandstetter, S.; Maass, R.; Hodge, A. M.; El-Dasher, B. S.; Biener, J.; Schmitt, B.; Borca, C.; Van Swygenhoven, H. Van. On the Microstructure of Nanoporous Gold: An X-Ray Diffraction Study. *Nano Lett.* **2009**, *9*, 1158−1163.
(37) Wittstock, A.; Wichmann, A.; Bäumer, M. Nanoporous Gold as a Platform for a Building Block Catalyst. *ACS Catal.* **2012**, *2*, 2199−2215.
(38) Wittstock, A.; Biener, J.; Bäumer, M. *Nanoporous Gold*; Wittstock, A., Biener, J., Erlebacher, J., Bäumer, M., Eds.; Nanoscience & Nanotechnology Series; Royal Society of Chemistry: Cambridge, 2012; pp 1−10.
(39) Wismann, S. T.; Engbæk, J. S.; Vendelbo, S. B.; Bendixen, F. B.; Eriksen, W. L.; Aasberg-Petersen, K.; Frandsen, C.; Chorkendorff, I.; Mortensen, P. M. Electrified Methane Reforming: A Compact Approach to Greener Industrial Hydrogen Production. *Science* **2019**, *364*, 756−759.
(40) Qi, Z.; Biener, M. M.; Kashi, A. R.; Hunegnaw, S.; Leung, A.; Ma, S.; Huo, Z.; Kuhl, K. P.; Biener, J. Scalable Fabrication of High Activity Nanoporous Copper Powders for Electrochemical $CO_2$ Reduction via Ball Milling and Dealloying. *J. CO2 Util.* **2021**, *45*, 101454.
(41) Qi, Z.; Biener, M. M.; Kashi, A. R.; Hunegnaw, S.; Leung, A.; Ma, S.; Huo, Z.; Kuhl, K. P.; Biener, J. Electrochemical $CO_2$ to CO Reduction at High Current Densities Using a Nanoporous Gold Catalyst. *Mater. Res. Lett.* **2021**, *9*, 99−104.
(42) Qi, Z.; Biener, J.; Biener, M. Surface Oxide-Derived Nanoporous Gold Catalysts for Electrochemical $CO_2$-to-CO Reduction. *ACS Appl. Energy Mater.* **2019**, *2*, 7717−7721.
(43) Rösner, H.; Parida, S.; Kramer, D.; Volkert, C. A.; Weissmüller, J. Reconstructing a Nanoporous Metal in Three Dimensions: An Electron Tomography Study of Dealloyed Gold Leaf. *Adv. Eng. Mater.* **2007**, *9*, 535−541.
(44) Tappan, B. C.; Steiner, S. A.; Luther, E. P. Nanoporous Metal Foams. *Angew. Chemie Int. Ed.* **2010**, *49*, 4544−4565.
(45) Zhang, J.; Li, C. M. Nanoporous Metals: Fabrication Strategies and Advanced Electrochemical Applications in Catalysis, Sensing and Energy Systems. *Chem. Soc. Rev.* **2012**, *41*, 7016−7031.
(46) Koya, A. N.; Zhu, X.; Ohannesian, N.; Yanik, A. A.; Alabastri, A.; Proietti Zaccaria, R.; Krahne, R.; Shih, W.-C.; Garoli, D. Nanoporous Metals: From Plasmonic Properties to Applications in Enhanced Spectroscopy and Photocatalysis. *ACS Nano* **2021**, *15*, 6038−6060.
(47) Shan, J.; Janvelyan, N.; Li, H.; Liu, J.; Egle, T. M.; Ye, J.; Biener, M. M.; Biener, J.; Friend, C. M.; Flytzani-Stephanopoulos, M. Selective Non-Oxidative Dehydrogenation of Ethanol to Acetaldehyde and Hydrogen on Highly Dilute NiCu Alloys. *Appl. Catal. B Environ.* **2017**, *205*, 541−550.
(48) Erlebacher, J.; Aziz, M. J.; Karma, A.; Dimitrov, N.; Sieradzki, K. Evolution of Nanoporosity in Dealloying. *Nature* **2001**, *410*, 450−453.
(49) Fujita, T.; Qian, L.-H.; Inoke, K.; Erlebacher, J.; Chen, M.-W. Three-Dimensional Morphology of Nanoporous Gold. *Appl. Phys. Lett.* **2008**, *92*, 251902.
(50) Hayes, J. R.; Hodge, A. M.; Biener, J.; Hamza, A. V.; Sieradzki, K. Monolithic Nanoporous Copper by Dealloying Mn-Cu. *J. Mater. Res.* **2006**, *21*, 2611−2616.
(51) Biener, J.; Nyce, G. W.; Hodge, A. M.; Biener, M. M.; Hamza, A. V.; Maier, S. A. Nanoporous Plasmonic Metamaterials. *Adv. Mater.* **2008**, *20*, 1211−1217.
(52) Egle, T. M.; Barroo, C.; Janvelyan, N.; Baumgaertel, A. C.; Akey, A. J.; Biener, M. M.; Friend, C. M.; Bell, D. C.; Biener, J. Multiscale Morphology of Nanoporous Copper Made from Intermetallic Phases. *ACS Appl. Mater. Interfaces* **2017**, *9*, 25615−25622.
(53) Chapman, C. A. R.; Wang, L.; Biener, J.; Seker, E.; Biener, M. M.; Matthews, M. J. Engineering On-Chip Nanoporous Gold Material Libraries via Precision Photothermal Treatment. *Nanoscale* **2016**, *8*, 785−795.
(54) Nyce, G. W.; Hayes, J. R.; Hamza, A. V.; Satcher, J. H. Synthesis and Characterization of Hierarchical Porous Gold Materials. *Chem. Mater.* **2007**, *19*, 344−346.
(55) Personick, M. L.; Zugic, B.; Biener, M. M.; Biener, J.; Madix, R. J.; Friend, C. M. Ozone-Activated Nanoporous Gold: A Stable and Storable Material for Catalytic Oxidation. *ACS Catal.* **2015**, *5*, 4237−4241.
(56) Wada, T.; Yubuta, K.; Inoue, A.; Kato, H. Dealloying by Metallic Melt. *Mater. Lett.* **2011**, *65*, 1076−1078.
(57) Lu, Z.; Li, C.; Han, J.; Zhang, F.; Liu, P.; Wang, H.; Wang, Z.; Cheng, C.; Chen, L.; Hirata, A.; et al. Three-Dimensional Bicontinuous Nanoporous Materials by Vapor Phase Dealloying. *Nat. Commun.* **2018**, *9*, 276.
(58) Biener, M. M.; Biener, J.; Wichmann, A.; Wittstock, A.; Baumann, T. F.; Bäumer, M.; Hamza, A. V. ALD Functionalized Nanoporous Gold: Thermal Stability, Mechanical Properties, and Catalytic Activity. *Nano Lett.* **2011**, *11*, 3085−3090.
(59) Li, Y.; Dinh Ngô, B.-N.; Markmann, J.; Weissmüller, J. Topology Evolution during Coarsening of Nanoscale Metal Network Structures. *Phys. Rev. Mater.* **2019**, *3*, 076001.
(60) Giannakakis, G.; Trimpalis, A.; Shan, J.; Qi, Z.; Cao, S.; Liu, J.; Ye, J.; Biener, J.; Flytzani-Stephanopoulos, M. NiAu Single Atom Alloys for the Non-Oxidative Dehydrogenation of Ethanol to Acetaldehyde and Hydrogen. *Top. Catal.* **2018**, *61*, 475−486.
(61) Vega, A. A.; Newman, R. C. Nanoporous Metals Fabricated through Electrochemical Dealloying of Ag-Au-Pt with Systematic Variation of Au:Pt Ratio. *J. Electrochem. Soc.* **2014**, *161*, C1−C10.
(62) Zugic, B.; Wang, L.; Heine, C.; Zakharov, D. N.; Lechner, B. A. J.; Stach, E. A.; Biener, J.; Salmeron, M.; Madix, R. J.; Friend, C. M. Dynamic Restructuring Drives Catalytic Activity on Nanoporous Gold-Silver Alloy Catalysts. *Nat. Mater.* **2017**, *16*, 558−564.
(63) Barroo, C.; Janvelyan, N.; Zugic, B.; Magyar, A. P.; Akey, A. J.; Biener, J.; Friend, C. M.; Bell, D. C. Surface Modifications during a Catalytic Reaction: A Combined APT and FIB/SEM Analysis of Surface Segregation. *Microsc. Microanal.* **2016**, *22*, 356−357.


https://doi.org/10.1021/acs.chemrev.1c00967
*Chem. Rev.* 2022, 122, 8758−8808

(64) Zhang, Z.; Wang, Y.; Qi, Z.; Somsen, C.; Wang, X.; Zhao, C. Fabrication and Characterization of Nanoporous Gold Composites through Chemical Dealloying of Two Phase Al-Au Alloys. *J. Mater. Chem.* **2009**, *19*, 6042−6050.
(65) Qi, Z.; Zhao, C.; Wang, X.; Lin, J.; Shao, W.; Zhang, Z.; Bian, X. Formation and Characterization of Monolithic Nanoporous Copper by Chemical Dealloying of Al-Cu Alloys. *J. Phys. Chem. C* **2009**, *113*, 6694−6698.
(66) Wang, X.; Qi, Z.; Zhao, C.; Wang, W.; Zhang, Z. Influence of Alloy Composition and Dealloying Solution on the Formation and Microstructure of Monolithic Nanoporous Silver through Chemical Dealloying of Al-Ag Alloys. *J. Phys. Chem. C* **2009**, *113*, 13139−13150.
(67) Falcucci, G.; Succi, S.; Montessori, A.; Melchionna, S.; Prestininzi, P.; Barroo, C.; Bell, D. C.; Biener, M. M.; Biener, J.; Zugic, B.; et al. Mapping Reactive Flow Patterns in Monolithic Nanoporous Catalysts. *Microfluid. Nanofluidics* **2016**, *20*, 105.
(68) Zhu, C.; Qi, Z.; Beck, V. A.; Luneau, M.; Lattimer, J.; Chen, W.; Worsley, M. A.; Ye, J.; Duoss, E. B.; Spadaccini, C. M.; et al. Toward Digitally Controlled Catalyst Architectures: Hierarchical Nanoporous Gold via 3D Printing. *Sci. Adv.* **2018**, *4*, No. eaas9459.
(69) Janvelyan, N.; van Spronsen, M. A.; Wu, C. H.; Qi, Z.; Montemore, M. M.; Shan, J.; Zakharov, D. N.; Xu, F.; Boscoboinik, J. A.; Salmeron, M. B.; et al. Stabilization of a Nanoporous NiCu Dilute Alloy Catalyst for Non-Oxidative Ethanol Dehydrogenation. *Catal. Sci. Technol.* **2020**, *10*, 5207−5217.
(70) King, J. S.; Wittstock, A.; Biener, J.; Kucheyev, S. O.; Wang, Y. M.; Baumann, T. F.; Giri, S. K.; Hamza, A. V.; Baeumer, M.; Bent, S. F. Ultralow Loading Pt Nanocatalysts Prepared by Atomic Layer Deposition on Carbon Aerogels. *Nano Lett.* **2008**, *8*, 2405−2409.
(71) Zielasek, V.; Jürgens, B.; Schulz, C.; Biener, J.; Biener, M. M.; Hamza, A. V.; Bäumer, M. Gold Catalysts: Nanoporous Gold Foams. *Angew. Chemie Int. Ed.* **2006**, *45*, 8241−8244.
(72) Kameoka, S.; Tsai, A. P. CO Oxidation Over a Fine Porous Gold Catalyst Fabricated by Selective Leaching from an Ordered $AuCu_3$ Intermetallic Compound. *Catal. Lett.* **2008**, *121*, 337−341.
(73) Wittstock, A.; Zielasek, V.; Biener, J.; Friend, C. M.; Baumer, M. Nanoporous Gold Catalysts for Selective Gas-Phase Oxidative Coupling of Methanol at Low Temperature. *Science* **2010**, *327*, 319−322.
(74) Zugic, B.; van Spronsen, M. A.; Heine, C.; Montemore, M. M.; Li, Y.; Zakharov, D. N.; Karakalos, S.; Lechner, B. A. J.; Crumlin, E.; Biener, M. M.; et al. Evolution of Steady-State Material Properties during Catalysis: Oxidative Coupling of Methanol over Nanoporous $Ag_{0.03}Au_{0.97}$. *J. Catal.* **2019**, *380*, 366−374.
(75) Stowers, K. J.; Madix, R. J.; Biener, M. M.; Biener, J.; Friend, C. M. Facile Ester Synthesis on Ag-Modified Nanoporous Au: Oxidative Coupling of Ethanol and 1-Butanol Under UHV Conditions. *Catal. Lett.* **2015**, *145*, 1217−1223.
(76) Karakalos, S.; Zugic, B.; Stowers, K. J.; Biener, M. M.; Biener, J.; Friend, C. M.; Madix, R. J. Catalytic Production of Methyl Acrylates by Gold-Mediated Cross Coupling of Unsaturated Aldehydes with Methanol. *Surf. Sci.* **2016**, *652*, 58−66.
(77) Wang, L.-C.; Stowers, K. J.; Zugic, B.; Personick, M. L.; Biener, M. M.; Biener, J.; Friend, C. M.; Madix, R. J. Exploiting Basic Principles to Control the Selectivity of the Vapor Phase Catalytic Oxidative Cross-Coupling of Primary Alcohols over Nanoporous Gold Catalysts. *J. Catal.* **2015**, *329*, 78−86.
(78) Zugic, B.; Karakalos, S.; Stowers, K. J.; Biener, M. M.; Biener, J.; Madix, R. J.; Friend, C. M. Continuous Catalytic Production of Methyl Acrylates from Unsaturated Alcohols by Gold: The Strong Effect of C═C Unsaturation on Reaction Selectivity. *ACS Catal.* **2016**, *6*, 1833−1839.
(79) van Deelen, T. W.; Hernández Mejía, C.; de Jong, K. P. Control of Metal-Support Interactions in Heterogeneous Catalysts to Enhance Activity and Selectivity. *Nat. Catal.* **2019**, *2*, 955−970.
(80) Ball, M. R.; Rivera-Dones, K. R.; Gilcher, E. B.; Ausman, S. F.; Hullfish, C. W.; Lebrón, E. A.; Dumesic, J. A. AgPd and CuPd Catalysts for Selective Hydrogenation of Acetylene. *ACS Catal.* **2020**, *10*, 8567−8581.
(81) Qian, K.; Luo, L.; Jiang, Z.; Huang, W. Alloying Au Surface with Pd Reduces the Intrinsic Activity in Catalyzing CO Oxidation. *Catal. Today* **2017**, *280*, 253−258.
(82) Hugon, A.; Delannoy, L.; Krafft, J.-M.; Louis, C. Selective Hydrogenation of 1,3-Butadiene in the Presence of an Excess of Alkenes over Supported Bimetallic Gold-Palladium Catalysts. *J. Phys. Chem. C* **2010**, *114*, 10823−10835.
(83) Kolli, N. El; Delannoy, L.; Louis, C. Bimetallic Au-Pd Catalysts for Selective Hydrogenation of Butadiene: Influence of the Preparation Method on Catalytic Properties. *J. Catal.* **2013**, *297*, 79−92.
(84) Yang, G.; Kuwahara, Y.; Mori, K.; Louis, C.; Yamashita, H. Pd-Cu Alloy Nanoparticles Confined within Mesoporous Hollow Carbon Spheres for the Hydrogenation of CO 2 to Formate. *J. Phys. Chem. C* **2021**, *125*, 3961−3971.
(85) Hutchings, G. J.; Kiely, C. J. Strategies for the Synthesis of Supported Gold Palladium Nanoparticles with Controlled Morphology and Composition. *Acc. Chem. Res.* **2013**, *46*, 1759−1772.
(86) Trimpalis, A.; Giannakakis, G.; Cao, S.; Flytzani-Stephanopoulos, M. NiAu Single Atom Alloys for the Selective Oxidation of Methacrolein with Methanol to Methyl Methacrylate. *Catal. Today* **2020**, *355*, 804−814.
(87) Boucher, M. B.; Zugic, B.; Cladaras, G.; Kammert, J.; Marcinkowski, M. D.; Lawton, T. J.; Sykes, E. C. H.; Flytzani-Stephanopoulos, M. Single Atom Alloy Surface Analogs in $Pd_{0.18}Cu_{15}$ Nanoparticles for Selective Hydrogenation Reactions. *Phys. Chem. Chem. Phys.* **2013**, *15*, 12187.
(88) da Silva, F. P.; Fiorio, J. L.; Gonçalves, R. V.; Teixeira-Neto, E.; Rossi, L. M. Synergic Effect of Copper and Palladium for Selective Hydrogenation of Alkynes. *Ind. Eng. Chem. Res.* **2018**, *57*, 16209−16216.
(89) Luo, S.; Song, H.; Philo, D.; Oshikiri, M.; Kako, T.; Ye, J. Solar-Driven Production of Hydrogen and Acetaldehyde from Ethanol on Ni-Cu Bimetallic Catalysts with Solar-to-Fuels Conversion Efficiency up to 3.8%. *Appl. Catal. B Environ.* **2020**, *272*, 118965.
(90) Cao, Y.; Guerrero-Sańchez, J.; Lee, I.; Zhou, X.; Takeuchi, N.; Zaera, F. Kinetic Study of the Hydrogenation of Unsaturated Aldehydes Promoted by CuPt x /SBA-15 Single-Atom Alloy (SAA) Catalysts. *ACS Catal.* **2020**, *10*, 3431−3443.
(91) Cargnello, M.; Chen, C.; Diroll, B. T.; Doan-Nguyen, V. V. T.; Gorte, R. J.; Murray, C. B. Efficient Removal of Organic Ligands from Supported Nanocrystals by Fast Thermal Annealing Enables Catalytic Studies on Well-Defined Active Phases. *J. Am. Chem. Soc.* **2015**, *137*, 6906−6911.
(92) Luo, J.; Lee, J. D.; Yun, H.; Wang, C.; Monai, M.; Murray, C. B.; Fornasiero, P.; Gorte, R. J. Base Metal-Pt Alloys: A General Route to High Selectivity and Stability in the Production of Biofuels from HMF. *Appl. Catal. B Environ.* **2016**, *199*, 439−446.
(93) Dong, A.; Ye, X.; Chen, J.; Kang, Y.; Gordon, T.; Kikkawa, J. M.; Murray, C. B. A Generalized Ligand-Exchange Strategy Enabling Sequential Surface Functionalization of Colloidal Nanocrystals. *J. Am. Chem. Soc.* **2011**, *133*, 998−1006.
(94) Taylor, M. J.; Beaumont, S. K.; Islam, M. J.; Tsatsos, S.; Parlett, C. A. M.; Issacs, M. A.; Kyriakou, G. Atom Efficient PtCu Bimetallic Catalysts and Ultra Dilute Alloys for the Selective Hydrogenation of Furfural. *Appl. Catal. B Environ.* **2021**, *284*, 119737.
(95) Bruno, J. E.; Dwarica, N. S.; Whittaker, T. N.; Hand, E. R.; Guzman, C. S.; Dasgupta, A.; Chen, Z.; Rioux, R. M.; Chandler, B. D. Supported Ni-Au Colloid Precursors for Active, Selective, and Stable Alkyne Partial Hydrogenation Catalysts. *ACS Catal.* **2020**, *10*, 2565−2580.
(96) Bartholomew, C. H.; Farrauto, R. J. Catalyst Deactivation: Causes, Mechanisms, and Treatment. *Fundamentals of Industrial Catalytic Processes*; John Wiley & Sons, Inc.: Hoboken, NJ, 2010; pp 260−336.


https://doi.org/10.1021/acs.chemrev.1c00967
*Chem. Rev.* 2022, 122, 8758−8808

(97) Cao, A.; Lu, R.; Veser, G. Stabilizing Metal Nanoparticles for Heterogeneous Catalysis. *Phys. Chem. Chem. Phys.* **2010**, *12*, 13499−13510.
(98) Farrusseng, D.; Tuel, A. Perspectives on Zeolite-Encapsulated Metal Nanoparticles and Their Applications in Catalysis. *New J. Chem.* **2016**, *40*, 3933−3949.
(99) Arnal, P. M.; Comotti, M.; Schüth, F. High-Temperature-Stable Catalysts by Hollow Sphere Encapsulation. *Angew. Chemie Int. Ed.* **2006**, *45*, 8224−8227.
(100) Liu, J.; Shan, J.; Lucci, F. R.; Cao, S.; Sykes, E. C. H.; Flytzani-Stephanopoulos, M. Palladium-Gold Single Atom Alloy Catalysts for Liquid Phase Selective Hydrogenation of 1-Hexyne. *Catal. Sci. Technol.* **2017**, *7*, 4276−4284.
(101) Shirman, E.; Shirman, T.; Shneidman, A. V.; Grinthal, A.; Phillips, K. R.; Whelan, H.; Bulger, E.; Abramovitch, M.; Patil, J.; Nevarez, R.; et al. Modular Design of Advanced Catalytic Materials Using Hybrid Organic-Inorganic Raspberry Particles. *Adv. Funct. Mater.* **2018**, *28*, 1704559.
(102) van der Hoeven, J. E. S.; Krämer, S.; Dussi, S.; Shirman, T.; Park, K. K.; Rycroft, C. H.; Bell, D. C.; Friend, C. M.; Aizenberg, J. On the Origin of Sinter-Resistance and Catalyst Accessibility in Raspberry-Colloid-Templated Catalyst Design. *Adv. Funct. Mater.* **2021**, *31*, 2106876.
(103) Guan, E.; Foucher, A. C.; Marcella, N.; Shirman, T.; Luneau, M.; Head, A. R.; Verbart, D. M. A.; Aizenberg, J.; Friend, C. M.; Stacchiola, D.; et al. New Role of Pd Hydride as a Sensor of Surface Pd Distributions in Pd-Au Catalysts. *ChemCatChem.* **2020**, *12*, 717−721.
(104) Luneau, M.; Guan, E.; Chen, W.; Foucher, A. C.; Marcella, N.; Shirman, T.; Verbart, D. M. A.; Aizenberg, J.; Aizenberg, M.; Stach, E. A.; et al. Enhancing Catalytic Performance of Dilute Metal Alloy Nanomaterials. *Commun. Chem.* **2020**, *3*, 46.
(105) Luneau, M.; Shirman, T.; Filie, A.; Timoshenko, J.; Chen, W.; Trimpalis, A.; Flytzani-Stephanopoulos, M.; Kaxiras, E.; Frenkel, A. I.; Aizenberg, J.; et al. Dilute Pd/Au Alloy Nanoparticles Embedded in Colloid-Templated Porous $SiO_2$: Stable Au-Based Oxidation Catalysts. *Chem. Mater.* **2019**, *31*, 5759−5768.
(106) Shan, J.; Liu, J.; Li, M.; Lustig, S.; Lee, S.; Flytzani-Stephanopoulos, M. NiCu Single Atom Alloys Catalyze the C H Bond Activation in the Selective Non- Oxidative Ethanol Dehydrogenation Reaction. *Appl. Catal. B Environ.* **2018**, *226*, 534−543.
(107) Shan, J.; Lucci, F. R.; Liu, J.; El-Soda, M.; Marcinkowski, M. D.; Allard, L. F.; Sykes, E. C. H.; Flytzani-Stephanopoulos, M. Water Co-Catalyzed Selective Dehydrogenation of Methanol to Formaldehyde and Hydrogen. *Surf. Sci.* **2016**, *650*, 121−129.
(108) Pei, G. X.; Liu, X. Y.; Yang, X.; Zhang, L.; Wang, A.; Li, L.; Wang, H.; Wang, X.; Zhang, T. Performance of Cu-Alloyed Pd Single-Atom Catalyst for Semihydrogenation of Acetylene under Simulated Front-End Conditions. *ACS Catal.* **2017**, *7*, 1491−1500.
(109) Liu, J.; Shan, J.; Lucci, F. R.; Cao, S.; Sykes, E. C. H.; Flytzani-Stephanopoulos, M. Palladium-Gold Single Atom Alloy Catalysts for Liquid Phase Selective Hydrogenation of 1-Hexyne. *Catal. Sci. Technol.* **2017**, *7*, 4276−4284.
(110) Liu, J.; Uhlman, M. B.; Montemore, M. M.; Trimpalis, A.; Giannakakis, G.; Shan, J.; Cao, S.; Hannagan, R. T.; Sykes, E. C. H.; Flytzani-Stephanopoulos, M. Integrated Catalysis-Surface Science-Theory Approach to Understand Selectivity in the Hydrogenation of 1-Hexyne to 1-Hexene on PdAu Single-Atom Alloy Catalysts. *ACS Catal.* **2019**, *9*, 8757−8765.
(111) Pei, G. X.; Liu, X. Y.; Wang, A.; Li, L.; Huang, Y.; Zhang, T.; Lee, J. W.; Jang, B. W. L.; Mou, C.-Y. Promotional Effect of Pd Single Atoms on Au Nanoparticles Supported on Silica for the Selective Hydrogenation of Acetylene in Excess Ethylene. *New J. Chem.* **2014**, *38*, 2043−2051.
(112) Luneau, M.; Shirman, T.; Foucher, A. C.; Duanmu, K.; Verbart, D. M. A.; Sautet, P.; Stach, E. A.; Aizenberg, J.; Madix, R. J.; Friend, C. M. Achieving High Selectivity for Alkyne Hydrogenation at High Conversions with Compositionally Optimized PdAu Nanoparticle Catalysts in Raspberry Colloid-Templated $SiO_2$. *ACS Catal.* **2020**, *10*, 441−450.
(113) McCue, A. J.; Anderson, J. A. CO Induced Surface Segregation as a Means of Improving Surface Composition and Enhancing Performance of CuPd Bimetallic Catalysts. *J. Catal.* **2015**, *329*, 538−546.
(114) McCue, A. J.; Gibson, A.; Anderson, J. A. Palladium Assisted Copper/Alumina Catalysts for the Selective Hydrogenation of Propyne, Propadiene and Propene Mixed Feeds. *Chem. Eng. J.* **2016**, *285*, 384−391.
(115) Haruta, M. Size- and Support-Dependency in the Catalysis of Gold. *Catal. Today* **1997**, *36*, 153−166.
(116) Guzman, J.; Gates, B. C. Catalysis by Supported Gold: Correlation between Catalytic Activity for CO Oxidation and Oxidation States of Gold. *J. Am. Chem. Soc.* **2004**, *126*, 2672−2673.
(117) Bamwenda, G. R.; Tsubota, S.; Nakamura, T.; Haruta, M. The Influence of the Preparation Methods on the Catalytic Activity of Platinum and Gold Supported on $TiO_2$ for CO Oxidation. *Catal. Lett.* **1997**, *44*, 83−87.
(118) Deng, W.; Carpenter, C.; Yi, N.; Flytzani-Stephanopoulos, M. Comparison of the Activity of Au/$CeO_2$ and Au/$Fe_2O_3$ Catalysts for the CO Oxidation and the Water-Gas Shift Reactions. *Top. Catal.* **2007**, *44*, 199−208.
(119) Valden, M.; Lai, X.; Goodman, D. W. Onset of Catalytic Activity of Gold Clusters on Titania with the Appearance of Nonmetallic Properties. *Science* **1998**, *281*, 1647−1650.
(120) Herzing, A. A.; Kiely, C. J.; Carley, A. F.; Landon, P.; Hutchings, G. J. Identification of Active Gold Nanoclusters on Iron Oxide Supports for CO Oxidation. *Science* **2008**, *321*, 1331−1335.
(121) Remediakis, I. N.; Lopez, N.; Nørskov, J. K. CO Oxidation on Gold Nanoparticles: Theoretical Studies. *Appl. Catal. A Gen.* **2005**, *291*, 13−20.
(122) Déronzier, T.; Morfin, F.; Massin, L.; Lomello, M.; Rousset, J.-L. Pure Nanoporous Gold Powder: Synthesis and Catalytic Properties. *Chem. Mater.* **2011**, *23*, 5287−5289.
(123) Xu, C.; Su, J.; Xu, X.; Liu, P.; Zhao, H.; Tian, F.; Ding, Y. Low Temperature CO Oxidation over Unsupported Nanoporous Gold. *J. Am. Chem. Soc.* **2007**, *129*, 42−43.
(124) Fujita, T.; Guan, P.; McKenna, K.; Lang, X.; Hirata, A.; Zhang, L.; Tokunaga, T.; Arai, S.; Yamamoto, Y.; Tanaka, N.; et al. Atomic Origins of the High Catalytic Activity of Nanoporous Gold. *Nat. Mater.* **2012**, *11*, 775−780.
(125) Montemore, M. M.; Madix, R. J.; Kaxiras, E. How Does Nanoporous Gold Dissociate Molecular Oxygen? *J. Phys. Chem. C* **2016**, *120*, 16636−16640.
(126) Fajín, J. L. C.; Cordeiro, M. N. D. S.; Gomes, J. R. B. On the Theoretical Understanding of the Unexpected $O_2$ Activation by Nanoporous Gold. *Chem. Commun.* **2011**, *47*, 8403−8405.
(127) Fujita, T.; Tokunaga, T.; Zhang, L.; Li, D.; Chen, L.; Arai, S.; Yamamoto, Y.; Hirata, A.; Tanaka, N.; Ding, Y.; et al. Atomic Observation of Catalysis-Induced Nanopore Coarsening of Nanoporous Gold. *Nano Lett.* **2014**, *14*, 1172−1177.
(128) Montemore, M. M.; Montessori, A.; Succi, S.; Barroo, C.; Falcucci, G.; Bell, D. C.; Kaxiras, E. Effect of Nanoscale Flows on the Surface Structure of Nanoporous Catalysts. *J. Chem. Phys.* **2017**, *146*, 214703.
(129) Wang, A.; Liu, J.; Lin, S.; Lin, T.; Mou, C. A Novel Efficient Au-Ag Alloy Catalyst System: Preparation, Activity, and Characterization. *J. Catal.* **2005**, *233*, 186−197.
(130) Déronzier, T.; Morfin, F.; Lomello, M.; Rousset, J.-L. Catalysis on Nanoporous Gold-Silver Systems: Synergistic Effects toward Oxidation Reactions and Influence of the Surface Composition. *J. Catal.* **2014**, *311*, 221−229.
(131) Xu, J.; White, T.; Li, P.; He, C.; Yu, J.; Yuan, W.; Han, Y.-F. Biphasic Pd-Au Alloy Catalyst for Low-Temperature CO Oxidation. *J. Am. Chem. Soc.* **2010**, *132*, 10398−10406.
(132) Kim, S. M.; Mun, J. H.; Lee, S. W.; An, H.; Kim, H. Y.; Kim, S. O.; Park, J. Y. Compositional Effect of Two-Dimensional Monodisperse AuPd Bimetallic Nanoparticle Arrays Fabricated by Block


https://doi.org/10.1021/acs.chemrev.1c00967
*Chem. Rev.* 2022, 122, 8758−8808

Copolymer Nanopatterning on Catalytic Activity of CO Oxidation. *Chem. Commun.* **2018**, *54*, 13734−13737.
(133) Alayoglu, S.; Tao, F.; Altoe, V.; Specht, C.; Zhu, Z.; Aksoy, F.; Butcher, D. R.; Renzas, R. J.; Liu, Z.; Somorjai, G. A. Surface Composition and Catalytic Evolution of $Au_xPd_{1-x}$ (x = 0.25, 0.50 and 0.75) Nanoparticles Under $CO/O_2$ Reaction in Torr Pressure Regime and at 200 °C. *Catal. Lett.* **2011**, *141*, 633−640.
(134) Ward, T.; Delannoy, L.; Hahn, R.; Kendell, S.; Pursell, C. J.; Louis, C.; Chandler, B. D. Effects of Pd on Catalysis by Au: CO Adsorption, CO Oxidation, and Cyclohexene Hydrogenation by Supported Au and Pd-Au Catalysts. *ACS Catal.* **2013**, *3*, 2644−2653.
(135) Gibson, E. K.; Beale, A. M.; Catlow, C. R. A.; Chutia, A.; Gianolio, D.; Gould, A.; Kroner, A.; Mohammed, K. M. H.; Perdjon, M.; Rogers, S. M.; et al. Restructuring of AuPd Nanoparticles Studied by a Combined XAFS/DRIFTS Approach. *Chem. Mater.* **2015**, *27*, 3714−3720.
(136) Garcia, C.; Truttmann, V.; Lopez, I.; Haunold, T.; Marini, C.; Rameshan, C.; Pittenauer, E.; Kregsamer, P.; Dobrezberger, K.; Stöger-Pollach, M.; et al. Dynamics of Pd Dopant Atoms inside Au Nanoclusters during Catalytic CO Oxidation. *J. Phys. Chem. C* **2020**, *124*, 23626−23636.
(137) Gao, F.; Wang, Y.; Goodman, D. W. Reaction Kinetics and Polarization-Modulation Infrared Reflection Absorption Spectroscopy (PM-IRAS) Investigation of CO Oxidation over Supported Pd-Au Alloy Catalysts. *J. Phys. Chem. C* **2010**, *114*, 4036−4043.
(138) Shirman, T.; Toops, T. J.; Shirman, E.; Shneidman, A. V.; Liu, S.; Gurkin, K.; Alvarenga, J.; Lewandowski, M. P.; Aizenberg, M.; Aizenberg, J. Raspberry Colloid-Templated Approach for the Synthesis of Palladium-Based Oxidation Catalysts with Enhanced Hydrothermal Stability and Low-Temperature Activity. *Catal. Today* **2021**, *360*, 241−251.
(139) Mars, P.; van Krevelen, D. W. Oxidations Carried out by Means of Vanadium Oxide Catalysts. *Chem. Eng. Sci.* **1954**, *3*, 41−59.
(140) Cordatos, H.; Gorte, R. J. CO, NO, and $H_2$ Adsorption on Ceria-Supported Pd. *J. Catal.* **1996**, *159*, 112−118.
(141) Cargnello, M.; Doan-Nguyen, V. V. T.; Gordon, T. R.; Diaz, R. E.; Stach, E. A.; Gorte, R. J.; Fornasiero, P.; Murray, C. B. Control of Metal Nanocrystal Size Reveals Metal-Support Interface Role for Ceria Catalysts. *Science* **2013**, *341*, 771−773.
(142) Hill, A. J.; Seo, C. Y.; Chen, X.; Bhat, A.; Fisher, G. B.; Lenert, A.; Schwank, J. W. Thermally Induced Restructuring of $Pd@CeO_2$ and $Pd@SiO_2$ Nanoparticles as a Strategy for Enhancing Low-Temperature Catalytic Activity. *ACS Catal.* **2020**, *10*, 1731−1741.
(143) Ewers, B. W.; Crampton, A. S.; Biener, M. M.; Friend, C. M. Thermally Activated Formation of Reactive Lattice Oxygen in Titania on Nanoporous Gold. *J. Phys. Chem. C* **2017**, *121*, 21405−21410.
(144) Kotobuki, M.; Leppelt, R.; Hansgen, D. A.; Widmann, D.; Behm, R. J. Reactive Oxygen on a $Au/TiO_2$ Supported Catalyst. *J. Catal.* **2009**, *264*, 67−76.
(145) Widmann, D.; Behm, R. J. Active Oxygen on a $Au/TiO_2$ Catalyst: Formation, Stability, and CO Oxidation Activity. *Angew. Chemie Int. Ed.* **2011**, *50*, 10241−10245.
(146) Qiao, B.; Liang, J.-X.; Wang, A.; Xu, C.-Q.; Li, J.; Zhang, T.; Liu, J. J. Ultrastable Single-Atom Gold Catalysts with Strong Covalent Metal-Support Interaction (CMSI). *Nano Res.* **2015**, *8*, 2913−2924.
(147) Wang, J.; Tan, H.; Yu, S.; Zhou, K. Morphological Effects of Gold Clusters on the Reactivity of Ceria Surface Oxygen. *ACS Catal.* **2015**, *5*, 2873−2881.
(148) Spezzati, G.; Su, Y.; Hofmann, J. P.; Benavidez, A. D.; DeLaRiva, A. T.; McCabe, J.; Datye, A. K.; Hensen, E. J. M. Atomically Dispersed Pd-O Species on $CeO_2$ (111) as Highly Active Sites for Low-Temperature CO Oxidation. *ACS Catal.* **2017**, *7*, 6887−6891.
(149) Friend, C. M.; Xu, B. Heterogeneous Catalysis: A Central Science for a Sustainable Future. *Acc. Chem. Res.* **2017**, *50*, 517−521.
(150) Filie, A.; Shirman, T.; Foucher, A. C.; Stach, E. A.; Aizenberg, M.; Aizenberg, J.; Friend, C. M.; Madix, R. J. Dilute Pd-in-Au Alloy RCT-SiO2 Catalysts for Enhanced Oxidative Methanol Coupling. *J. Catal.* **2021**, *404*, 943−953.
(151) Karakalos, S.; Xu, Y.; Cheenicode Kabeer, F.; Chen, W.; Rodríguez-Reyes, J. C. F.; Tkatchenko, A.; Kaxiras, E.; Madix, R. J.; Friend, C. M. Noncovalent Bonding Controls Selectivity in Heterogeneous Catalysis: Coupling Reactions on Gold. *J. Am. Chem. Soc.* **2016**, *138*, 15243−15250.
(152) Hayashi, T.; Tanaka, K.; Haruta, M. Selective Vapor-Phase Epoxidation of Propylene over Au/TiO2Catalysts in the Presence of Oxygen and Hydrogen. *J. Catal.* **1998**, *178*, 566−575.
(153) Bravo-Suárez, J. J.; Bando, K. K.; Lu, J.; Fujitani, T.; Oyama, S. T. Oxidation of Propane to Propylene Oxide on Gold Catalysts. *J. Catal.* **2008**, *255*, 114−126.
(154) Neurock, M. The Microkinetics of Heterogeneous Catalysis. By J. A. Dumesic, D. F. Rudd, L. M. Aparicio, J. E. Rekoske, and A. A. Treviño, ACS Professional Reference Book, American Chemical Society, Washington, DC, 1993, 315 Pp. *AIChE J.* **1994**, *40*, 1085−1087.
(155) Reece, C.; Luneau, M.; Madix, R. J. Dissecting the Performance of Nanoporous Gold Catalysts for Oxygen-Assisted Coupling of Methanol with Fundamental Mechanistic and Kinetic Information. *ACS Catal.* **2019**, *9*, 4477−4487.
(156) Outka, D. A.; Madix, R. J. Broensted Basicity of Atomic Oxygen on the Gold(110) Surface: Reactions with Methanol, Acetylene, Water, and Ethylene. *J. Am. Chem. Soc.* **1987**, *109*, 1708−1714.
(157) Outka, D. A.; Madix, R. J. Acid-Base and Nucleophilic Chemistry of Atomic Oxygen on the Au(110) Surface: Reactions with Formic Acid and Formaldehyde. *Surf. Sci.* **1987**, *179*, 361−376.
(158) Wang, L.-C.; Personick, M. L.; Karakalos, S.; Fushimi, R.; Friend, C. M.; Madix, R. J. Active Sites for Methanol Partial Oxidation on Nanoporous Gold Catalysts. *J. Catal.* **2016**, *344*, 778−783.
(159) Reece, C.; Madix, R. J. Moving from Fundamental Knowledge of Kinetics and Mechanisms on Surfaces to Prediction of Catalyst Performance in Reactors. *ACS Catal.* **2021**, *11*, 3048−3066.
(160) Personick, M. L.; Montemore, M. M.; Kaxiras, E.; Madix, R. J.; Biener, J.; Friend, C. M. Catalyst Design for Enhanced Sustainability through Fundamental Surface Chemistry. *Philos. Trans. R. Soc. A Math. Phys. Eng. Sci.* **2016**, *374*, 20150077.
(161) Xu, Y.; Chen, W.; Kaxiras, E.; Friend, C. M.; Madix, R. J. General Effect of van Der Waals Interactions on the Stability of Alkoxy Intermediates on Metal Surfaces. *J. Phys. Chem. B* **2018**, *122*, 555−560.
(162) Cheenicode Kabeer, F.; Chen, W.; Madix, R. J.; Friend, C. M.; Tkatchenko, A. First-Principles Study of Alkoxides Adsorbed on Au(111) and Au(110) Surfaces: Assessing the Roles of Noncovalent Interactions and Molecular Structures in Catalysis. *J. Phys. Chem. C* **2017**, *121*, 27905−27914.
(163) O'Connor, C. R.; Hiebel, F.; Chen, W.; Kaxiras, E.; Madix, R. J.; Friend, C. M. Identifying Key Descriptors in Surface Binding: Interplay of Surface Anchoring and Intermolecular Interactions for Carboxylates on Au(110). *Chem. Sci.* **2018**, *9*, 3759−3766.
(164) Hiebel, F.; Shong, B.; Chen, W.; Madix, R. J.; Kaxiras, E.; Friend, C. M. Self-Assembly of Acetate Adsorbates Drives Atomic Rearrangement on the Au(110) Surface. *Nat. Commun.* **2016**, *7*, 13139.
(165) Muttaqien, F.; Hamamoto, Y.; Hamada, I.; Inagaki, K.; Shiozawa, Y.; Mukai, K.; Koitaya, T.; Yoshimoto, S.; Yoshinobu, J.; Morikawa, Y. CO2 Adsorption on the Copper Surfaces: Van Der Waals Density Functional and TPD Studies. *J. Chem. Phys.* **2017**, *147*, 094702.
(166) Yuan, D.; Zhang, Y.; Ho, W.; Wu, R. Effects of van Der Waals Dispersion Interactions in Density Functional Studies of Adsorption, Catalysis, and Tribology on Metals. *J. Phys. Chem. C* **2020**, *124*, 16926−16942.
(167) Barabás, J.; Vanbuel, J.; Ferrari, P.; Janssens, E.; Höltzl, T. Non-covalent Interactions and Charge Transfer between Propene and Neutral Yttrium-Doped and Pure Gold Clusters. *Chem. - A Eur. J.* **2019**, *25*, 15795−15804.
(168) Yuan, D.; Liao, H.; Hu, W. Assessment of van Der Waals Inclusive Density Functional Theory Methods for Adsorption and


https://doi.org/10.1021/acs.chemrev.1c00967
*Chem. Rev.* 2022, 122, 8758−8808

Selective Dehydrogenation of Formic Acid on Pt(111) Surface. *Phys. Chem. Chem. Phys.* **2019**, *21*, 21049−21056.
(169) Pham, T. L. M.; Vo, D.-V. N.; Nguyen, H. N. T.; Pham-Tran, N.-N. C H versus O H Bond Scission in Methanol Decomposition on Pt(111): Role of the Dispersion Interaction. *Appl. Surf. Sci.* **2019**, *481*, 1327−1334.
(170) Su, G.; Yang, S.; Jiang, Y.; Li, J.; Li, S.; Ren, J.-C.; Liu, W. Modeling Chemical Reactions on Surfaces: The Roles of Chemical Bonding and van Der Waals Interactions. *Prog. Surf. Sci.* **2019**, *94*, 100561.
(171) Jasper-Tönnies, T.; Poltavsky, I.; Ulrich, S.; Moje, T.; Tkatchenko, A.; Herges, R.; Berndt, R. Stability of Functionalized Platform Molecules on Au(111). *J. Chem. Phys.* **2018**, *149*, 244705.
(172) Montemore, M. M.; van Spronsen, M. A.; Madix, R. J.; Friend, C. M. $O_2$ Activation by Metal Surfaces: Implications for Bonding and Reactivity on Heterogeneous Catalysts. *Chem. Rev.* **2018**, *118*, 2816−2862.
(173) Pia, G.; Sogne, E.; Falqui, A.; Delogu, F. Ag Surface Segregation in Nanoporous Au Catalysts during CO Oxidation. *Sci. Rep.* **2018**, *8*, 15208.
(174) Jacobs, L.; von Boehn, B.; Homann, M.; Barroo, C.; Visart de Bocarmé, T.; Imbihl, R. On the Importance of the Structure in the Catalytic Reactivity of Au-Based Catalysts. *Appl. Surf. Sci.* **2020**, *525*, 146568.
(175) Sensoy, M. G.; Montemore, M. M. Density Functional Theory Investigation of Oxidation Intermediates on Gold and Gold-Silver Surfaces. *J. Phys. Chem. C* **2020**, *124*, 8843−8853.
(176) Hoppe, S.; Li, Y.; Moskaleva, L. V.; Müller, S. How Silver Segregation Stabilizes 1D Surface Gold Oxide: A Cluster Expansion Study Combined with Ab Initio MD Simulations. *Phys. Chem. Chem. Phys.* **2017**, *19*, 14845−14853.
(177) Hiebel, F.; Montemore, M. M.; Kaxiras, E.; Friend, C. M. Direct Visualization of Quasi-Ordered Oxygen Chain Structures on Au(110)-(1 × 2). *Surf. Sci.* **2016**, *650*, 5−10.
(178) Xu, F.; Montemore, M. M.; O'Connor, C. R.; Muramoto, E.; van Spronsen, M. A.; Madix, R. J.; Friend, C. M. Oxygen Adsorption on Spontaneously Reconstructed Au(511). *Surf. Sci.* **2019**, *679*, 296−303.
(179) Xu, F.; Madix, R. J.; Friend, C. M. Spatially Nonuniform Reaction Rates during Selective Oxidation on Gold. *J. Am. Chem. Soc.* **2018**, *140*, 12210−12215.
(180) Barroo, C.; Montemore, M. M.; Janvelyan, N.; Zugic, B.; Akey, A. J.; Magyar, A. P.; Ye, J.; Kaxiras, E.; Biener, J.; Bell, D. C. Macroscopic 3D Nanoporosity Formation by Dry Oxidation of AgAu Alloys. *J. Phys. Chem. C* **2017**, *121*, 5115−5122.
(181) Montemore, M. M.; Cubuk, E. D.; Klobas, J. E.; Schmid, M.; Madix, R. J.; Friend, C. M.; Kaxiras, E. Controlling O Coverage and Stability by Alloying Au and Ag. *Phys. Chem. Chem. Phys.* **2016**, *18*, 26844−26853.
(182) Tomaschun, G.; Dononelli, W.; Li, Y.; Bäumer, M.; Klüner, T.; Moskaleva, L. V. Methanol Oxidation on the Au(310) Surface: A Theoretical Study. *J. Catal.* **2018**, *364*, 216−227.
(183) Su, S.; Zaza, P.; Renken, A. Catalytic Dehydrogenation of Methanol to Water-Free Formaldehyde. *Chem. Eng. Technol.* **1994**, *17*, 34−40.
(184) Žilnik, L. F.; Golob, J. Analysis of Separation of a Water-Methanol-Formaldehyde Mixture. *Acta Chim. Slov.* **2003**, *50*, 451−460.
(185) Shylesh, S.; Kim, D.; Ho, C. R.; Johnson, G. R.; Wu, J.; Bell, A. T. Non-Oxidative Dehydrogenation Pathways for the Conversion of $C_2$-$C_4$ Alcohols to Carbonyl Compounds. *ChemSusChem* **2015**, *8*, 3959−3962.
(186) Huber, G. W.; Iborra, S.; Corma, A. Synthesis of Transportation Fuels from Biomass: Chemistry, Catalysts, and Engineering. *Chem. Rev.* **2006**, *106*, 4044−4098.
(187) Rass-Hansen, J.; Falsig, H.; Jørgensen, B.; Christensen, C. H. Bioethanol: Fuel or Feedstock? *J. Chem. Technol. Biotechnol.* **2007**, *82*, 329−333.
(188) Prasad, R. Highly Active Copper Chromite Catalyst Produced by Thermal Decomposition of Ammoniac Copper Oxalate Chromate. *Mater. Lett.* **2005**, *59*, 3945−3949.
(189) Wang, Z.-T.; Xu, Y.; El-Soda, M.; Lucci, F. R.; Madix, R. J.; Friend, C. M.; Sykes, E. C. H. Surface Structure Dependence of the Dry Dehydrogenation of Alcohols on Cu(111) and Cu(110). *J. Phys. Chem. C* **2017**, *121*, 12800−12806.
(190) Sato, A. G.; Volanti, D. P.; de Freitas, I. C.; Longo, E.; Bueno, J. M. C. Site-Selective Ethanol Conversion over Supported Copper Catalysts. *Catal. Commun.* **2012**, *26*, 122−126.
(191) Cassinelli, W. H.; Martins, L.; Passos, A. R.; Pulcinelli, S. H.; Rochet, A.; Briois, V.; Santilli, C. V. Correlation between Structural and Catalytic Properties of Copper Supported on Porous Alumina for the Ethanol Dehydrogenation Reaction. *ChemCatChem.* **2015**, *7*, 1668−1677.
(192) Morales, M. V.; Asedegbega-Nieto, E.; Bachiller-Baeza, B.; Guerrero-Ruiz, A. Bioethanol Dehydrogenation over Copper Supported on Functionalized Graphene Materials and a High Surface Area Graphite. *Carbon N. Y.* **2016**, *102*, 426−436.
(193) Conesa, J. M.; Morales, M. V.; López-Olmos, C.; Rodríguez-Ramos, I.; Guerrero-Ruiz, A. Comparative Study of Cu, Ag and Ag-Cu Catalysts over Graphite in the Ethanol Dehydrogenation Reaction: Catalytic Activity, Deactivation and Regeneration. *Appl. Catal. A Gen.* **2019**, *576*, 54−64.
(194) He, X.; Wang, Y.; Zhang, X.; Dong, M.; Wang, G.; Zhang, B.; Niu, Y.; Yao, S.; He, X.; Liu, H. Controllable in Situ Surface Restructuring of Cu Catalysts and Remarkable Enhancement of Their Catalytic Activity. *ACS Catal.* **2019**, *9*, 2213−2221.
(195) Guan, Y.; Hensen, E. J. M. Ethanol Dehydrogenation by Gold Catalysts: The Effect of the Gold Particle Size and the Presence of Oxygen. *Appl. Catal. A Gen.* **2009**, *361*, 49−56.
(196) Hoyt, R. A.; Montemore, M. M.; Sykes, E. C. H.; Kaxiras, E. Anhydrous Methanol and Ethanol Dehydrogenation at Cu(111) Step Edges. *J. Phys. Chem. C* **2018**, *122*, 21952−21962.
(197) Chen, A.; Masel, R. Direct Conversion of Methanol to Formaldehyde in the Absence of Oxygen on Cu(210). *Surf. Sci.* **1995**, *343*, 17−23.
(198) Wang, Z.-T.; Hoyt, R. A.; El-Soda, M.; Madix, R. J.; Kaxiras, E.; Sykes, E. C. H. Dry Dehydrogenation of Ethanol on Pt-Cu Single Atom Alloys. *Top. Catal.* **2018**, *61*, 328−335.
(199) Li, H.; Evans, E. J.; Mullins, C. B.; Henkelman, G. Ethanol Decomposition on Pd-Au Alloy Catalysts. *J. Phys. Chem. C* **2018**, *122*, 22024−22032.
(200) Evans, E. J.; Li, H.; Yu, W.-Y.; Mullen, G. M.; Henkelman, G.; Mullins, C. B. Mechanistic Insights on Ethanol Dehydrogenation on Pd-Au Model Catalysts: A Combined Experimental and DFT Study. *Phys. Chem. Chem. Phys.* **2017**, *19*, 30578−30589.
(201) Li, H.; Chai, W.; Henkelman, G. Selectivity for Ethanol Partial Oxidation: The Unique Chemistry of Single-Atom Alloy Catalysts on Au, Ag, and Cu(111). *J. Mater. Chem. A* **2019**, *7*, 23868−23877.
(202) Khan, T. S.; Jalid, F.; Haider, M. A. First-Principle Microkinetic Modeling of Ethanol Dehydrogenation on Metal Catalyst Surfaces in Non-Oxidative Environment: Design of Bimetallic Alloys. *Top. Catal.* **2018**, *61*, 1820−1831.
(203) Schlosser, D. A.; Yehorova, D.; Kaleem, H.; Maxwell, E. M.; Baker, J. S.; Gillum, M. Z.; DePonte, M. C.; Letchworth-Weaver, K.; Baber, A. E. Effect of Undercoordinated Ag(111) Defect Sites on the Adsorption of Ethanol. *J. Vac. Sci. Technol. A* **2020**, *38*, 033213.
(204) Takei, T.; Iguchi, N.; Haruta, M. Synthesis of Acetoaldehyde, Acetic Acid, and Others by the Dehydrogenation and Oxidation of Ethanol. *Catal. Surv. from Asia* **2011**, *15*, 80−88.
(205) Wachs, I. E.; Madix, R. J. The Selective Oxidation of $CH_3OH$ to $H_2CO$ on a Copper(110) Catalyst. *J. Catal.* **1978**, *53*, 208−227.
(206) Chen, W.; Cubuk, E. D.; Montemore, M. M.; Reece, C.; Madix, R. J.; Friend, C. M.; Kaxiras, E. A Comparative Ab Initio Study of Anhydrous Dehydrogenation of Linear-Chain Alcohols on Cu(110). *J. Phys. Chem. C* **2018**, *122*, 7806−7815.


https://doi.org/10.1021/acs.chemrev.1c00967
*Chem. Rev.* 2022, 122, 8758−8808

(207) Bos, A. N. R.; Westerterp, K. R. Mechanism and Kinetics of the Selective Hydrogenation of Ethyne and Ethene. *Chem. Eng. Process. Process Intensif.* **1993**, *32*, 1−7.
(208) Schbib, N. S.; García, M. A.; Gígola, C. E.; Errazu, A. F. Kinetics of Front-End Acetylene Hydrogenation in Ethylene Production. *Ind. Eng. Chem. Res.* **1996**, *35*, 1496−1505.
(209) Chen, B.; Dingerdissen, U.; Krauter, J. G. E.; Lansink Rotgerink, H. G. J.; Möbus, K.; Ostgard, D. J.; Panster, P.; Riermeier, T. H.; Seebald, S.; Tacke, T.; et al. New Developments in Hydrogenation Catalysis Particularly in Synthesis of Fine and Intermediate Chemicals. *Appl. Catal. A Gen.* **2005**, *280*, 17−46.
(210) Studt, F.; Abild-Pedersen, F.; Bligaard, T.; Sorensen, R. Z.; Christensen, C. H.; Norskov, J. K. Identification of Non-Precious Metal Alloy Catalysts for Selective Hydrogenation of Acetylene. *Science* **2008**, *320*, 1320−1322.
(211) Teschner, D.; Vass, E.; Havecker, M.; Zafeiratos, S.; Schnorch, P.; Sauer, H.; Knopgericke, A.; Schlogl, R.; Chamam, M.; Wootsch, A. Alkyne Hydrogenation over Pd Catalysts: A New Paradigm. *J. Catal.* **2006**, *242*, 26−37.
(212) Teschner, D.; Borsodi, J.; Wootsch, A.; Revay, Z.; Havecker, M.; Knop-Gericke, A.; Jackson, S. D.; Schlogl, R. The Roles of Subsurface Carbon and Hydrogen in Palladium-Catalyzed Alkyne Hydrogenation. *Science* **2008**, *320*, 86−89.
(213) Armbrüster, M.; Behrens, M.; Cinquini, F.; Föttinger, K.; Grin, Y.; Haghofer, A.; Klötzer, B.; Knop-Gericke, A.; Lorenz, H.; Ota, A.; et al. How to Control the Selectivity of Palladium-Based Catalysts in Hydrogenation Reactions: The Role of Subsurface Chemistry. *ChemCatChem.* **2012**, *4*, 1048−1063.
(214) Benavidez, A. D.; Burton, P. D.; Nogales, J. L.; Jenkins, A. R.; Ivanov, S. A.; Miller, J. T.; Karim, A. M.; Datye, A. K. Improved Selectivity of Carbon-Supported Palladium Catalysts for the Hydrogenation of Acetylene in Excess Ethylene. *Appl. Catal. A Gen.* **2014**, *482*, 108−115.
(215) Studt, F.; Abild-Pedersen, F.; Bligaard, T.; Sørensen, R. Z.; Christensen, C. H.; Nørskov, J. K. On the Role of Surface Modifications of Palladium Catalysts in the Selective Hydrogenation of Acetylene. *Angew. Chemie Int. Ed.* **2008**, *47*, 9299−9302.
(216) Heuchel, M.; Snurr, R. Q.; Buss, E. Adsorption of CH 4 -CF 4 Mixtures in Silicalite: Simulation, Experiment, and Theory. *Langmuir* **1997**, *13*, 6795−6804.
(217) McLeod, A. S.; Blackwell, R. Monte Carlo Simulation of the Selective Hydrogenation of Acetylene. *Chem. Eng. Sci.* **2004**, *59*, 4715−4721.
(218) Jia, J.; Haraki, K.; Kondo, J. N.; Domen, K.; Tamaru, K. Selective Hydrogenation of Acetylene over $Au/Al_2O_3$ Catalyst. *J. Phys. Chem. B* **2000**, *104*, 11153−11156.
(219) Choudhary, T. V.; Sivadinarayana, C.; Datye, A. K.; Kumar, D.; Goodman, D. W. Acetylene Hydrogenation on Au-Based Catalysts. *Catal. Lett.* **2003**, *86*, 1−8.
(220) Azizi, Y.; Petit, C.; Pitchon, V. Formation of Polymer-Grade Ethylene by Selective Hydrogenation of Acetylene over Au/CeO2 Catalyst. *J. Catal.* **2008**, *256*, 338−344.
(221) Masoud, N.; Delannoy, L.; Schaink, H.; van der Eerden, A.; de Rijk, J. W.; Silva, T. A. G.; Banerjee, D.; Meeldijk, J. D.; de Jong, K. P.; Louis, C.; et al. Superior Stability of $Au/SiO_2$ Compared to $Au/TiO_2$ Catalysts for the Selective Hydrogenation of Butadiene. *ACS Catal.* **2017**, *7*, 5594−5603.
(222) Wang, S.; Xin, Z.; Huang, X.; Yu, W.; Niu, S.; Shao, L. Nanosized Pd-Au Bimetallic Phases on Carbon Nanotubes for Selective Phenylacetylene Hydrogenation. *Phys. Chem. Chem. Phys.* **2017**, *19*, 6164−6168.
(223) McCue, A. J.; Baker, R. T.; Anderson, J. A. Acetylene Hydrogenation over Structured Au-Pd Catalysts. *Faraday Discuss.* **2016**, *188*, 499−523.
(224) Lucci, F. R.; Marcinkowski, M. D.; Lawton, T. J.; Sykes, E. C. H. $H_2$ Activation and Spillover on Catalytically Relevant Pt-Cu Single Atom Alloys. *J. Phys. Chem. C* **2015**, *119*, 24351−24357.
(225) Fu, Q.; Luo, Y. Active Sites of Pd-Doped Flat and Stepped Cu(111) Surfaces for $H_2$ Dissociation in Heterogeneous Catalytic Hydrogenation. *ACS Catal.* **2013**, *3*, 1245−1252.
(226) McCue, A. J.; McRitchie, C. J.; Shepherd, A. M.; Anderson, J. A. $Cu/Al_2O_3$ Catalysts Modified with Pd for Selective Acetylene Hydrogenation. *J. Catal.* **2014**, *319*, 127−135.
(227) McCue, A. J.; Shepherd, A. M.; Anderson, J. A. Optimisation of Preparation Method for Pd Doped $Cu/Al_2O_3$ Catalysts for Selective Acetylene Hydrogenation. *Catal. Sci. Technol.* **2015**, *5*, 2880−2890.
(228) Biener, J.; Wittstock, A.; Baumann, T.; Weissmüller, J.; Bäumer, M.; Hamza, A. Surface Chemistry in Nanoscale Materials. *Materials (Basel).* **2009**, *2*, 2404−2428.
(229) O'Connor, C. R.; van Spronsen, M. A.; Egle, T.; Xu, F.; Kersell, H. R.; Oliver-Meseguer, J.; Karatok, M.; Salmeron, M.; Madix, R. J.; Friend, C. M. Hydrogen Migration at Restructuring Palladium-Silver Oxide Boundaries Dramatically Enhances Reduction Rate of Silver Oxide. *Nat. Commun.* **2020**, *11*, 1844.
(230) Skriver, H. L.; Rosengaard, N. M. Surface Energy and Work Function of Elemental Metals. *Phys. Rev. B* **1992**, *46*, 7157−7168.
(231) Gao, F.; Wang, Y.; Goodman, D. W. CO Oxidation over AuPd(100) from Ultrahigh Vacuum to Near-Atmospheric Pressures: The Critical Role of Contiguous Pd Atoms. *J. Am. Chem. Soc.* **2009**, *131*, 5734−5735.
(232) Gao, F.; Wang, Y.; Goodman, D. W. CO Oxidation over AuPd(100) from Ultrahigh Vacuum to Near-Atmospheric Pressures: CO Adsorption-Induced Surface Segregation and Reaction Kinetics. *J. Phys. Chem. C* **2009**, *113*, 14993−15000.
(233) Languille, M. A.; Ehret, E.; Lee, H. C.; Jeong, C. K.; Toyoshima, R.; Kondoh, H.; Mase, K.; Jugnet, Y.; Bertolini, J. C.; Aires, F. J. C. S.; et al. In-Situ Surface Analysis of AuPd(110) under Elevated Pressure of CO. *Catal. Today* **2016**, *260*, 39−45.
(234) Saint-Lager, M.-C.; Languille, M.-A.; Cadete Santos Aires, F. J.; Bailly, A.; Garaudee, S.; Ehret, E.; Robach, O. Oxygen-Induced Changes of the $Au_{30}Pd_{70}(110)$ Surface Structure and Composition under Increasing $O_2$ Pressure. *J. Phys. Chem. C* **2018**, *122*, 22588−22596.
(235) Boes, J. R.; Kitchin, J. R. Modeling Segregation on AuPd(111) Surfaces with Density Functional Theory and Monte Carlo Simulations. *J. Phys. Chem. C* **2017**, *121*, 3479−3487.
(236) Takehiro, N.; Liu, P.; Bergbreiter, A.; Nørskov, J. K.; Behm, R. J. Hydrogen Adsorption on Bimetallic PdAu(111) Surface Alloys: Minimum Adsorption Ensemble, Ligand and Ensemble Effects, and Ensemble Confinement. *Phys. Chem. Chem. Phys.* **2014**, *16*, 23930−23943.
(237) Yu, W.-Y.; Zhang, L.; Mullen, G. M.; Henkelman, G.; Mullins, C. B. Oxygen Activation and Reaction on Pd-Au Bimetallic Surfaces. *J. Phys. Chem. C* **2015**, *119*, 11754−11762.
(238) Lim, J. S.; Vandermause, J.; van Spronsen, M. A.; Musaelian, A.; Xie, Y.; Sun, L.; O'Connor, C. R.; Egle, T.; Molinari, N.; Florian, J.; et al. Evolution of Metastable Structures at Bimetallic Surfaces from Microscopy and Machine-Learning Molecular Dynamics. *J. Am. Chem. Soc.* **2020**, *142*, 15907−15916.
(239) Engstfeld, A. K.; Hoster, H. E.; Behm, R. J. Formation, Atomic Distribution and Mixing Energy in Two-Dimensional PdxAg1-x Surface Alloys on Pd(111). *Phys. Chem. Chem. Phys.* **2012**, *14*, 10754−10761.
(240) Ma, Y.; Diemant, T.; Bansmann, J.; Behm, R. J. The Interaction of CO with PdAg/Pd(111) Surface Alloys—A Case Study of Ensemble Effects on a Bimetallic Surface. *Phys. Chem. Chem. Phys.* **2011**, *13*, 10741.
(241) Wouda, P. T.; Schmid, M.; Nieuwenhuys, B. E.; Varga, P. STM Study of the (111) and (100) Surfaces of PdAg. *Surf. Sci.* **1998**, *417*, 292−300.
(242) Walle, L. E.; Grönbeck, H.; Fernandes, V. R.; Blomberg, S.; Farstad, M. H.; Schulte, K.; Gustafson, J.; Andersen, J. N.; Lundgren, E.; Borg, A. Surface Composition of Clean and Oxidized Pd75Ag25(100) from Photoelectron Spectroscopy and Density Functional Theory Calculations. *Surf. Sci.* **2012**, *606*, 1777−1782.


https://doi.org/10.1021/acs.chemrev.1c00967
*Chem. Rev.* 2022, 122, 8758−8808

(243) Fernandes, V. R.; Gustafson, J.; Svenum, I.-H.; Farstad, M. H.; Walle, L. E.; Blomberg, S.; Lundgren, E.; Borg, A. Reduction Behavior of Oxidized Pd(100) and Pd75Ag25(100) Surfaces Using CO. *Surf. Sci.* **2014**, *621*, 31−39.
(244) Simonovis, J. P.; Hunt, A.; Palomino, R. M.; Senanayake, S. D.; Waluyo, I. Enhanced Stability of Pt-Cu Single-Atom Alloy Catalysts: In Situ Characterization of the Pt/Cu(111) Surface in an Ambient Pressure of CO. *J. Phys. Chem. C* **2018**, *122*, 4488−4495.
(245) Lim, J. S.; Molinari, N.; Duanmu, K.; Sautet, P.; Kozinsky, B. Automated Detection and Characterization of Surface Restructuring Events in Bimetallic Catalysts. *J. Phys. Chem. C* **2019**, *123*, 16332−16344.
(246) Prins, R. Hydrogen Spillover. Facts and Fiction. *Chem. Rev.* **2012**, *112*, 2714−2738.
(247) Levy, R. B.; Boudart, M. The Kinetics and Mechanism of Spillover. *J. Catal.* **1974**, *32*, 304−314.
(248) Goodman, D. W.; Yates, J. T.; Peden, C. H. F. The Reaction of Atomic Copper with Chemisorbed Hydrogen on Ruthenium. *Surf. Sci.* **1985**, *164*, 417−424.
(249) Marcinkowski, M. D.; Jewell, A. D.; Stamatakis, M.; Boucher, M. B.; Lewis, E. A.; Murphy, C. J.; Kyriakou, G.; Sykes, E. C. H. Controlling a Spillover Pathway with the Molecular Cork Effect. *Nat. Mater.* **2013**, *12*, 523−528.
(250) Lewis, E. A.; Marcinkowski, M. D.; Murphy, C. J.; Liriano, M. L.; Sykes, E. C. H. Hydrogen Dissociation, Spillover, and Desorption from Cu-Supported Co Nanoparticles. *J. Phys. Chem. Lett.* **2014**, *5*, 3380−3385.
(251) Lucci, F. R.; Darby, M. T.; Mattera, M. F. G.; Ivimey, C. J.; Therrien, A. J.; Michaelides, A.; Stamatakis, M.; Sykes, E. C. H. Controlling Hydrogen Activation, Spillover, and Desorption with Pd-Au Single-Atom Alloys. *J. Phys. Chem. Lett.* **2016**, *7*, 480−485.
(252) Yao, Y.; Goodman, D. W. Direct Evidence of Hydrogen Spillover from Ni to Cu on Ni-Cu Bimetallic Catalysts. *J. Mol. Catal. A Chem.* **2014**, *383*−*384*, 239−242.
(253) Darby, M. T.; Stamatakis, M.; Michaelides, A.; Sykes, E. C. H. Lonely Atoms with Special Gifts: Breaking Linear Scaling Relationships in Heterogeneous Catalysis with Single-Atom Alloys. *J. Phys. Chem. Lett.* **2018**, *9*, 5636−5646.
(254) Muir, M.; Trenary, M. Adsorption of CO to Characterize the Structure of a Pd/Ag(111) Single-Atom Alloy Surface. *J. Phys. Chem. C* **2020**, *124*, 14722−14729.
(255) O'Connor, C. R.; Duanmu, K.; Patel, D. A.; Muramoto, E.; van Spronsen, M. A.; Stacchiola, D.; Sykes, E. C. H.; Sautet, P.; Madix, R. J.; Friend, C. M. Facilitating Hydrogen Atom Migration via a Dense Phase on Palladium Islands to a Surrounding Silver Surface. *Proc. Natl. Acad. Sci. U. S. A.* **2020**, *117*, 22657−22664.
(256) Mehar, V.; O'Connor, C. R.; Egle, T.; Karatok, M.; Madix, R. J.; Friend, C. M.; Weaver, J. F. Growth and Auto-Oxidation of Pd on Single-Layer $AgO_x$/Ag(111). *Phys. Chem. Chem. Phys.* **2020**, *22*, 6202−6209.
(257) Mehar, V.; Almithn, A.; Egle, T.; Yu, M.-H.; O'Connor, C. R.; Karatok, M.; Madix, R. J.; Hibbitts, D.; Weaver, J. F. Oxophilicity Drives Oxygen Transfer at a Palladium-Silver Interface for Increased CO Oxidation Activity. *ACS Catal.* **2020**, *10*, 13878−13889.
(258) Karatok, M.; Egle, T.; Mehar, V.; O'Connor, C. R.; Yu, M.-H.; Friend, C. M.; Weaver, J. F. Reduction of Oxidized Pd/Ag(111) Surfaces by H 2 : Sensitivity to PdO Island Size and Dispersion. *ACS Catal.* **2020**, *10*, 10117−10124.
(259) Egle, T.; O'Connor, C. R.; Friend, C. M. Regeneration of Active Surface Alloys during Cyclic Oxidation and Reduction: Oxidation of H 2 on Pd/Ag(111). *J. Phys. Chem. Lett.* **2021**, *12*, 6752−6759.
(260) Martin, N. M.; Van den Bossche, M.; Grönbeck, H.; Hakanoglu, C.; Gustafson, J.; Blomberg, S.; Arman, M. A.; Antony, A.; Rai, R.; Asthagiri, A.; et al. Dissociative Adsorption of Hydrogen on PdO(101) Studied by HRCLS and DFT. *J. Phys. Chem. C* **2013**, *117*, 13510−13519.
(261) Mohammad, A. B.; Yudanov, I. V.; Lim, K. H.; Neyman, K. M.; Rösch, N. Hydrogen Activation on Silver: A Computational Study on Surface and Subsurface Oxygen Species. *J. Phys. Chem. C* **2008**, *112*, 1628−1635.
(262) Mohammad, A. B.; Hwa Lim, K.; Yudanov, I. V.; Neyman, K. M.; Rösch, N. A Computational Study of $H_2$ Dissociation on Silver Surfaces: The Effect of Oxygen in the Added Row Structure of Ag(110). *Phys. Chem. Chem. Phys.* **2007**, *9*, 1247−1254.
(263) Schilling, A. C.; Groden, K.; Simonovis, J. P.; Hunt, A.; Hannagan, R. T.; Çınar, V.; McEwen, J.-S.; Sykes, E. C. H.; Waluyo, I. Accelerated $Cu_2O$ Reduction by Single Pt Atoms at the Metal-Oxide Interface. *ACS Catal.* **2020**, *10*, 4215−4226.
(264) Weaver, J. F.; Choi, J.; Mehar, V.; Wu, C. Kinetic Coupling among Metal and Oxide Phases during CO Oxidation on Partially Reduced PdO(101): Influence of Gas-Phase Composition. *ACS Catal.* **2017**, *7*, 7319−7331.
(265) Weaver, J. F.; Zhang, F.; Pan, L.; Li, T.; Asthagiri, A. Vacancy-Mediated Processes in the Oxidation of CO on PdO(101). *Acc. Chem. Res.* **2015**, *48*, 1515−1523.
(266) Zhang, F.; Pan, L.; Li, T.; Diulus, J. T.; Asthagiri, A.; Weaver, J. F. CO Oxidation on PdO(101) during Temperature-Programmed Reaction Spectroscopy: Role of Oxygen Vacancies. *J. Phys. Chem. C* **2014**, *118*, 28647−28661.
(267) Zhang, F.; Li, T.; Pan, L.; Asthagiri, A.; Weaver, J. F. CO Oxidation on Single and Multilayer Pd Oxides on Pd(111): Mechanistic Insights from RAIRS. *Catal. Sci. Technol.* **2014**, *4*, 3826−3834.
(268) Klust, A.; Madix, R. J. Mesoscopic Restructuring and Mass Transport of Metal Atoms during Reduction of the Ag(111)-p(4 × 4)-O Surface with CO. *J. Chem. Phys.* **2007**, *126*, 084707.
(269) Koningsberger, D. C.; Prins, R. *X-ray Absorption: Principles, Applications, Techniques of EXAFS, SEXAFS, and XANES*; John Wiley and Sons Inc., 1988; p viii.
(270) Bunker, G. *Introduction to XAFS*; Cambridge University Press: Cambridge, 2010; pp 96−100.
(271) Rehr, J. J.; Albers, R. C. Theoretical Approaches to X-Ray Absorption Fine Structure. *Rev. Mod. Phys.* **2000**, *72*, 621−654.
(272) Penner-Hahn, J. E. X-Ray Absorption Spectroscopy in Coordination Chemistry. *Coord. Chem. Rev.* **1999**, *190*−*192*, 1101−1123.
(273) Russell, A. E.; Rose, A. X-Ray Absorption Spectroscopy of Low Temperature Fuel Cell Catalysts. *Chem. Rev.* **2004**, *104*, 4613−4636.
(274) Wende, H. Recent Advances in X-Ray Absorption Spectroscopy. *Rep. Prog. Phys.* **2004**, *67*, 2105−2181.
(275) Nashner, M. S.; Frenkel, A. I.; Adler, D. L.; Shapley, J. R.; Nuzzo, R. G. Structural Characterization of Carbon-Supported Platinum-Ruthenium Nanoparticles from the Molecular Cluster Precursor $PtRu_5C(CO)_{16}$. *J. Am. Chem. Soc.* **1997**, *119*, 7760−7771.
(276) Singh, J.; Lamberti, C.; van Bokhoven, J. A. Advanced X-Ray Absorption and Emission Spectroscopy: In Situ Catalytic Studies. *Chem. Soc. Rev.* **2010**, *39*, 4754−4766.
(277) Timoshenko, J.; Roldan Cuenya, B. In Situ/Operando Electrocatalyst Characterization by X-Ray Absorption Spectroscopy. *Chem. Rev.* **2021**, *121*, 882−961.
(278) Filipponi, A. EXAFS for Liquids. *J. Phys.: Condens. Matter* **2001**, *13*, R23−R60.
(279) Hardacre, C. Application of EXAFS to Molten Salts and Ionic Liquid Technology. *Annu. Rev. Mater. Res.* **2005**, *35*, 29−49.
(280) Frenkel, A. I.; Wang, Q.; Sanchez, S. I.; Small, M. W.; Nuzzo, R. G. Short Range Order in Bimetallic Nanoalloys: An Extended X-Ray Absorption Fine Structure Study. *J. Chem. Phys.* **2013**, *138*, 064202.
(281) Frenkel, A. I. Applications of Extended X-Ray Absorption Fine-Structure Spectroscopy to Studies of Bimetallic Nanoparticle Catalysts. *Chem. Soc. Rev.* **2012**, *41*, 8163.
(282) Glasner, D.; Frenkel, A. I. Geometrical Characteristics of Regular Polyhedra: Application to EXAFS Studies of Nanoclusters. *AIP Conference Proceedings*; AIP, 2007; Vol. *882*, pp 746−748.
(283) Marx, D.; Hutter, J. Ab Initio Molecular Dynamics: Theory and Implementation. In *Modern Methods and Algorithms of Quantum*


https://doi.org/10.1021/acs.chemrev.1c00967
*Chem. Rev.* 2022, 122, 8758−8808

*Chemistry*; Grotendorst, J., Ed.; John von Neumann Institute for Computing, 2000; Vol. *1*, pp 301−449.
(284) Roy, S.; Liu, Y.; Topsakal, M.; Dias, E.; Gakhar, R.; Phillips, W. C.; Wishart, J. F.; Leshchev, D.; Halstenberg, P.; Dai, S.; et al. A Holistic Approach for Elucidating Local Structure, Dynamics, and Speciation in Molten Salts with High Structural Disorder. *J. Am. Chem. Soc.* **2021**, *143*, 15298−15308.
(285) Gill, S. K.; Huang, J.; Mausz, J.; Gakhar, R.; Roy, S.; Vila, F.; Topsakal, M.; Phillips, W. C.; Layne, B.; Mahurin, S.; et al. Connections between the Speciation and Solubility of Ni(II) and Co(II) in Molten ZnCl 2. *J. Phys. Chem. B* **2020**, *124*, 1253−1258.
(286) Kraynis, O.; Timoshenko, J.; Huang, J.; Singh, H.; Wachtel, E.; Frenkel, A. I.; Lubomirsky, I. Modeling Strain Distribution at the Atomic Level in Doped Ceria Films with Extended X-Ray Absorption Fine Structure Spectroscopy. *Inorg. Chem.* **2019**, *58*, 7527−7536.
(287) Timoshenko, J.; Lu, D.; Lin, Y.; Frenkel, A. I. Supervised Machine-Learning-Based Determination of Three-Dimensional Structure of Metallic Nanoparticles. *J. Phys. Chem. Lett.* **2017**, *8*, 5091−5098.
(288) Schmeide, K.; Rossberg, A.; Bok, F.; Shams Aldin Azzam, S.; Weiss, S.; Scheinost, A. C. Technetium Immobilization by Chukanovite and Its Oxidative Transformation Products: Neural Network Analysis of EXAFS Spectra. *Sci. Total Environ.* **2021**, *770*, 145334.
(289) Martini, A.; Bugaev, A. L.; Guda, S. A.; Guda, A. A.; Priola, E.; Borfecchia, E.; Smolders, S.; Janssens, K.; De Vos, D.; Soldatov, A. V. Revisiting the Extended X-Ray Absorption Fine Structure Fitting Procedure through a Machine Learning-Based Approach. *J. Phys. Chem. A* **2021**, *125*, 7080−7091.
(290) Terry, J.; Lau, M. L.; Sun, J.; Xu, C.; Hendricks, B.; Kise, J.; Lnu, M.; Bagade, S.; Shah, S.; Makhijani, P.; et al. Analysis of Extended X-Ray Absorption Fine Structure (EXAFS) Data Using Artificial Intelligence Techniques. *Appl. Surf. Sci.* **2021**, *547*, 149059.
(291) Timoshenko, J.; Wrasman, C. J.; Luneau, M.; Shirman, T.; Cargnello, M.; Bare, S. R.; Aizenberg, J.; Friend, C. M.; Frenkel, A. I. Probing Atomic Distributions in Mono- and Bimetallic Nanoparticles by Supervised Machine Learning. *Nano Lett.* **2019**, *19*, 520−529.
(292) Frenkel, A. I.; Nemzer, S.; Pister, I.; Soussan, L.; Harris, T.; Sun, Y.; Rafailovich, M. H. Size-Controlled Synthesis and Characterization of Thiol-Stabilized Gold Nanoparticles. *J. Chem. Phys.* **2005**, *123*, 184701.
(293) Marcella, N.; Liu, Y.; Timoshenko, J.; Guan, E.; Luneau, M.; Shirman, T.; Plonka, A. M.; van der Hoeven, J. E. S.; Aizenberg, J.; Friend, C. M.; et al. Neural Network Assisted Analysis of Bimetallic Nanocatalysts Using X-Ray Absorption near Edge Structure Spectroscopy. *Phys. Chem. Chem. Phys.* **2020**, *22*, 18902−18910.
(294) Zafeiratos, S.; Piccinin, S.; Teschner, D. Alloys in Catalysis: Phase Separation and Surface Segregation Phenomena in Response to the Reactive Environment. *Catal. Sci. Technol.* **2012**, *2*, 1787−1801.
(295) Davis, R. J.; Landry, S. M.; Horsley, J. A.; Boudart, M. X-Ray-Absorption Study of the Interaction of Hydrogen with Clusters of Supported Palladium. *Phys. Rev. B* **1989**, *39*, 10580−10583.
(296) Tew, M. W.; Miller, J. T.; van Bokhoven, J. A. Particle Size Effect of Hydride Formation and Surface Hydrogen Adsorption of Nanosized Palladium Catalysts: L-3 Edge vs K Edge X-Ray Absorption Spectroscopy. *J. Phys. Chem. C* **2009**, *113*, 15140−15147.
(297) Wang, J.; Wang, Q.; Jiang, X.; Liu, Z.; Yang, W.; Frenkel, A. I. Determination of Nanoparticle Size by Measuring the Metal-Metal Bond Length: The Case of Palladium Hydride. *J. Phys. Chem. C* **2015**, *119*, 854−861.
(298) Bugaev, A. L.; Guda, A. A.; Lazzarini, A.; Lomachenko, K. A.; Groppo, E.; Pellegrini, R.; Piovano, A.; Emerich, H.; Soldatov, A. V.; Bugaev, L. A.; et al. In Situ Formation of Hydrides and Carbides in Palladium Catalyst: When XANES Is Better than EXAFS and XRD. *Catal. Today* **2017**, *283*, 119−126.
(299) Hansen, T. W., Wagner, J. B., Eds. *Controlled Atmosphere Transmission Electron Microscopy*; Springer International Publishing: Cham, Switzerland, 2016; Vol. *August*, pp 237−258.
(300) Wang, D.; Xin, H. L.; Hovden, R.; Wang, H.; Yu, Y.; Muller, D. A.; DiSalvo, F. J.; Abruña, H. D. Structurally Ordered Intermetallic Platinum-Cobalt Core-Shell Nanoparticles with Enhanced Activity and Stability as Oxygen Reduction Electrocatalysts. *Nat. Mater.* **2013**, *12*, 81−87.
(301) Jung, U.; Elsen, A.; Li, Y.; Smith, J. G.; Small, M. W.; Stach, E. A.; Frenkel, A. I.; Nuzzo, R. G. Comparative in Operando Studies in Heterogeneous Catalysis: Atomic and Electronic Structural Features in the Hydrogenation of Ethylene over Supported Pd and Pt Catalysts. *ACS Catal.* **2015**, *5*, 1539−1551.
(302) Liu, D.; Li, Y.; Kottwitz, M.; Yan, B.; Yao, S.; Gamalski, A.; Grolimund, D.; Safonova, O. V.; Nachtegaal, M.; Chen, J. G.; et al. Identifying Dynamic Structural Changes of Active Sites in Pt-Ni Bimetallic Catalysts Using Multimodal Approaches. *ACS Catal.* **2018**, *8*, 4120−4131.
(303) Carter, C. B.; Williams, D. B. Transmission Electron Microscopy. In *Transmission Electron Microscopy: Diffraction, Imaging, and Spectrometry*; Carter, C. B., Williams, D. B., Eds.; Springer International Publishing: Cham, Switzerland, 2016; pp 30−33.
(304) Zou, L.; Li, J.; Zakharov, D.; Stach, E. A.; Zhou, G. In Situ Atomic-Scale Imaging of the Metal/Oxide Interfacial Transformation. *Nat. Commun.* **2017**, *8*, 307.
(305) Wang, C.-M.; Genc, A.; Cheng, H.; Pullan, L.; Baer, D. R.; Bruemmer, S. M. In-Situ TEM Visualization of Vacancy Injection and Chemical Partition during Oxidation of Ni-Cr Nanoparticles. *Sci. Rep.* **2015**, *4*, 3683.
(306) Bohra, M.; Grammatikopoulos, P.; Singh, V.; Zhao, J.; Toulkeridou, E.; Steinhauer, S.; Kioseoglou, J.; Bobo, J.-F.; Nordlund, K.; Djurabekova, F.; et al. Tuning the Onset of Ferromagnetism in Heterogeneous Bimetallic Nanoparticles by Gas Phase Doping. *Phys. Rev. Mater.* **2017**, *1*, 066001.
(307) Xia, W.; Yang, Y.; Meng, Q.; Deng, Z.; Gong, M.; Wang, J.; Wang, D.; Zhu, Y.; Sun, L.; Xu, F.; et al. Bimetallic Nanoparticle Oxidation in Three Dimensions by Chemically Sensitive Electron Tomography and in Situ Transmission Electron Microscopy. *ACS Nano* **2018**, *12*, 7866−7874.
(308) Han, L.; Meng, Q.; Wang, D.; Zhu, Y.; Wang, J.; Du, X.; Stach, E. A.; Xin, H. L. Interrogation of Bimetallic Particle Oxidation in Three Dimensions at the Nanoscale. *Nat. Commun.* **2016**, *7*, 13335.
(309) Li, Y.; Zakharov, D.; Zhao, S.; Tappero, R.; Jung, U.; Elsen, A.; Baumann, P.; Nuzzo, R. G.; Stach, E. A.; Frenkel, A. I. Complex Structural Dynamics of Nanocatalysts Revealed in Operando Conditions by Correlated Imaging and Spectroscopy Probes. *Nat. Commun.* **2015**, *6*, 7583.
(310) Hammer, B.; Norskov, J. K. Why Gold Is the Noblest of All the Metals. *Nature* **1995**, *376*, 238−240.
(311) Hammer, B.; Nørskov, J. K. Theoretical Surface Science and Catalysis—Calculations and Concepts. *Advances in Catalysis*; Academic Press, 2000; Vol. *45*, pp 71−129.
(312) Gao, W.; Baker, T. A.; Zhou, L.; Pinnaduwage, D. S.; Kaxiras, E.; Friend, C. M. Chlorine Adsorption on Au(111): Chlorine Overlayer or Surface Chloride? *J. Am. Chem. Soc.* **2008**, *130*, 3560−3565.
(313) Ulissi, Z. W.; Medford, A. J.; Bligaard, T.; Nørskov, J. K. To Address Surface Reaction Network Complexity Using Scaling Relations Machine Learning and DFT Calculations. *Nat. Commun.* **2017**, *8*, 14621.
(314) Campbell, C.; Bowker, M.; Stamatakis, M.; Hutchings, G.; Davies, P.; Earley, J.; Howard, M.; Garrett, B.; Oloye, F.; Gross, E.; et al. Bridging Model and Real Catalysts: General Discussion. *Faraday Discuss.* **2016**, *188*, 565−589.
(315) Wang, Y.-G.; Cantu, D. C.; Lee, M.-S.; Li, J.; Glezakou, V.-A.; Rousseau, R. CO Oxidation on $Au/TiO_2$: Condition-Dependent Active Sites and Mechanistic Pathways. *J. Am. Chem. Soc.* **2016**, *138*, 10467−10476.
(316) Cheng, T.; Xiao, H.; Goddard, W. A. Full Atomistic Reaction Mechanism with Kinetics for CO Reduction on Cu(100) from Ab Initio Molecular Dynamics Free-Energy Calculations at 298 K. *Proc. Natl. Acad. Sci. U. S. A.* **2017**, *114*, 1795−1800.


https://doi.org/10.1021/acs.chemrev.1c00967
*Chem. Rev.* 2022, 122, 8758−8808

(317) He, Y.; Liu, J.-C.; Luo, L.; Wang, Y.-G.; Zhu, J.; Du, Y.; Li, J.; Mao, S. X.; Wang, C. Size-Dependent Dynamic Structures of Supported Gold Nanoparticles in CO Oxidation Reaction Condition. *Proc. Natl. Acad. Sci. U. S. A.* **2018**, *115*, 7700−7705.
(318) Xu, C.-Q.; Lee, M.-S.; Wang, Y.-G.; Cantu, D. C.; Li, J.; Glezakou, V.-A.; Rousseau, R. Structural Rearrangement of Au-Pd Nanoparticles under Reaction Conditions: An Ab Initio Molecular Dynamics Study. *ACS Nano* **2017**, *11*, 1649−1658.
(319) Yang, Y.; Shen, X.; Han, Y.-F. Diffusion Mechanisms of Metal Atoms in Pd Au Bimetallic Catalyst under CO Atmosphere Based on Ab Initio Molecular Dynamics. *Appl. Surf. Sci.* **2019**, *483*, 991−1005.
(320) Zhu, B.; Creuze, J.; Mottet, C.; Legrand, B.; Guesmi, H. CO Adsorption-Induced Surface Segregation and Formation of Pd Chains on AuPd(100) Alloy: Density Functional Theory Based Ising Model and Monte Carlo Simulations. *J. Phys. Chem. C* **2016**, *120*, 350−359.
(321) Vignola, E.; Steinmann, S. N.; Le Mapihan, K.; Vandegehuchte, B. D.; Curulla, D.; Sautet, P. Acetylene Adsorption on Pd-Ag Alloys: Evidence for Limited Island Formation and Strong Reverse Segregation from Monte Carlo Simulations. *J. Phys. Chem. C* **2018**, *122*, 15456−15463.
(322) Senftle, T. P.; Hong, S.; Islam, M. M.; Kylasa, S. B.; Zheng, Y.; Shin, Y. K.; Junkermeier, C.; Engel-Herbert, R.; Janik, M. J.; Aktulga, H. M.; et al. The ReaxFF Reactive Force-Field: Development, Applications and Future Directions. *npj Comput. Mater.* **2016**, *2*, 15011.
(323) Liang, T.; Shan, T.-R.; Cheng, Y.-T.; Devine, B. D.; Noordhoek, M.; Li, Y.; Lu, Z.; Phillpot, S. R.; Sinnott, S. B. Classical Atomistic Simulations of Surfaces and Heterogeneous Interfaces with the Charge-Optimized Many Body (COMB) Potentials. *Mater. Sci. Eng. R Reports* **2013**, *74*, 255−279.
(324) Fantauzzi, D.; Bandlow, J.; Sabo, L.; Mueller, J. E.; van Duin, A. C. T.; Jacob, T. Development of a ReaxFF Potential for Pt-O Systems Describing the Energetics and Dynamics of Pt-Oxide Formation. *Phys. Chem. Chem. Phys.* **2014**, *16*, 23118−23133.
(325) Ludwig, J.; Vlachos, D. G.; van Duin, A. C. T.; Goddard, W. A. Dynamics of the Dissociation of Hydrogen on Stepped Platinum Surfaces Using the ReaxFF Reactive Force Field. *J. Phys. Chem. B* **2006**, *110*, 4274−4282.
(326) Hu, X.; Schuster, J.; Schulz, S. E. Multiparameter and Parallel Optimization of ReaxFF Reactive Force Field for Modeling the Atomic Layer Deposition of Copper. *J. Phys. Chem. C* **2017**, *121*, 28077−28089.
(327) Cheng, T.; Jaramillo-Botero, A.; Goddard, W. A.; Sun, H. Adaptive Accelerated ReaxFF Reactive Dynamics with Validation from Simulating Hydrogen Combustion. *J. Am. Chem. Soc.* **2014**, *136*, 9434−9442.
(328) Senftle, T. P.; Janik, M. J.; van Duin, A. C. T. A ReaxFF Investigation of Hydride Formation in Palladium Nanoclusters via Monte Carlo and Molecular Dynamics Simulations. *J. Phys. Chem. C* **2014**, *118*, 4967−4981.
(329) Shin, Y. K.; Gai, L.; Raman, S.; van Duin, A. C. T. Development of a ReaxFF Reactive Force Field for the Pt-Ni Alloy Catalyst. *J. Phys. Chem. A* **2016**, *120*, 8044−8055.
(330) Zou, C.; van Duin, A. C. T.; Sorescu, D. C. Theoretical Investigation of Hydrogen Adsorption and Dissociation on Iron and Iron Carbide Surfaces Using the ReaxFF Reactive Force Field Method. *Top. Catal.* **2012**, *55*, 391−401.
(331) Blank, T. B.; Brown, S. D.; Calhoun, A. W.; Doren, D. J. Neural Network Models of Potential Energy Surfaces. *J. Chem. Phys.* **1995**, *103*, 4129−4137.
(332) Behler, J. Representing Potential Energy Surfaces by High-Dimensional Neural Network Potentials. *J. Phys.: Condens. Matter* **2014**, *26*, 183001.
(333) Behler, J. Neural Network Potential-Energy Surfaces in Chemistry: A Tool for Large-Scale Simulations. *Phys. Chem. Chem. Phys.* **2011**, *13*, 17930.
(334) Sun, G.; Sautet, P. Toward Fast and Reliable Potential Energy Surfaces for Metallic Pt Clusters by Hierarchical Delta Neural Networks. *J. Chem. Theory Comput.* **2019**, *15*, 5614−5627.
(335) Bartók, A. P.; Payne, M. C.; Kondor, R.; Csányi, G. Gaussian Approximation Potentials: The Accuracy of Quantum Mechanics, without the Electrons. *Phys. Rev. Lett.* **2010**, *104*, 136403.
(336) Schütt, K. T.; Sauceda, H. E.; Kindermans, P.-J.; Tkatchenko, A.; Müller, K.-R. SchNet - A Deep Learning Architecture for Molecules and Materials. *J. Chem. Phys.* **2018**, *148*, 241722.
(337) Shapeev, A. V. Moment Tensor Potentials: A Class of Systematically Improvable Interatomic Potentials. *Multiscale Model. Simul.* **2016**, *14*, 1153−1173.
(338) Thompson, A. P.; Swiler, L. P.; Trott, C. R.; Foiles, S. M.; Tucker, G. J. Spectral Neighbor Analysis Method for Automated Generation of Quantum-Accurate Interatomic Potentials. *J. Comput. Phys.* **2015**, *285*, 316−330.
(339) Zeni, C.; Rossi, K.; Glielmo, A.; Fekete, Á.; Gaston, N.; Baletto, F.; De Vita, A. Building Machine Learning Force Fields for Nanoclusters. *J. Chem. Phys.* **2018**, *148*, 241739.
(340) Zhang, L.; Han, J.; Wang, H.; Car, R.; E, W. Deep Potential Molecular Dynamics: A Scalable Model with the Accuracy of Quantum Mechanics. *Phys. Rev. Lett.* **2018**, *120*, 143001.
(341) Vandermause, J.; Torrisi, S. B.; Batzner, S.; Xie, Y.; Sun, L.; Kolpak, A. M.; Kozinsky, B. On-the-Fly Active Learning of Interpretable Bayesian Force Fields for Atomistic Rare Events. *npj Comput. Mater.* **2020**, *6*, 20.
(342) Xie, Y.; Vandermause, J.; Sun, L.; Cepellotti, A.; Kozinsky, B. Bayesian Force Fields from Active Learning for Simulation of Inter-Dimensional Transformation of Stanene. *npj Comput. Mater.* **2021**, *7*, 40.
(343) FLARE: Fast Learning of Atomistic Rare Events; https://github.com/mir-group/flare (accessed 2022-03-01).
(344) Batzner, S.; Smidt, T. E.; Sun, L.; Mailoa, J. P.; Kornbluth, M.; Molinari, N.; Kozinsky, B. SE(3)-Equivariant Graph Neural Networks for Data-Efficient and Accurate Interatomic Potentials. *arXiv* **2021**; https://arxiv.org/abs/2101.03164.
(345) Artrith, N.; Kolpak, A. M. Grand Canonical Molecular Dynamics Simulations of Cu-Au Nanoalloys in Thermal Equilibrium Using Reactive ANN Potentials. *Comput. Mater. Sci.* **2015**, *110*, 20−28.
(346) Artrith, N.; Hiller, B.; Behler, J. Neural Network Potentials for Metals and Oxides - First Applications to Copper Clusters at Zinc Oxide. *Phys. status solidi* **2013**, *250*, 1191−1203.
(347) Behler, J.; Reuter, K.; Scheffler, M. Nonadiabatic Effects in the Dissociation of Oxygen Molecules at the Al(111) Surface. *Phys. Rev. B* **2008**, *77*, 115421.
(348) Shakouri, K.; Behler, J.; Meyer, J.; Kroes, G.-J. Accurate Neural Network Description of Surface Phonons in Reactive Gas-Surface Dynamics: $N_2$ + Ru(0001). *J. Phys. Chem. Lett.* **2017**, *8*, 2131−2136.
(349) Lorenz, S.; Scheffler, M.; Gross, A. Descriptions of Surface Chemical Reactions Using a Neural Network Representation of the Potential-Energy Surface. *Phys. Rev. B* **2006**, *73*, 115431.
(350) Kolb, B.; Luo, X.; Zhou, X.; Jiang, B.; Guo, H. High-Dimensional Atomistic Neural Network Potentials for Molecule-Surface Interactions: HCl Scattering from Au(111). *J. Phys. Chem. Lett.* **2017**, *8*, 666−672.
(351) Steinmann, S. N.; Ferreira De Morais, R.; Götz, A. W.; Fleurat-Lessard, P.; Iannuzzi, M.; Sautet, P.; Michel, C. Force Field for Water over Pt(111): Development, Assessment, and Comparison. *J. Chem. Theory Comput.* **2018**, *14*, 3238−3251.
(352) del Cueto, M.; Zhou, X.; Zhou, L.; Zhang, Y.; Jiang, B.; Guo, H. New Perspectives on $CO_2$-Pt(111) Interaction with a High-Dimensional Neural Network Potential Energy Surface. *J. Phys. Chem. C* **2020**, *124*, 5174−5181.
(353) Weinreich, J.; Römer, A.; Paleico, M. L.; Behler, J. Properties of α-Brass Nanoparticles. 1. Neural Network Potential Energy Surface. *J. Phys. Chem. C* **2020**, *124*, 12682−12695.
(354) Nyshadham, C.; Rupp, M.; Bekker, B.; Shapeev, A. V.; Mueller, T.; Rosenbrock, C. W.; Csányi, G.; Wingate, D. W.; Hart, G. L. W. Machine-Learned Multi-System Surrogate Models for Materials Prediction. *npj Comput. Mater.* **2019**, *5*, 51.


https://doi.org/10.1021/acs.chemrev.1c00967
*Chem. Rev.* 2022, 122, 8758−8808

(355) Gubaev, K.; Podryabinkin, E. V.; Hart, G. L. W.; Shapeev, A. V. Accelerating High-Throughput Searches for New Alloys with Active Learning of Interatomic Potentials. *Comput. Mater. Sci.* **2019**, *156*, 148−156.
(356) Zeni, C.; Rossi, K.; Glielmo, A.; Baletto, F. On Machine Learning Force Fields for Metallic Nanoparticles. *Adv. Phys. X* **2019**, *4*, 1654919.
(357) Artrith, N.; Kolpak, A. M. Understanding the Composition and Activity of Electrocatalytic Nanoalloys in Aqueous Solvents: A Combination of DFT and Accurate Neural Network Potentials. *Nano Lett.* **2014**, *14*, 2670−2676.
(358) Kolsbjerg, E. L.; Peterson, A. A.; Hammer, B. Neural-Network-Enhanced Evolutionary Algorithm Applied to Supported Metal Nanoparticles. *Phys. Rev. B* **2018**, *97*, 195424.
(359) Rosenbrock, C. W.; Gubaev, K.; Shapeev, A. V.; Pártay, L. B.; Bernstein, N.; Csányi, G.; Hart, G. L. W. Machine-Learned Interatomic Potentials for Alloys and Alloy Phase Diagrams. *npj Comput. Mater.* **2021**, *7*, 24.
(360) Chiriki, S.; Jindal, S.; Bulusu, S. S. C-T Phase Diagram and Landau Free Energies of (AgAu) 55 Nanoalloy via Neural-Network Molecular Dynamic Simulations. *J. Chem. Phys.* **2017**, *147*, 154303.
(361) Andolina, C. M.; Bon, M.; Passerone, D.; Saidi, W. A. Robust, Multi-Length-Scale, Machine Learning Potential for Ag-Au Bimetallic Alloys from Clusters to Bulk Materials. *J. Phys. Chem. C* **2021**, *125*, 17438−17447.
(362) Hajinazar, S.; Sandoval, E. D.; Cullo, A. J.; Kolmogorov, A. N. Multitribe Evolutionary Search for Stable Cu-Pd-Ag Nanoparticles Using Neural Network Models. *Phys. Chem. Chem. Phys.* **2019**, *21*, 8729−8742.
(363) Kang, J.; Noh, S. H.; Hwang, J.; Chun, H.; Kim, H.; Han, B. First-Principles Database Driven Computational Neural Network Approach to the Discovery of Active Ternary Nanocatalysts for Oxygen Reduction Reaction. *Phys. Chem. Chem. Phys.* **2018**, *20*, 24539−24544.
(364) Glielmo, A.; Sollich, P.; De Vita, A. Accurate Interatomic Force Fields via Machine Learning with Covariant Kernels. *Phys. Rev. B* **2017**, *95*, 214302.
(365) Vandermause, J.; Xie, Y.; Lim, J. S.; Owen, C. J.; Kozinsky, B. Active Learning of Reactive Bayesian Force Fields: Application to Heterogeneous Hydrogen-Platinum Catalysis Dynamics *arXiv* **2021**; https://arxiv.org/abs/2106.01949.
(366) Kahle, L.; Musaelian, A.; Marzari, N.; Kozinsky, B. Unsupervised Landmark Analysis for Jump Detection in Molecular Dynamics Simulations. *Phys. Rev. Mater.* **2019**, *3*, 055404.
(367) Seh, Z. W.; Kibsgaard, J.; Dickens, C. F.; Chorkendorff, I.; Nørskov, J. K.; Jaramillo, T. F. Combining Theory and Experiment in Electrocatalysis: Insights into Materials Design. *Science* **2017**, *355*, No. eaad4998.
(368) Zaera, F. The Surface Chemistry of Metal-Based Hydrogenation Catalysis. *ACS Catal.* **2017**, *7*, 4947−4967.
(369) Yu, W.-Y.; Zhang, L.; Mullen, G. M.; Evans, E. J.; Henkelman, G.; Mullins, C. B. Effect of Annealing in Oxygen on Alloy Structures of Pd-Au Bimetallic Model Catalysts. *Phys. Chem. Chem. Phys.* **2015**, *17*, 20588−20596.
(370) Habas, S. E.; Lee, H.; Radmilovic, V.; Somorjai, G. A.; Yang, P. Shaping Binary Metal Nanocrystals through Epitaxial Seeded Growth. *Nat. Mater.* **2007**, *6*, 692−697.
(371) Gilroy, K. D.; Ruditskiy, A.; Peng, H.-C.; Qin, D.; Xia, Y. Bimetallic Nanocrystals: Syntheses, Properties, and Applications. *Chem. Rev.* **2016**, *116*, 10414−10472.
(372) Tao, A. R.; Habas, S.; Yang, P. Shape Control of Colloidal Metal Nanocrystals. *Small* **2008**, *4*, 310−325.
(373) Lee, J. D.; Jishkariani, D.; Zhao, Y.; Najmr, S.; Rosen, D.; Kikkawa, J. M.; Stach, E. A.; Murray, C. B. Tuning the Electrocatalytic Oxygen Reduction Reaction Activity of Pt-Co Nanocrystals by Cobalt Concentration with Atomic-Scale Understanding. *ACS Appl. Mater. Interfaces* **2019**, *11*, 26789−26797.
(374) Wang, M.; Zhou, C.; Akter, N.; Tysoe, W. T.; Boscoboinik, J. A.; Lu, D. Mechanism of the Accelerated Water Formation Reaction under Interfacial Confinement. *ACS Catal.* **2020**, *10*, 6119−6128.
(375) Mark, L. O.; Chen, W.; Eads, C. N.; Lu, D.; Boscoboinik, J. A.; Stacchiola, D.; Medlin, J. W.; Tenney, S. A. Confinement Effects on Furfuryl Alcohol Reactions over Porous Bilayer Silica-Modified Pd(111). *J. Phys. Chem. C* **2020**, *124*, 25437−25446.
(376) Eads, C. N.; Boscoboinik, J. A.; Head, A. R.; Hunt, A.; Waluyo, I.; Stacchiola, D. J.; Tenney, S. A. Enhanced Catalysis under 2D Silica: A CO Oxidation Study. *Angew. Chemie Int. Ed.* **2021**, *60*, 10888−10894.
(377) Sun, L.; Vandermause, J.; Batzner, S.; Xie, Y.; Clark, D.; Chen, W.; Kozinsky, B. Multitask Machine Learning of Collective Variables for Enhanced Sampling of Rare Events. *arXiv* **2020**; https://arxiv.org/abs/2012.03909.
(378) Kitchin, J. R.; Gellman, A. J. High-Throughput Methods Using Composition and Structure Spread Libraries. *AIChE J.* **2016**, *62*, 3826−3835.




https://doi.org/10.1021/acs.chemrev.1c00967
*Chem. Rev.* 2022, 122, 8758−8808